# Unintended Consequences of Environmental Regulation of Maritime Shipping: Carbon Leakage to Air Shipping*

Volodymyr Lugovskyy† Alexandre Skiba‡ David Terner§

16th June 2023
First draft: October 2022

**Abstract**

We evaluate the expected impact of the International Maritime Organization's 2023 regulatory regime that will cap $CO_2$ emissions from global maritime shipping. Focusing on U.S. imports— for which we compile granular vessel, route, emission, and trade data— we structurally estimate a model featuring substitution between maritime and air transportation. We demonstrate that the cap will instigate a shift towards much more carbon-intensive air transportation, causing a short-term increase in total transportation-related $CO_2$ emissions! Additionally, the cap will induce substantial welfare losses in both the short and long run. We conclude by advocating for alternative, more efficient policy options.

*We are grateful for the excellent feedback provided by Tibor Besedeš, Bruce Blonigen, Anca Cristea, Phillip Economides, Jan Hoffmann, David Hummels, Sam Kortum, Ahmad Lashkaripor, Joseph Shapiro, Woan Foong Wong, Joshua Graff Zivin, and the participants at (the): University of Oregon Economics Seminar (Fall 2022); Midwest Macroeconomics Meetings (Fall 2022); Empirical Investigations in International Trade (Fall 2022); Midwest Economic Theory and International Trade Conference (Fall 2022); NERA Economic Consulting (Fall 2022); Indiana University Microeconomics Workshop (Fall 2022); Midwest Economic Theory and International Trade Conference (Spring 2022); Indiana University Trade Seminar (Spring 2022); and, Southern Economics Association Meetings (Fall 2021). We thank BlueWater Reporting for providing access to their data on the maritime containerized ocean routes and carrier composition. All mistakes are our own.

†Department of Economics, Indiana University, Wylie Hall Rm 301, 100 S. Woodlawn, Bloomington, IN 47405-7104; e-mail: vlugovsk@iu.edu

‡Department of Economics, University of Wyoming; 1000 E. University Ave, Laramie, WY 82071; e-mail: askiba@uwyo.edu

§Department of Economics, Indiana University, Wylie Hall Rm 101, 100 S. Woodlawn, Bloomington, IN 47405-7104; e-mail: dmterner@iu.edu

# 1 Introduction

The United Nations (U.N.) has identified global decarbonization as a top priority (Guterres, 2020). In line with this agenda, the U.N. mandated its International Maritime Organization (IMO) to spearhead the decarbonization of maritime transport, an industry responsible for about 3% of global anthropogenic $CO_2$ emissions—an amount equivalent to the combined emissions of Germany and France (UN, 2021)—and projected to rise by 50% to 250% by 2050 (IMO, 2014).[1] In response, the IMO adopted Initial IMO Strategy on Reduction of GHG Emissions. This strategy aims to restrict $CO_2$ emissions from maritime transport and is expected to come into effect following the conclusion of negotiations in July 2023 (IMO, 2022). We will refer to these forthcoming regulations as IMO2023.

Our paper offers an ex-ante examination of the impacts of the yet-to-be-implemented IMO2023. Our core argument revolves around the unintended consequences of IMO2023: (i) carbon leakage from maritime to air transportation, and (ii) a decrease in consumer surplus. To quantitatively analyze these and other effects of IMO2023, we focus exclusively on the U.S. imports of manufactured goods. This focus is justified by two facts. Firstly, manufactured goods bound for the U.S. are predominantly transported via maritime or air transport. These modes of transport account for the majority of U.S. imports from virtually all exporting countries, excluding Mexico and Canada. Secondly, previous research exploring the interchangeability between air and maritime transportation has focused on the U.S. imports of manufacturers (Harrigan, 2010; Hummels and Schaur, 2010, 2013).

We begin our examination by outlining the proposed IMO2023 regulations and analyzing the observed carbon emissions from specific vessels. This initial analysis reveals that a large proportion of vessels are currently exceeding the emission thresholds proposed in IMO2023, indicating a significant need for emissions reduction. Expert opinions and official IMO documents suggest that the existing abatement technology is either inadequate or economically unfeasible for meeting the IMO2023 requirements. Instead, both IMO members and industry practitioners stress that, at least

[1] Our paper's analysis centers on containerized emissions. Based on bottom-up emissions accounting for 2018 (IMO, 2020, p.126-129), containerized emissions are the largest across all maritime freight market segments, accounting for roughly 22% maritime freight emissions. Put differently, liner emissions are approximately 0.65% of global emissions and are comparable to Spain's $CO_2$ output.

in the short-run, slow-steaming—i.e., operating vessels at slower speeds—is the only viable method to achieve the carbon intensity thresholds established by IMO2023.

Our calculation of the required speed reduction is based on comprehensive data on vessel emissions and technical details and application of naval engineering formulas . According to the calculations U.S.-bound containerized vessels will need to reduce their speed, on average, by 5.2%. We also show that containerized maritime transportation is a capacity-constrained industry. Therefore, in the short run, slow-steaming will effectively shrink its capacity. We then calculate the corresponding capacity reduction for each specific route, defined at the level of an individual exporting country to a U.S. Customs District. Our calculations reveal that capacity reductions will vary substantially across different routes, showing an average decrease of 6%—a figure that aligns with estimates provided by industry experts.

To structurally estimate crucial parameters necessary for the quantitative evaluation of IMO2023, we need a model of U.S. imports which allows for substitution between air and containerized ocean (hereafter referred to as ocean) transportation within and across routes. Building on Hummels and Schaur (2013), we provide such a model, which includes important structural parameters such as the elasticity of substitution between air and ocean transportation and the preference parameter for expedited versus delayed delivery via ocean transport. We then estimate these parameters by employing U.S. Census Imports granular data on freight rates, quantities, and product prices by mode of transportation.

Estimated demand- and supply-side parameters enable us to predict both the short-run and long-run impacts of IMO2023. By applying these parameters to our model's short-run predictions, we show that, for the U.S.-bound containerized ocean fleet, IMO2023 will (i) more than double the average freight rate and (ii) decrease $CO_2$ emissions by 16.5%. That is, IMO2023 will indeed achieve its targeted reduction in $CO_2$ emissions from ocean transportation. However, it will concurrently instigate a significant pollution leakage into air transportation: Our model predicts an increase in $CO_2$ emissions related to air transportation by up to 31%. Consequently, the combined $CO_2$ emissions from both ocean and air transport will increase by up to 18%. This implies that in the short run,

the unintended consequences of IMO2023 will effectively negate its intended benefits, leading to an overall increase (!) in total emissions.

Furthermore, the implications of IMO2023 extend beyond environmental consequences. The reform will also impact the economic dynamics of U.S. imports. Imported goods will be delivered at slower speeds, arrive in reduced quantities, and at much higher freight rates. These factors collectively contribute to significant welfare losses for American consumers, which we estimate to range between 5 to 7 billion USD annually. IMO members are the only player in this policy proposal that stand to accrue material benefits: the reform will enhance industry's image by reducing emissions produced by ocean transportation, increase short-run profits of carriers, and boost demand for new vessels in the medium and long run.

We extend our analysis to consider the long-term impact of the reform. Over time, the combined $CO_2$ emissions from ocean and air transportation are projected to decrease due to entry of new vessels and reclaiming some market share from air transportation. However, these annual reductions will be modest. Considering that carbon emissions have a cumulative impact on climate change (Solomon et al., 2009; IPCC, 2014), it's expected to take a decade to offset the environmental harm wrought by the IMO2023 in the short term. Moreover, the economic burdens borne by American consumers due to increased costs are anticipated to persist, raising serious questions about the overall efficacy of IMO2023 even in the long run.

Our analysis underscores the potential conflict of interest that emerges when self-regulating organizations are responsible for environmental regulations. The IMO, comprising representatives from carriers, shipbuilders, and ship-building financiers, is likely to prioritize the interests of its members over broader societal goals, as previously suggested by Apuzzo and Hurtes (2021). While the reorganization and coordination of U.N. agency mandates is a complex task, assigning broader responsibilities to specialized agencies can aid the U.N. in achieving its climate objectives. In the case of the IMO, despite its direct control being limited to vessels, it still has the potential to reduce *combined* emissions from both air and ocean transportation.

For instance, in our counterfactual analysis, we demonstrate that an effective, albeit perhaps un-

expected, short-run policy would be to increase the speed of containerized vessels. This would not only decrease total combined emissions but it would also enhance consumer surplus. In the long run, a more beneficial policy could be to subsidize goods transported by sea. This approach could reduce overall emissions by shifting demand from air transportation, which has a high carbon footprint, to a more carbon-efficient ocean transportation. In addition, we show that such approach would also enhance total welfare even after factoring in the cost of subsidies.

Finally, touching on the desirable features of future technologies, we stress the importance of innovations that can accelerate ocean transportation. As an illustration, we consider the introduction of black-box technology that keeps fuel consumption constant for a modest increase in speed over the current speed. Quicker delivery times from container ships employing carbon-efficient technologies can once again help shift and amplify demand for such carbon-efficient ships, reducing *net* $CO_2$ emissions and improving overall welfare.

Our paper contributes to several bodies of literature. First, we contribute to the literature on government regulation of pollution and pollution leakages. In general, government intervention is a textbook solution for dealing with externalities, including environmental externalities (Pigou, 1920). Such intervention compels producers to internalize the external cost of pollution, thereby mitigating the impacts of market failure. However, the effects of regulation become ambiguous if controlling one market leads to increased pollution in another, a phenomenon known as leakage.

Pollution leakage has been thoroughly examined within the context of geographic markets, where regulation in one country or U.S. county increases pollution in others (e.g., Becker and Henderson, 2000; Greenstone, 2002).[2] We contribute to this literature by highlighting a different type of pollution leakage: inter-sectoral leakage from ocean to air transportation, where stricter regulations exclusively on ocean transportation will shift import demand from ocean to air transportation.

This unintended consequence of IMO2023 will be especially severe given that air transportation

[2]There is a large body of literature on trade and environmental regulations, which focuses on the environmental aspects of trade, including international leakage and free riding across countries. A very incomplete list of papers in this literature includes Markusen (1975); Copeland (1996); Elliott et al. (2010); Hanna (2010); Nordhaus (2015); Shapiro (2020); Farrokhi and Lashkaripour (2021); Kortum and Weisbach (2021); Tanaka et al. (2022).

is two orders of magnitude (!) more carbon-intensive than containerized maritime transportation.[3] This stark difference in carbon-intensity between the targeted ocean transportation and the leakage destination (air transportation) is unprecedented. Therefore, inter-modal leakage may not just undermine the effect of regulation, as in case of some other within-industry leakages,[4] but can even overturn it, increasing the overall emissions and creating a version of the *green paradox*.[5]

Second, our paper contributes to academic research on emissions from transportation. Most research on pollution from transportation does not focus on the issue of leakage. Walker et al. (2019) offers a comprehensive review of the environmental effects of maritime transportation, Ben-Hakoun et al. (2016) focuses on carbon pollution by maritime transport, and Chao (2014) studies the cost-effect of carbon pollution caused by air cargo transportation. Recent work by Wong and Fuchs (2022) analyzes the impacts of improving inter-modal transport infrastructure, including container ports, on both welfare and mode-specific greenhouse emissions. Even research on spatial leakage of carbon emissions produced by maritime transport tends to ignore intersectoral leakage. Unsurprisingly, this research advocates for either quantitative emissions restrictions or taxes on bunker fuel in ocean transportation (Parry et al., 2018; Mundaca et al., 2021). According to our results, such policies are likely to *increase* joint air and ocean transportation emissions.

Our paper proceeds as follows. Section 2 provides an overview of IMO2023, our shipping microdata, and IMO2023 impacts on vessel speed and attendant short-run U.S. ocean-transportation capacity removal. Section 3 presents our theoretical model. We estimate and calibrate model parameters in Section 4. In Section 5, we present our quantitative predictions on the effect of IMO2023 on ocean and air transportation emissions in the short-run and analyze long-run outcomes in Section 6. Section 7 discusses welfare-improving alternative policies, including tax/subsidy instruments and

[3] According to our calculations, the average ratio of grams of $CO_2$ per ton of goods transported by air relative to American container ship routes results in a 90-fold difference. This 90-fold difference grows to 156 if we compare grams of $CO_2$ per ton-mile since air routes are typically more direct than container ship routes. Cristea et al. (2013) and Shapiro (2016) have also highlighted much greater carbon intensity of air transportation compared to ocean and other modes of transportation.

[4] See, for example, literature on *Gruenspecht effect*, where the impact of stricter emission regulations of new vehicles is offset by the owners keeping older vehicles for longer time (Gruenspecht, 1982; Jacobsen and van Benthem, 2015).

[5] See der Werf and Maria (2012) for a review of green paradox literature related to pollution leakage.

technological advances. Section 8 concludes the paper.

## 2 The Anatomy of IMO2023

The IMO is one of the U.N.'s specialized agencies tasked with developing and promulgating global safety and environmental standards for freight shipping. In 2018, the IMO established its Initial IMO Strategy on Reduction of GHG Emissions to restrict $CO_2$ emissions from maritime transportation, beginning in the second half of 2023. The IMO's objective is to gradually increase the stringency of regulations and policy measures until 2050. Collectively, we refer to all of the regulations and policy changes proposed by the IMO as IMO2023.[6] IMO2023 aims to lower carbon emissions by prescribing more stringent standards expressed as $CO_2$ emissions in grams per ton-mile. The IMO coined the term "Carbon Intensity Indicator" (CII) to describe this measure. In any given year $t$ for a specific vessel $v$ two CII values are relevant: the observed CII denoted $CII^{obs}_{v,t}$, and the required CII denoted $CII^{req}_{v,t}$. The formulas for these measures are provided in Table 1. The IMO classifies individual ships into letter grades based on the ratio of $\frac{CII^{obs}_{v,t}}{CII^{req}_{v,t}}$ with grade thresholds outlined in Table 1. Beginning in 2023, only vessels that receive an "A", "B", or "C" grade can be chartered without extensive operational modifications.

Table 1: IMO2023 Letter Grade Classification of Carbon Efficiency

| $\frac{CII^{obs}_{v,t}}{CII^{req}_{v,t}} \times 100\%$ | $< 83\%$ | $83 - 94\%$ | $94 - 107\%$ | $107 - 119\%$ | $> 119\%$ |
|---|---|---|---|---|---|
| Grade | A | B | C | D | E |

*Note*: $CII^{obs}_{v,t} = \frac{\text{CO}_2 \text{ Emissions}_{v,t}}{Dwt_v \times Dist_{v,t}}$ and $CII^{req}_{v,t} = \left[1984 \times (Dwt_v)^{-0.489}\right](1 - Z_t)$, where $Dwt_v$—Deadweight Tonnage— is a measure of vessel size; $Dist_{v,t}$ is the total distance traveled by $v$ in year $t$; expression in $[.]$ is the reference line in year 2019; and $Z_t$ starts out at 5% in 2023 and increments by 2% each year with the rate likely to accelerate in 2027.[7]

In order to assign letter grades to vessels under the IMO2023 regulations, it is necessary to obtain specific information about each vessel, including its deadweight tonnage (Dwt), distance traveled,

[6]The origins of emission threshold policies can be traced back to the Initial IMO Strategy on Reduction of GHG Emissions adopted in April 2018 (IMO Resolution MEPC.304(72)), which was later expanded with new regulations approved in 2021 (refer to IMO Resolutions MEPC.335(76), MEPC.336(76), MEPC.337(76), MEPC.338(76)).

and $CO_2$ emissions. We obtain Dwt data for all containerized vessels from the *World Fleet Register* (WFR), which is maintained by Clarksons PLC, the world's leading shipbroker. However, at present, there is no comprehensive dataset with observed $CO_2$ emissions at the vessel level. To address this, we rely on a partial dataset from *THETIS-MRV* (alternatively THETIS), an online database maintained by the European Maritime Safety Agency (EMSA) that provides information on carbon emissions (as well as distance traveled) for the years 2018-2020. This dataset covers 39.7% of the global containerized ocean fleet by count and 54.1% by capacity. For more information on this and other datasets used in the paper, see Online Appendix A.1.

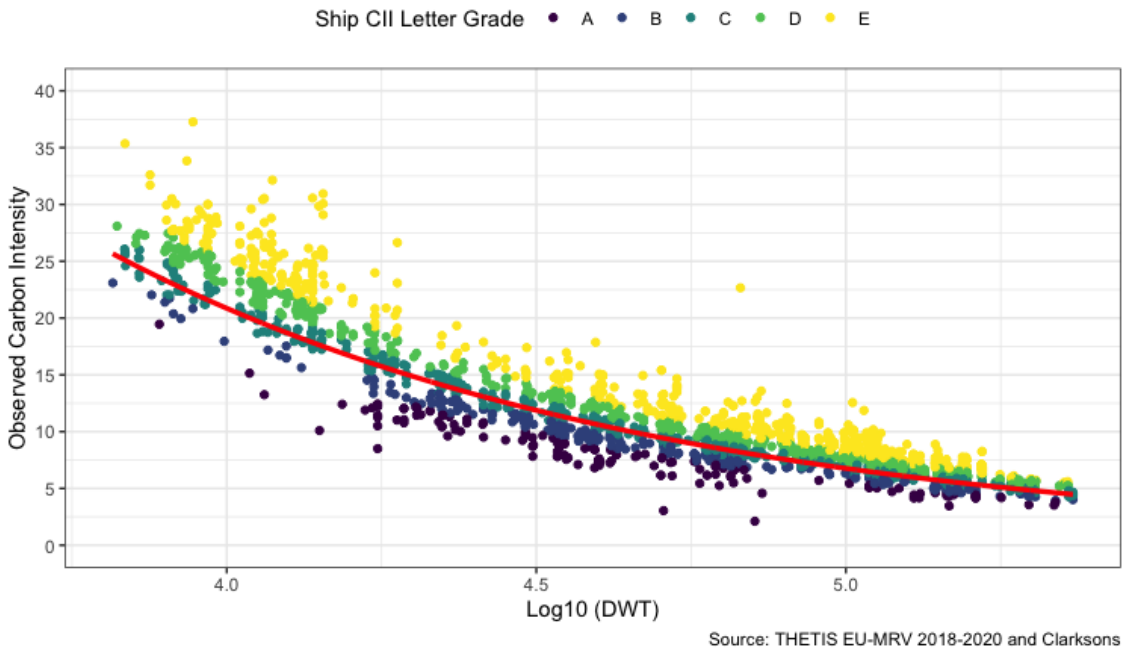


Figure 1: Observed Carbon Intensity
*Note*: Each dot represents a vessel. Based on Dwt capacity, our sample has the following distribution of CII letter grades going based on the IMO2023 required CII: 5.1% are A, 12.8% are B; 25.0% are C; 27.3% are D; and, 29.8% are E.

Using the data, we conduct two key analyses. First, we calculate IMO2023 letter grades for 1,903 containerized vessels reported in the THETIS dataset, and display the results in Figure 1. If there are multiple observations per vessel, we average the data at the vessel level to calculate $\overline{CII}_v^{obs}$. Second, we estimate $CO_2$ emissions for the remaining vessels to calculate their letter grades.

Figure 1 displays the relationship between vessel Dwt (obtained from Clarksons) and observed

$CO_2$ emissions per *Dwt* ton-mile, along with the IMO2023 required CII (red) benchmark efficiency line for 2023; the benchmark efficiency line is 95% of the required CII or, equally, represents at 5% efficiency improvement relative to the base year (2019). The figure reveals two main insights. First, a 5% reduction in vessel operational carbon intensity under IMO2023 is an uninformative summary statistic, as the reduction varies greatly across container ships. To avoid an "D" or "E" rating, vessels need to achieve an average $CO_2$ reduction of 8.9%, which includes vessels with "A-C" ratings. For vessels with "D" or "E" ratings, the average reduction required is 15.9%. Second, vessel size is an excellent predictor of observed carbon intensity, as evidenced by a simple linear model estimated on the THETIS sample (standard errors reported below coefficients):

$$\ln\left(\overline{CII}_v^{obs}\right) = \underset{(0.04)}{7.62} - \underset{(0.004)}{0.49}\ln(Dwt_v) + \varepsilon_v \quad (R^2 = 0.87; \text{N Obs} = 1903), \tag{1}$$

This model explains 87% of the variation in log-transformed observed carbon intensity. Given the strong explanatory power of Dwt, we aim to estimate the $CII_{v,t}^{obs}$ for vessels outside of the THETIS sample. To do this, we adopt a training and testing approach. We randomly divide our THETIS sample into a training dataset (80% of the sample) and a testing dataset (20% of the sample) 10,000 times. For each iteration, we fit a simple linear model similar to Equation (1), and calculate the in-sample and out-of-sample $R^2$ and RMSE.

As $CII_{v,t}^{obs}$ is in levels, while our fitted values are expressed in logs, we exponentiate our fitted values and adjust for Duan's smear of $\approx 1.02$ as per Duan (1983). Our in-sample $R^2$ based on levels for our chosen model is 0.818 with a 95% CI of [0.754, 0.877]. Standard errors are derived using 10,000 bootstrapped samples. Furthermore, our out-of-sample $R^2$ based on levels is 0.883 with a 95% CI of [0.860,0.907].

To select our predictive model, we choose the slope term with the highest frequency in 10,000 trials. Notably, the model's coefficient matches Equation (1). With this model, we estimate the $CII_{v,t}^{obs} = \widehat{\overline{CII}}_v^{obs}$ and assign letter grades to the remaining vessels.

## 2.1 Calculating the required slow-steaming in response to IMO2023

Compliance for letter grades D and E vessels, based on IMO2023 requirements, poses a significant challenge. Container ship carbon abatement has so far been achieved through three channels: (1) adoption of lower carbon content fuels; (2) incorporation of more fuel-efficient ship designs; and (3) construction of larger vessels. Of these channels, the first two offer limited potential for lasting environmental improvement: Alternative fuel sources, such as liquefied natural gas and methanol, release comparable carbon emissions over their lifetime use, and reductions achieved through vessel design are only realized when vessels operate at slow speeds (Winnes et al., 2015). Consequently, both the IMO and industry practitioners highlight slow steaming, i.e., speed reduction, as the primary approach for complying with IMO2023.[8]

In order to assess the impact of IMO2023 on vessel speed, we utilize a naval engineering formula from Corbett et al. (2009) to express the per trip fuel consumption $F$ of a vessel as a function of its speed:

$$F_{ijv}(s_v) = \left[F_v^{\text{Main}}\left(\frac{s_v}{s_v^{\text{Des}}}\right)^3 + F_v^{\text{Aux}}\right]\frac{d_{ij}}{24 s_v}, \tag{2}$$

where $F_v^{\text{Main}}$ and $F_v^{\text{Aux}}$ are vessel $v$'s main and auxiliary engine fuel consumption per day, respectively; $s^{\text{Des}}$ and $s_v$ are $v$'s design and operational speeds, respectively; and $d_{ij}$ is the total distance of the $ij$ route defined by the U.S. importing Customs District $i$ and the exporting country $j$. We then calculate the ratio of fuel consumption for a vessel slowing down to meet the IMO requirements to $s_v^{\text{IMO}}$ relative to operational speed $s_v$ assuming $s_v^{\text{IMO}} = \rho_v s_v$, where $\rho_v \equiv s_{2v}/s_{1v} \leq 1$ represents the reduction in speed necessary for a vessel to meet new operational efficiency standards:

$$\frac{F_{ijv}(s_v^{\text{IMO}})}{F_{ijv}(s_v)} = \frac{F_v^{\text{Main}}(\rho_v s_v / s_v^{\text{Des}})^3 + F_v^{\text{Aux}}}{\rho_v\left(F_v^{\text{Main}}(s_v/s_v^{\text{Des}})^3 + F_v^{\text{Aux}}\right)}. \tag{3}$$

[8] ZIM's executive vice president, Xavier Destriau, noted in an August 2021 interview with Szakonyi (2021) that reducing carbon emissions requires changes in engine power and vessel speed. That means the industry is going "to need more vessels to handle the same amount of cargo," he said. This sentiment was echoed by Gulfstream Shippers Association's President, Garret Bowman, who predicts that many ships will slow down in response to IMO2023 (Slaughter, 2022).

Given that vessel $CO_2$ emissions are directly proportional to fuel consumption, comparing the fuel consumption at different speeds allows us to estimate the change in $CO_2$ output (per ton-mile). We then use the IMO's $CII^{req}_{v,t}$ operational efficiency standard to calculate the slowdown factor $\rho_v$ required for vessels with a "D" or "E" rating to achieve a "C" grade or higher. To find the appropriate slowdown adjustment $\rho_v$, we minimize the function $H(\rho_v)$, defined as

$$H(\rho_v) \equiv \Big[\frac{F_v^{\text{Main}}(\rho_v s_v / s_v^{\text{Des}})^3 + F_v^{\text{Aux}}}{\rho_v (F_v^{\text{Main}}(s_v / s_v^{\text{Des}})^3 + F_v^{\text{Aux}})} - \Big(1 - \Big(\frac{\overline{CII}_v^{obs}}{\overline{CII}_v^{req}} - 1.07\Big)\Big)\Big]^2. \tag{4}$$

This ensures that the vessel achieves the necessary reduction in $CO_2$ emissions while balancing the competing objectives of speed and efficiency.[9] For vessels that are currently rated "C" or better, we set $\rho_v = 1$.

To use equation (3), we require data on container ship routes, vessel speeds, fixed technical characteristics (main engine fuel consumption, auxiliary fuel consumption, and design speed), and observed operational carbon intensity $CII^{obs}_{v,t}$. We identify U.S.-bound container ships using Panjiva bill of lading data and BlueWater Reporting ship rotation data, and calculate vessel operational speeds using THETIS-MRV and BlueWater Reporting data. Fixed technical characteristics are measured or imputed using Clarkson's WFR data, and missing values of $CII^{obs}_{v,t}$ are measured or imputed based on the relationship between vessel size and operational carbon efficiency captured by equation (1).[10]

In Figure 2, we present our estimates of vessel slowdown as a function of vessel size measured

[9] A quick explanation of the formula. The left hand side term comes from equation (3): the ratio of fuel consumption at new (slower) speeds relative to initial speed. $\overline{CII}_v^{obs}/\overline{CII}_v^{req} - 1.07$ comes from comparing a vessel's current operational rating to its IMO2023 standard. We use vessel averages if multiple observations per vessel are available. We subtract off 1.07 because +7% higher score is the largest deviation a vessel can have and still achieve a "C" grade. Thus, if a vessel's $\overline{CII}_v^{obs}/\overline{CII}_v^{req} = 1.08$, said vessel would need a 1 percentage point improvement in its operational rating to achieve a "C" grade. $1 - (\overline{CII}_v^{obs}/\overline{CII}_v^{req} - 1.07)$ thus gives us an estimate of what the fuel ratio should equal given a new (slower) speed; to continue with the example, given vessel characteristics and current speed, how much slower should a vessel move such that it is consuming 1% less fuel (or 0.99 in ratio terms)? Finally, we try to the minimize the squared difference between IMO2023 required improvements (e.g. the right-hand side) and the attendant speed-induced relative change in fuel consumption (e.g the left-hand side).

[10] See Online Appendix A.3.1 for details on identifying U.S.-bound container ships, Online Appendix A.3.2 for calculating vessel speed, Online Appendix A.3.3 for modeling technical characteristics, and Online Appendix A.3.4 for imputing $CII^{obs}_{v,t}$. Table A4 summarizes data sources and methods, while Online Appendix A.3.6 provides more details on the speed adjustment factor $\rho_v$.

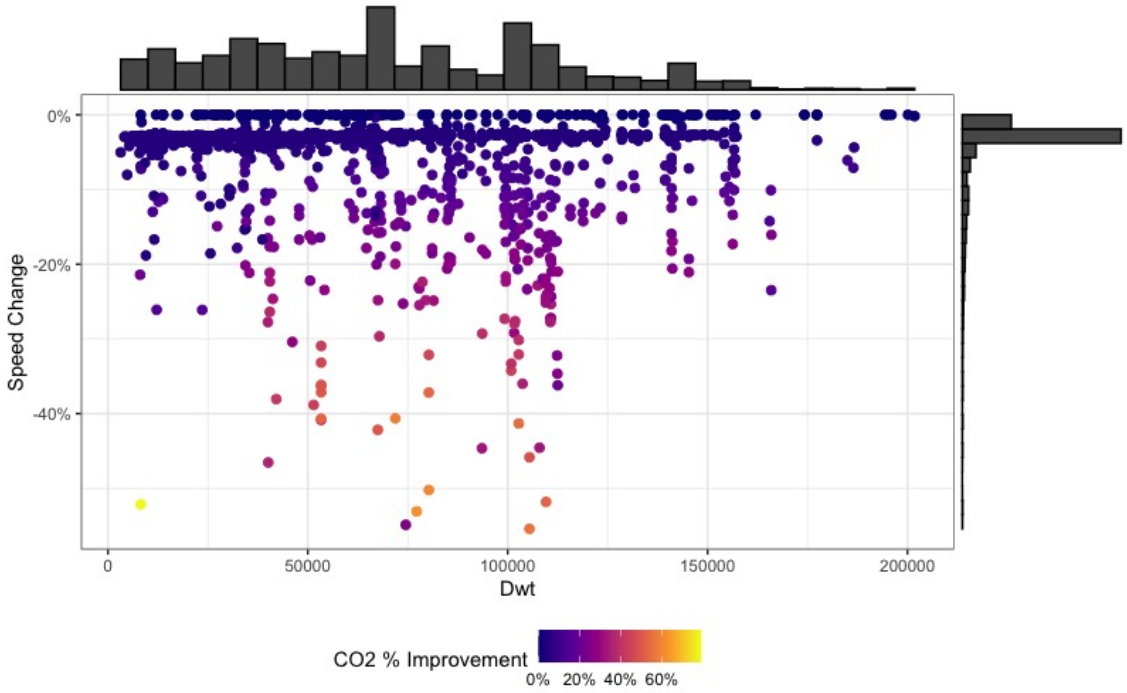


Figure 2: IMO2023 slowdown calculations ($\rho_v$)
*Note*: The unit of observation in this Figure is a vessel. The horizontal axis corresponds to deadweight tonnage (a measure of vessel size) whereas the vertical axis corresponds to how much a vessel needs to slow down (e.g. $\rho_v$) in percentage terms to meet IMO2023 standards. The unweighted marginal densities of both vessel size and slowdown are plotted alongside the appropriate axis. Each vessel/point is colored according to how much the slowdown will improve the vessel's operational efficiency rating: brighter (darker) colors correspond to greater (lesser) operational efficiency improvements.

in Dwt. Each vessel is color-coded according to the size of the carbon operational efficiency increase needed to attain a "C" grade or better. The results highlight significant heterogeneity across vessel size and speed adjustments. On average, the Dwt capacity-weighted vessel slowdown is approximately **5.2%**, leading to a corresponding **7.3%** increase in carbon operational efficiency. When we restrict our attention to vessels that must slow down, the Dwt capacity-weighted average speed reduction rises to 6.4%, with a corresponding 8.7% increase in carbon operational efficiency.

## 2.2 Calculating effective capacity reduction

We begin by verifying that the assumption of binding capacity constraint accurately describes capacity use in maritime transportation. This step is necessary to establish that slow steaming reduces the effective capacity of the ocean fleet in the short run due to full utilization and slow vessel con-

struction. We use Clarksons *Shipping Intelligence Network* (SIN) to assess fleet capacity utilization, calculating idle TEU capacity daily between 2014 and 2022. Figure 3 indicates that idle capacity fluctuates between 1.3% and 6.8% within this period, averaging 2-3%. Some instances of idle capacity stem from low demand, port congestion,[11] maintenance, and schedule adjustments. Therefore, we conclude the observed idle rates support full utilization of the containerized ocean fleet.

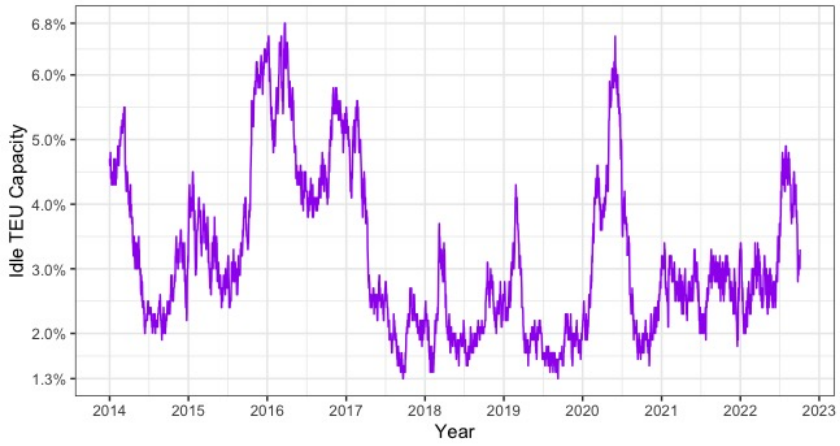


Figure 3: Historic Daily Idle Ocean TEU Capacity
*Sources*: Figure 3 relies on data from Clarksons Shipping Intelligence Network (SIN).

In the short run, ocean shipping is capacity constrained, as building a new vessel can take up to three (3) years (Kalouptsidi, 2014; Chokshi, 2020). Therefore, the required slow-down of the ocean fleet will result in a reduction of ocean fleet capacity. To quantify this effect, we first use the calculated vessel speed reduction $\rho_v$ to determine a more aggregated route-level slowdown, $\rho_{ij}$, where the route is defined between an exporting country $j$ and an importing U.S. Customs District $i$.[12] Assuming a representative vessel on route $ij$, the number of corresponding round trips $n_{ij}$ is

$$n_{ij} = A \Big/ 2(TIME_{ij} + \text{port}(\text{port traffic}_{ij})), \tag{5}$$

where $A$ is the number of sailing days in the year and $TIME_{ij}$ is the average route time. The time spent at port is modeled as a function of port traffic $\text{port}(\text{port traffic}_{ij})$ using Automatic Identification

[11] For example, wait times outside of ports may reach up to 22 days at the most congested ports (Thomsen, 2021).
[12] Towards this goal, we map individual vessels to route $ij$. For details, see Online Appendix A.3.8.

System (AIS) tracking data. AIS does not report time at port for all ports. We overcome this issue by computing the weighted average for the ports where the data are available, which is $\overline{\text{port}}$ =2.53 days, and assign it to all ports in our sample.[13] Our port time elasticity, $\kappa$, estimate suggests that a 10% increase in port traffic is associated with a 1.97% increase in a vessel's time at port.[14] These estimates are based on fixed-effects regression models that include vessel, time, and port fixed effects.[15] We will use the relationship between the port traffic and time at port when analyzing various policies which affect port traffic.

Reducing vessel speed has two opposing effects in our model. First, it increases the time spent on a route, which reduces the number of round trips and capacity for the year. Second, slower vessels result in fewer vessels in ports, reducing traffic. This, in turn, means that a vessel's time in port is reduced, leading to more round trips and partially restored capacity. We calculate the change in route $ij$ capacity brought on by IMO2023's slower speeds as:

$$\underline{\omega}_{ij} \equiv \frac{n_{ijT}(\rho_{ij})}{n_{ijt}} = \frac{TIME_{ij} + \overline{\text{port}}}{\frac{1}{\rho_{ij}} TIME_{ij} + \overline{\text{port}}\left(\underline{\omega}_{ij}\right)^{\kappa}}, \tag{6}$$

where $t$ and $T$ refer respectively to time periods pre and post implementation of IMO2023. We solve for $\underline{\omega}_{ij}$ numerically. Our aggregated results reveal that IMO2023 will lead to a 5.9% reduction in U.S. imports' capacity and increase the average route shipping times by 0.54 days.[16] The required capacity reduction varies across countries. Figure 4 displays our $\underline{\omega}_{ij}$ calculations aggregated at the level of importing country. For example, Chinese ocean export capacity will decrease by approximately 4.2%, Brazilian export capacity by 8.2%, and German export capacity by over 10.3%.

Our results align with industry reports on the impact of IMO2023 on shipping capacity. For

[13] We use AIS tracking data on container ships serving U.S. ports from Marine Cadastre to estimate time at port and how it depends on traffic. Refer to Online Appendix A.3.7 for more information on data and estimation details.

[14] This point estimate comes from Column (4) of Table A6 in Online Appendix A.3.7. Our elasticity is qualitatively similar to Wong and Fuchs (2022)'s range of vessel dwell time elasticity estimates.

[15] Moreover, our port time elasticity estimates are qualitatively similar to those found by Wong and Fuchs (2022).

[16] Using route traffic volumes as weights, we compute both summary statistics as weighted averages. We then compute standard errors via boot-strap with 1,000 replications. Accordingly, we find short run capacity reductions to have a 95% confidence interval (CI) of [5.34%, 6.40%]. Likewise, short run shipping time increases have a 95% CI of [0.40 days 0.69 days]. Additional boot-strap standard errors/confidence intervals for other summary statistics are available upon request.

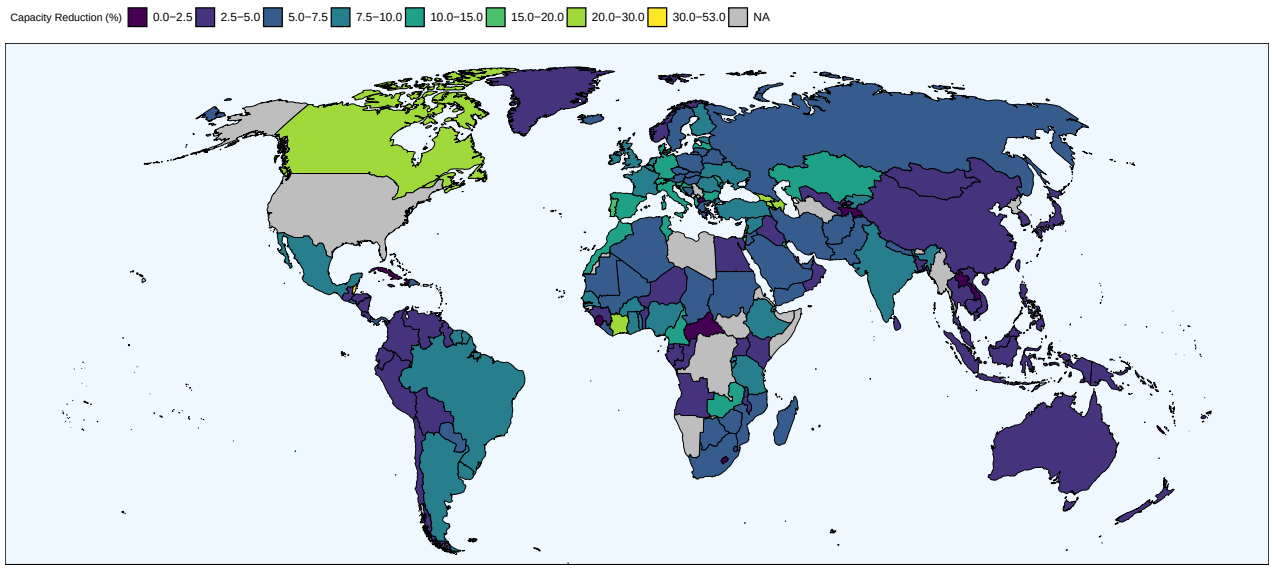


(a)

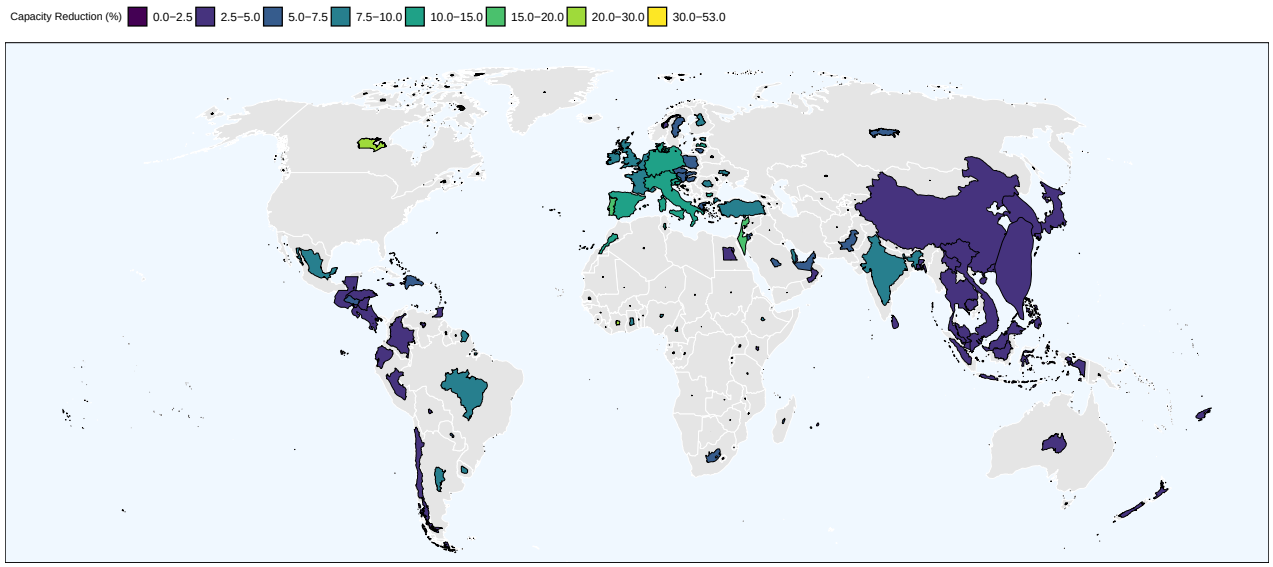


(b)

Figure 4: IMO2023 US Capacity Impacts

*Note*: Both panels depict changes in country containerized export capacity to the US post IMO2023. Changes in country $j$'s capacity are calculated via $(\sum_i \underline{\omega}_{ij}\underline{q}_{ijt})/(\sum_i \underline{q}_{ij}) - 1$; this calculation informs how we color-code each country. The difference between (a) and (b) is that (b) is cartogram, where country geometries are scaled according to trade volume with the US. In this way, panel (b) shows that East Asian and Western European capacity reductions will be (numerically) more significant.

instance, Maersk CEO Søren Skou asserted that the ocean company would require 5-15% more capacity to comply with the regulations due to slow steaming (Mandra, 2022). Similarly, Hapag-Lloyd CEO Rolf Habben Jansen reported that the company would need an extra 5-10% capacity (Kershaw,

2022). Furthermore, our projections regarding decreases in speed and imports align with the findings presented by the U.N. Conference on Trade and Development (UNCTAD, 2021).[17]

## 2.3 A Note on Enforcement Mechanism

Enforcement of IMO regulations is generally left to member states, and implementation details are often left to MARPOL signatories.[18] For example, in the U.S., MARPOL Annex IV regulations have been incorporated into law by the Act to Prevent Pollution from Ships (APPS) and implemented within 33 USC 1901 and 33 CFR 151 (USCG, 2022). The U.S. Coast Guard enforces maritime emissions standards, including Annex IV's regulations on sulfur content in commercial vessels' bunker fuels (Hansen-Lewis and Marcus, 2022).

Proponents of the IMO's efforts to improve maritime emissions by collaborating with port states, i.e., MARPOL signatories, highlight the success of IMO2020. That set of regulations lowered the maximum sulfur content in fuel used by vessels outside of emission control areas from 3.5% m/m to 0.50% m/m. Even after accounting for the reduction in commercial freight traffic due to COVID-19, IMO2020 was a success, resulting in a 46% reduction in $SO_2$ aerosol volume (Yuan et al., 2022).

Despite the success of IMO2020, effective enforcement of emissions regulations for both owners and charters remains a challenge, which may delay the implementation of IMO2023 (Kinyua, 2023). The Baltic and International Maritime Council (BIMCO) has created a contractual framework called the "CII Operations Clause for Time Charter Parties," which purports to facilitate cooperation between shipowners and charters to achieve the IMO2020 carbon intensity goals. However, the "Clause" does not transfer regulatory responsibility for compliance to charters, and it is the shipowners who will ultimately be accountable for meeting IMO2023 compliance requirements. As a result, charters have little incentive to adopt the "Clause" (Keys, 2022a). Keys (2022b) suggests that the real enforcement of IMO2023 may come from a vessel's flag state's ability to issue or withhold a State-

[17] Specifically, with their HIGH scenario results as reported in Table 1. UNCTAD's analysis includes all modes of ocean transportation, including liner, dry-bulk, tankers, and ro-ro, and offers a broad geographical coverage.

[18] MARPOL stands for "International Convention for the Prevention of Pollution from Ships, 1973 as modified by the Protocol of 1978" and is one of the world's most significant international marine environmental conventions; see the U.S. Coast Guard's summary page here.

ment of Compliance: vessels without "SoC" are unchartable.[19]

# 3 Model

Our model builds upon that of Hummels and Schaur (2013), which also focuses on ocean and air transportation of goods. However, our approach is more aggregated. While Hummels and Schaur (2013) explored shipping of the same product by either ocean or air, our model emphasizes the total demand for goods transported by air versus those transported by ocean. For instance, in our model, an increase in the ocean freight rate for imported cars will boost demand for air-transported imported watches. That is, in addition to considering substitution of transportation modes within products, we also explore that across products. This additional aspect could potentially amplify the magnitude of ocean-to-air substitution compared to that found in Hummels and Schaur (2013).

**Preferences.** The model is set from the perspective of one country, Home, which consists of multiple regions indexed by $i$ and imports foreign goods via two modes of transportation: ocean and air shipping (in the empirical exercise regions are the U.S. Customs Districts). Consumers have Cobb-Douglas preferences defined over a domestically-produced composite good 0 and composite differentiated good. Differentiation is based on the national origin [20] $j$ and goods' perishability: perishable (transported by air) vs. non-perishable (transported by ocean). We use the lower-bar and upper-bar notation for parameters of non-perishables and perishables, respectively. Formally, a Home's representative consumer in region $i$ in year $t$ has preferences given by:

$$U_{it} = q_{0,it}^{1-\mu}\left[\sum_j\left(\nu_{it}\nu_j\underline{q}_{ijt}^{\frac{\varepsilon-1}{\varepsilon}}+\overline{q}_{ijt}^{\frac{\varepsilon-1}{\varepsilon}}\right)\right]^{\mu\frac{\varepsilon}{\varepsilon-1}} \qquad \varepsilon>1, \quad 1>\mu>0, \tag{7}$$

where $\underline{q}_{0,it}$ is the quantity of the domestic numeraire good;

[19] Adopting 'flags of convenience' is common in international shipping, where vessels are registered in port states with open registries. These countries impose lower taxes and fewer inspections, making them attractive to shipowners (Stopford, 2009). Around 45% of TEU US imports are carried by ships from Liberia, Panama, and Malta, which have open registries; US-registered containerships account only for 5%.

[20] The national origin, or Armington, differentiation is quite common in trade literature and has also been used in the related paper on emissions from transportation of traded goods by Shapiro (2016).

$\underline{q}_{ijt}$ and $\overline{q}_{ijt}$ are the imported from $j$ quantities of non-perishables and perishables, respectively;

$\nu_{it}$ and $\nu_j$ are the region-time- and origin-specific preference shifters of non-perishable imports, which, among other things (captured by $\vartheta_{jt}$), depend on the delivery time, which is a function of distance $d_{ij}$, speed per hour $s_{ij}$, and time spent in $i$'s port:

$$\nu_{it}\nu_j = \vartheta_{jt}(d_{ij}/(24s_{ij}) + port_i)^{\beta_k} \qquad \vartheta_{jt} > 0, \quad \beta_k < 0. \tag{8}$$

**Production of Goods and Transportation.** Production costs may vary across countries of origin, over time, and between perishable and non-perishable goods. Prices, freight rates, and tariffs are set exogenously. Perishable goods are imported by air, while non-perishables—by ocean. We assume that the air freight rate is always much greater than the ocean one: $\overline{f}_{ijt} >> \underline{f}_{ijt}$, and therefore firms choose to transport non-perishable goods by vessel. Following Hummels et al. (2009), we express the delivered prices of imported goods imported by $i$ from $j$ in $t$, and denoted by $P_{ijt}$, as a function of the free-on-board (FOB) prices, $p_{ijt}$, iceberg tariffs, $\tau_{ijt} \geq 1$, and specific transport cost, $f_{ijt}$:

$$\underline{P}_{ijt} = \underline{p}_{ijt}(\underline{\tau}_{ijt} + \underline{f}_{ijt}/\underline{p}_{ijt}), \qquad \overline{P}_{ijt} = \overline{p}_{ijt}(\overline{\tau}_{ijt} + \overline{f}_{ijt}/\overline{p}_{ijt}). \tag{9}$$

To keep our model tractable, we simplify it by abstracting away from critical issues that affect freight rate formation, including port efficiency (Blonigen and Wilson, 2008), average vessel size (Asturias, 2020), average unit values (Hummels and Skiba, 2004), geography and networks in ocean transportation (Ganapati et al., 2020), and backhaul effects (Ishikawa and Tarui, 2018; Wong, 2020).[21]

Instead, we focus on such determinants of the freight costs as the number of carriers (Hummels et al., 2009; Ardelean and Lugovskyy, 2023), fuel and non-fuel costs components, speed ($s_{ij}$), and time spent in ports. Following Hummels et al. (2009), we assume that, on each route $ij$, a fixed number of containerized ocean carriers, $N_{ij}$, compete in quantities à la Cournot. Each $ij$ transportation market is treated as a segmented market with all carriers in $ij$ having access to the same symmetric technology.

[21] We justify this assumption in the estimation section by stating that these determinants are already incorporated into the observed freight rates. When analyzing policy-induced changes, we assume that any changes to these determinants resulting from the policy will have a secondary effect on freight rates compared to the policy's direct impact.

The technology is characterized by an annual fixed cost of $\Gamma_{ij}$ and a marginal cost per trip of $c_{ij}$, which consists of fuel and non-fuel cost components:

$$c_{ij} = b_{ij}F_{ij}(s_{ij}) + D_{ij}((d_{ij}/24s_{ij}) + port_i), \tag{10}$$

where $b_{ij}$ is the bunker fuel price, $F_{ij}$ is the fuel amount per trip, previously defined by equation (2), $d_{ij}$ is distance between $i$ and $j$, and $s_{ij}$ is speed per hour, and $D_{ij}$ daily non-fuel costs (i.e., labor costs, financing costs, etc.).

Based on the evidence presented in Section 2.2, we assume that ocean transportation is operating at full capacity. Similar assumption is less justifiable for air transportation, where on average only 24.3% of payload is used to transport cargo with most of the under-utilized capacity coming from the passenger airplanes (Besedeš and Murshidb, 2022).[22] We confirm these statements, using Domestic and International Segment T100 Traffic Data, by plotting the utilized air capacity over time and across airplane types in Figure 5. Therefore, in our model, we assume that air transportation is subject to significant excess capacity.

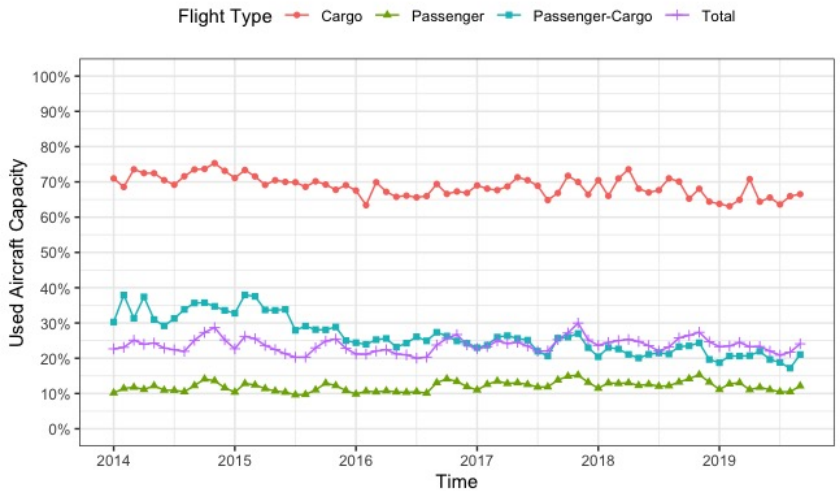


Figure 5: US Air Import Capacity Utilization over Time
*Sources*: Figure 5 relies on Domestic and International Segment T100 Traffic Data reported by U.S. and Foreign Carriers and provided by the Bureau of Transportation Statistics (BTS). The figure shows percentages of utilized cargo capacity in cargo, passenger, and cargo-passenger airplane types.

[22]Passenger airplanes are responsible for 44% of cargo transported by air (Budd and Ison, 2017).

**Equilibrium Demands and Ocean Freight Rates.** In equilibrium, the ratio of marginal utilities is equal to the ratio of the delivered prices, from which we can derive demand functions:

$$\underline{q}_{ijt} = \left(\nu_{it}\nu_j q_{0,it}\right)^{\varepsilon}\left(K_{it}\underline{p}_{ijt}(\underline{\tau}_{ijt} + \underline{f}_{ijt}/\underline{p}_{ijt})\right)^{-\varepsilon} \qquad \overline{q}_{ijt} = (q_{0,it})^{\varepsilon}\left(K_{it}\overline{p}_{ijt}(\overline{\tau}_{ijt} + \overline{f}_{ijt}/\overline{p}_{ijt})\right)^{-\varepsilon}, \quad (11)$$

where $K_{it} = \frac{1-\mu}{\mu}\left[\sum_j\left(\nu_{it}\nu_j\underline{q}_{ijt}^{\frac{\varepsilon-1}{\varepsilon}} + \overline{q}_{ijt}^{\frac{\varepsilon-1}{\varepsilon}}\right)\right]$ is treated by all market participants as given. Notably, the demand for any differentiated variety depends on the freight rates of all other imported varieties delivered to district $i$. Next, we build on the solution outlined in Hummels et al. (2009) to get the equilibrium freight rate in ocean transportation:[23]

$$\underline{f}_{ij} = c_{ij} + \frac{c_{ij} + \underline{p}_{ij}\underline{\tau}_{ij}}{N_{ij}\sigma_{ij} - 1}, \quad (12)$$

where $\sigma_{ij} = \varepsilon\left(1 + \frac{(\varepsilon-1)\nu_{ij}\underline{q}_{ij}^{\frac{\varepsilon-1}{\varepsilon}}}{\sum_j\left(\nu_{ij}\underline{q}_{ij}^{\frac{\varepsilon-1}{\varepsilon}} + \overline{q}_{ij}^{\frac{\varepsilon-1}{\varepsilon}}\right)}\right)^{-1}$. While in Hummels et al. (2009) the equilibrium freight rate on a given route is self-contained, our model contrasts this result by having rates depend on trade from other routes. Our result converges to Hummels et al. (2009) if we assume that ocean imports on $ij$ are negligible compared to the total imports by $i$, in which case $\sigma_{ij} \to \varepsilon\ \forall ij$. With these results in mind, we will next outline the implications of various policies; their quantitative assessments will be provided in Sections 5, 6, and 7, respectively.

**Short-Run Effects of IMO2023.** To analyze the impact of IMO2023, we derive the relative vessel-to-air demand by taking the ratio of and log-linearizing the mode-specific demands in equation (11):

$$\ln\left(\frac{\underline{q}_{ijt}}{\overline{q}_{ijt}}\right) = \varepsilon\ln(\nu_j\nu_{it}) - \varepsilon\ln\left(\frac{\underline{p}_{ijt}}{\overline{p}_{ijt}}\right) - \varepsilon\ln\left(\frac{\underline{\tau}_{ijt} + \underline{f}_{jt}/\underline{p}_{ijt}}{\overline{\tau}_{ijt} + \overline{f}_{ijt}/\overline{p}_{ijt}}\right). \quad (13)$$

As a result of the reduction in average speed in ocean transportation caused by IMO2023, the preference multiplier for non-perishables $(\nu_j\nu_{it})$ will be lowered, as indicated by equation (8). Furthermore, since containerized ocean capacity is already at its limit, the decrease in speed will reduce the quan-

[23] For completeness, we provide derivations in Appendix A.5.

tity of goods shipped via ocean transportation, which will in turn put upward pressure on ocean freight rates. These effects will collectively contribute to a reduction in ocean transportation and an increase in air shipping, resulting in carbon leakage from ocean to air transport.

**Long-Run Effects of IMO2023** In the long-run, ocean capacity will no longer be binding, and changes in relative demand will primarily result from (i) the lower $\nu_j \nu_{it}$ due to reduced average speed and (ii) the potential change in ocean freight rates resulting from new marginal costs imposed by IMO2023 (as seen in equations (10) and (12)).

**Alternative Policies: Subsidizing ocean-delivered imports or taxing air-delivered imports.** Either of these policies will increase demand for ocean transportation and decrease demand for air transportation, thus reallocating transportation towards more carbon-efficient mode of transportation. This result follows directly from equations (11) and (13).

# 4 Estimating and Calibrating Model Parameters

In this section, we structurally estimate and calibrate model parameters which we will then use to evaluate the effects of IMO2023. We will restrict our attention to imports by the U.S. There are two reasons for this choice. First, detailed data on the import prices and freight rates by the mode of transportation is rather limited for other countries. Second, the U.S. ideally fits our model with only two modes of transportation: air and ocean, as there are only two countries, Canada and Mexico, which use land transportation for exporting to the U.S.

## 4.1 Data Sources

For the demand estimation, we use monthly U.S. Census import data from 2013-2019. These data are freight-mode specific (e.g., vessel containerized, vessel non-containerized, air), are reported at the HS6 level of dis-aggregation, and specify the U.S. Customs District of entry and the exporting country. We limit our attention to two freight import modes: vessel containerized and air. Within these data, we observe freight charges (USD), import values (USD), and import weight (kg).

Our first aggregation step is to build up mode-route-time-HS6 values for freight charges, import values, and import weight from these Census data. Next, we obtain annual-country-HS6 level U.S. import tariff data from the WITS. We use these tariff data alongside our mode-product import data to compute mode-route-time tariffs (e.g., $\underline{\tau}_{ijt}$ or $\overline{\tau}_{ijt}$ ) using HS6 import mode-route-time-HS6 value shares as part of this weighted average. Finally, we sum over HS6 product codes for our freight charges, import values, and import weight to arrive at the import *mode-route-time* data we use for estimation. Moreover, we aggregate our import data to quarterly time frequency. We define factory prices ($p_{ijt}$) as the ratio of import values to import weight, unit freight charges ($f_{ijt}$) as the ratio of freight charges to import weight, and ad-valorem freight costs ($f_{ijt}/p_{ijt}$) as the ratio of unit freight charges to factory prices.

## 4.2 Estimating Demand Parameters in the Benchmark Model

We start by estimating the key parameters of our model by using our theoretical relative demand equation (11). We log-linearize it: $\ln\left(\frac{q_{ijt}}{\overline{q}_{ijt}}\right) = \varepsilon\ln(\nu_j) + \varepsilon\ln(\nu_{it}) - \varepsilon\ln\left(\frac{\underline{p}_{ijt}}{\overline{p}_{ijt}}\right) - \varepsilon\ln\left(\frac{\underline{\tau}_{ijt}+\underline{f}_{jt}/\underline{p}_{ijt}}{\overline{\tau}_{ijt}+\overline{f}_{ijt}/\overline{p}_{ijt}}\right)$, and set our estimating equation as following:

$$\ln\left(\frac{\underline{q}_{ijt}}{\overline{q}_{ijt}}\right) = \theta_j + \theta_{it} + \beta_1\ln\left(\frac{\underline{p}_{ijt}}{\overline{p}_{ijt}}\right) + \beta_2\ln\left(\frac{\underline{\tau}_{ijt}+\underline{f}_{ijt}/\underline{p}_{ijt}}{\overline{\tau}_{ijt}+\overline{f}_{ijt}/\overline{p}_{ijt}}\right) + \mu_{ijt}, \tag{14}$$

where $\theta_j$ and $\theta_{it}$ are exporter and district-year fixed effects, respectively; and $\mu_{ijt}$ is the error term. Equation (14) has strong similarities with the estimation equation (9) of Hummels and Schaur (2013).[24] In addition to addressing multiple potential concerns with this specification,[25] they provided a detailed and convincing argument for why to identify the elasticity $\varepsilon$ from the relative trade cost coefficient $\beta_2$ rather than from the relative price coefficient $\beta_1$.[26] Following their approach, we identify

[24] Their LHS is in terms of relative revenues rather than relative quantities. When we re-ran our equation (14) with the relative revenues as the LHS. The only change is in the relative price coefficient, $\beta_1$ : its magnitude has increased by 1.

[25] E.g., trade costs endogeneity, unobserved (quality) terms correlated with prices, etc.

[26] As per the argument presented by Hummels and Schaur (2013), goods transported by air and ocean are likely to have varying degrees of bulkiness per kilogram, with goods transported by ocean tending to be bulkier. Consequently, the differences in unit values might exaggerate the actual price differences. This could result in a bias towards zero for the coefficient on unit values, even when the model perfectly controls for variations in unobserved quality.

$\widehat{\varepsilon} = -\widehat{\beta}_2$. Next, we will recover $\nu_j$ by $\widehat{\nu}_j = \exp\left(\widehat{\theta}_j/(-\widehat{\beta}_2)\right)$ and $\nu_{it}$ by $\widehat{\nu}_{it} = \exp\left(\widehat{\theta}_{it}/(-\widehat{\beta}_2)\right)$. Following Hummels and Skiba (2004) and Bellemare et al. (2017), we instrument for $\ln \frac{\underline{p}_{ijt}}{\overline{p}_{ijt}}$ and $\ln(\frac{\underline{\tau}_{ijt}+\underline{f}_{ijt}/\underline{p}_{ijt}}{\overline{\tau}_{ijt}+\overline{f}_{ijt}/\overline{p}_{ijt}})$ with their one-quartered lags.

Table 2: Equation (14) Results

| | (1:OLS) | (2:IV) |
|---|---|---|
| $\ln\left(\underline{p}_{ijt}/\overline{p}_{ijt}\right)$ | $-0.806^{***}$ | $-0.823^{***}$ |
| | (0.026) | (0.057) |
| $\ln\left(\frac{\underline{\tau}_{ijt}+\underline{f}_{ijt}/\underline{p}_{ijt}}{\overline{\tau}_{ijt}+\overline{f}_{ijt}/\overline{p}_{ijt}}\right), (-\widehat{\varepsilon})$ | $-7.298^{***}$ | $-10.299^{***}$ |
| | (0.561) | (2.181) |
| Num. obs. | 22,432 | 18,228 |
| Num. groups: $\theta_j$ | 214 | 210 |
| Num. groups: $\theta_{it}$ | 262 | 210 |
| $R^2$ (full model) | 0.583 | 0.588 |
| $R^2$ (proj model) | 0.230 | 0.209 |

$^{***}p < 0.01$; $^{**}p < 0.05$; $^{*}p < 0.1$

Table 2 reports estimation results. The elasticity of substitution $\hat{\varepsilon}$ is 7.3 for OLS and 10.3 for IV, respectively. For comparison, Hummels and Schaur (2013)'s equivalent estimates for $-\widehat{\varepsilon}$ are qualitatively similar to ours with a range between 2.7 and 6.5.[27] Both estimates are statistically significant at 1% level. The estimates of the fixed effect $\theta_j$ and $\theta_{it}$ allow us to get the estimates of $\widehat{\nu}$'s (see their distribution in Online Appendix Figure A6.)

We use estimates of $\widehat{\nu}_j\widehat{\nu}_{it}$ and the log-linearized equation (8) to estimate $\beta_k$. Towards this goal, we utilize annualized 2012-2019 BlueWater data on the average number of days in transit for every route $ij$, which we label as $TIME_{ijt}$. We regress $\widehat{\nu}_j\widehat{\nu}_{it}$ on $TIME_{ijt}$ and district-year fixed effects using OLS:

$$\ln(\widehat{\nu}_j\widehat{\nu}_{it}) = \beta_k \ln TIME_{ijt} + \ln(\vartheta_{jt}) + \epsilon_{ijt}.$$

[27] As mentioned in the theoretical section, our elasticities are expected to be of greater magnitudes because in addition to within-product substitution of transportation, we also consider across product changes in imports. The differences in our empirical approaches can be summarized as following. Hummels and Schaur (2013) used annual data from US Imports of Merchandise that: span 1991-2005; aggregate by East/West coast; and reflect HS6 level product detail. By contrast, we use product-aggregated, quarterly data from 2013-2019 at the custom district (rather than coastal) level. These differences likely contribute to the rather modest differences between elasticity estimates.

Table 3 presents the results. The two columns correspond to the two sets of results from Table 2 used to obtain $\ln(\widehat{\nu}_j\widehat{\nu}_{it})$. An intuitive interpretation of this estimate is that for a given U.S. region $i$, a 10% increase in travel time is associated with a $\beta_k \times 10\%$ change in the preference parameters for non-perishables. In practice, this marginal effect translates into a 0.3 to 0.41% decrease.

Table 3: Preferences for timely delivery

| | (1:OLS) | (2:IV) |
|---|---|---|
| $\ln TIME_{ijt}, (\widehat{\beta}_k)$ | $-0.041^{***}$ | $-0.030^{***}$ |
| | (0.011) | (0.009) |
| Num. obs. | 3806 | 3366 |
| Num. groups: $\ln(\vartheta_{jt})$ | 608 | 534 |
| $R^2$ | 0.370 | 0.368 |

$^{***}p < 0.01$; $^{**}p < 0.05$; $^{*}p < 0.1$

Finally, once we obtain estimates for $\widehat{\varepsilon}$ and $\widehat{\nu}_j\widehat{\nu}_{it}$, we invert equation (12) to express marginal costs as function of observables and estimated parameters.[28]

# 5 Short-Run Effects of IMO2023

In this section, we predict the short-run effects of IMO2023 on carbon emissions from maritime and air transportation of imported goods to the United States. For clarity of exposition, we will use blue color for the exogenously given shocks and red color for solution objects. In Section 2, we demonstrated that IMO2023 will decrease the capacity of containerized fleet and calculated these decreases as proportions $\underline{\omega}_{ij} \equiv \frac{q_{ijT}}{q_{ijt}}$ for each route $ij$ where $t$ and $T$ denote pre- and post-IMO2023 years, respectively. From our import demand functions, eq. (11), we derive the proportional changes in quantities as:

$$\underline{\omega}_{ij} \equiv \underline{q}_{ijT}/\underline{q}_{ijt} = \omega_{K_i}^{-\varepsilon}\underline{\omega}_P^{-\varepsilon}\omega_\nu^{\varepsilon} \qquad \overline{\omega}_{ij} \equiv \overline{q}_{ijT}/\overline{q}_{ijt} = \omega_{K_i}^{-\varepsilon}\overline{\omega}_P^{-\varepsilon}, \tag{15}$$

[28] Please see Online Appendix Section A.8 for a full treatment of how we calibrate marginal costs.

where $\omega_{K_i} \equiv \frac{K_{iT}}{K_{it}}$; $\underline{\omega}_P \equiv \frac{\underline{p}_{ijt}\underline{\tau}_{ijt}+\underline{f}_{ijT}}{\underline{p}_{ijt}\underline{\tau}_{ij}+\underline{f}_{ijt}}$ and $\overline{\omega}_P \equiv \frac{\overline{p}_{ijt}\overline{\tau}_{ijt}+\overline{f}_{ijT}}{\overline{p}_{ijt}\overline{\tau}_{ijt}+\overline{f}_{ijt}}$ are the changes in the delivered prices by ocean and air, respectively;[29] and $\omega_\nu \equiv \frac{(\nu_i\nu_j)_T}{(\nu_i\nu_j)_t}$ is the change in the preferences parameter due to slow-steaming, which we calculate using our estimates of $\beta_k$ as following:

$$\omega_\nu = \left(\frac{TIME_{ijT}}{TIME_{ijt}}\right)^{\beta_k} = \left(\frac{1/\underline{\omega}_{ij}TIME_{ijt}}{TIME_{ijt}}\right)^{\beta_k} = 1/\underline{\omega}_{ij}{}^{\beta_k}. \tag{16}$$

Using these notations, the utility function for the first post-IMO2023 year $T$ can be written as a function of pre-IMO2023 variables in year $t$, assuming constant consumption of the numeraire good:

$$U_{iT} = q_{0,it}^{1-\mu}\left[\sum_j\left(\omega_\nu\nu_{it}\nu_j(\underline{\omega}_{ij}\underline{q}_{ijt})^{\frac{\varepsilon-1}{\varepsilon}} + \overline{\omega}_{ij}\overline{q}_{ijt}^{\frac{\varepsilon-1}{\varepsilon}}\right)\right]^{\mu\frac{\varepsilon}{\varepsilon-1}}.$$

Given the substantial excess capacity previously identified in the air-shipping industry, it's unclear if an expected rise in ocean freight rates would correspondingly boost air freight rates. To further investigate, we analyze US imports data from 2013 to 2019 in Online Appendix A.6. We use these Census data—organized on a monthly-year-(HS6 product)-(customs district)-(exporting country) basis—to estimate the relationship between these two freight rates. We find the ad-valorem (iceberg) vessel-freight-rate elasticity of the iceberg air-freight-rate to be 0.021, an economically insignificant figure. For instance, a 5% increase in the average iceberg ocean freight rate in 2019 (from 1.048 to 1.10) would result in a mere 0.011% rise in the average iceberg air rate (from 1.123 to 1.1242). In other words, doubling the vessel freight rate would only lead to a 1% increase in air freight rates.[30]

Nevertheless, as a part of the sensitivity analysis, we aim to show our qualitative results stand even if air freight rates were much more sensitive to ocean freight rate. Towards this goal, we first denote the proportional change in ocean freight rates as $\underline{\alpha}_{ij} \equiv \underline{f}_{ijT}/\underline{f}_{ijt}$, and then the proportional

[29] In our analysis, including our later analysis of the long-run impacts of IMO2023, factory prices of goods and tariffs remain constant and thus changes in delivered prices can be solely attributed to changes in freight rates. This assumption allows us to isolate the effects of slower speeds and changes in capacity on the demand for transportation services.

[30] In this example, the normalized by price vessel freight rate would increase from 0.0.48 to 0.1 (roughly doubling), while the normalized by price air freight rate would increase from 0.123 to 0.1242 (a 1% increase).

increase in ad-valorem air freight rates as:

$$\overline{\alpha}_{ij} \equiv \overline{f}_{ijT}/\overline{f}_{ijt} = (1 + \zeta(\underline{\alpha}_j - 1)) \qquad \zeta \geq 0. \tag{17}$$

For our quantitative analysis, we consider two scenarios: (i) ocean freight rates have no effect on air freight rates with $\zeta = 0$, given their estimated negligible sensitivity; and (ii) ocean freight rates have a positive effect on air freight rates with $\zeta = \frac{1}{6}$. This $\zeta$ value implies an air freight rate sensitivity to ocean freight rates 17 times greater than our estimation, an exaggerated figure used to demonstrate our results' robustness to a very high sensitivity.

Using the structural parameters previously identified in the model, we will solve for $\underline{\alpha}_{ij}$, $\overline{\alpha}_{ij}$, $\omega_{K_i}$, and $\overline{\omega}_{ij}$. Our Identification Algorithm I relies on the fixed point argument and proceeds in the following steps.[31]

**Identification Algorithm I**

(Step 1) Use equation (6) to calculate change in ocean capacity $\underline{\omega}_{ij}$ for a given change in speed $\rho_{ij} = s_{ijT}/s_{ijt}$.

(Step 2) For each U.S. Customs District $i$, solve for $\omega_{K_i}$ that minimizes $g(\omega_{K_i}) = (\frac{K_{iT}(\omega_{K_i};\underline{\omega}_{ij})}{K_{it}} - \omega_{K_i})^2$ (since we are solving here per $i$, $\omega_{K_i}$ is singleton valued). Proceed in five steps.

(a) Calculate changes in delivered containerized price by manipulating eq. (15) such that: $\underline{\omega}_p(\omega_{K_i}) = \underline{\omega}_{ij}{}^{-\frac{1}{\varepsilon}} \times \omega_{K_i}{}^{-1} \times \omega_v(\underline{\omega}_{ij})$.

(b) Use the definition of $\underline{\omega}_P$ from eq. (15) to calculate changes in ocean freight rates: $\underline{\omega}_f(\omega_{K_i}) = \frac{\underline{\omega}_p(\omega_{K_i})(\underline{f}_{ijt} + \underline{p}_{ijt}\underline{\tau}_{ijt}) - \underline{p}_{ijt}\underline{\tau}_{ijt}}{\underline{f}_{ijt}}$.

(c) Calculate changes in air freight rates via: $\overline{\omega}_f = \zeta(\underline{\omega}_f - 1) + 1$.

(d) Determine air capacity changes:[32] $\overline{\omega}_{ij} = \omega_{K_i}{}^{-\varepsilon}\overline{\omega}_p^{-\varepsilon}$, where $\overline{\omega}_p = \frac{\overline{\omega}_f\overline{f}_{ijt} + \overline{p}_{ijt}\overline{\tau}_{ijt}}{\overline{f}_{ijt} + \overline{p}_{ijt}\overline{\tau}_{ijt}}$.

(e) Calculate $\omega_{K_i} = \frac{\sum_{j=1}^{n} \omega_v \nu_{ij} [\underline{\omega}_{ij}\underline{q}_{ij}]^{\frac{\varepsilon-1}{\varepsilon}} + [\overline{\omega}_{ij}\overline{q}_{ij}]^{\frac{\varepsilon-1}{\varepsilon}}}{\sum_{j=1}^{n} \nu_{ij}\overline{q}_{ij}^{\frac{\varepsilon-1}{\varepsilon}} + \overline{q}_{ij}^{\frac{\varepsilon-1}{\varepsilon}}}$

[31] See Online Appendix A.10 for existence and uniqueness proofs for **Identification Algorithm I**.

[32] If modeling a no inter-modal substitution scenario, set $\overline{\omega}_{ij} = 1$.

We use a standard Newton-Raphson method to find $\omega^*_{K_i}$ that minimizes $g$ :

$$\omega^*_{K_i} \in \text{argmin}\, g(\omega_{K_i}; \underline{\omega}_{ij}) \equiv \left( \frac{\sum_{j=1}^{n} \omega_\nu(\underline{\omega}_{ij}) \nu_{ij} [\underline{\omega}_{ij} \underline{q}_{ij}]^{\frac{\varepsilon-1}{\varepsilon}} + [\overline{\omega}_{ij}(\overline{\omega}_{K_{it}}) \overline{q}_{ij}]^{\frac{\varepsilon-1}{\varepsilon}}}{\sum_{j=1}^{n} \nu_{ij} \underline{q}_{ij}^{\frac{\varepsilon-1}{\varepsilon}} + \overline{q}_{ij}^{\frac{\varepsilon-1}{\varepsilon}}} - \omega_{K_i} \right)^2$$

(Step 3) Once we have $\omega^*_{K_{it}}$ for each U.S. Customs District, we recompute changes to containerized and air freight rates as well as changes to air capacity.

**Calculating Carbon Emissions.** We use the methodology outlined in Shapiro (2016) to calculate the carbon emissions associated with each mode of transportation. Specifically, we assume an emissions rate of 1439.49 g $CO_2$ per ton-mile for air transportation on each route.[33] Route air distance is calculated as the great circle distance between the U.S. Customs District $i$ and the country $j$.[34] For maritime transportation , we use route specific $CO_2$ emissions per ton-mile, calculated based on our shipping data. We estimate ocean mileage based on BlueWater's rotation schedule.

To calculate the total emissions levels before and after IMO2023, we combine the change in container capacity $(\underline{\omega}_{ij})$ and the change in air capacity $(\overline{\omega}_{ij})$ with 2019 trade volumes in tons transported by each respective mode. This approach enables us to incorporate mode-specific carbon efficiency (g $CO_2$ per ton-mile), mode-specific mileage (miles), and mode-specific volume (tons) in our analysis.

## 5.1 Results and Discussion

We present results for six scenarios: with and without adjustments in $\nu$ (preference multiplier for maritime imports) and with three types of adjustment of air transportation to IMO2023. The results are shown in Table 4.[35] In all six scenarios, ocean capacity decreases by 5.9%, ocean emissions decrease by 16.5%, and ocean freight rates increase by over 100%.[36] Moreover, each IMO2023 sce-

[33] This figure is derived from the International Air Transport Association (IATA)'s 2009 fuel economy of air freight transport of 985.97 g $CO_2$/ton-km, as reported by Shapiro (2016). We convert this figure to ton-miles. Further details can be found in Shapiro's Online Appendix A.4.

[34] We obtain country $j$ coordinates from CEPII's database.

[35] Please see our Online Appendix Table A11 for our IMO2023 predictions using our IV estimates of $\varepsilon$ and all other parameters.

[36] As rough check of freight rate change order of magnitude, consider the simplest version of our model where there is no inter-modal substitution and preferences for timely delivery remain unchanged. Assuming a uniform 6% reduction in capacity, delivered prices must increase by roughly 6.5%. Since freight rates are roughly 5% of delivered price, this implies freight rates must rise by $1.06 = (\alpha f + p\tau)/(f + p\tau) = (\alpha f + (1 - 0.05)f)/(f + (1 - 0.05)f) \implies \alpha = 112\%$. Moreover, ocean freight rates are historically capable even more dramatic swings; according to data from FBX Freightos,

nario has a materially adverse effect (between $4.6 and $7.1 billion) on U.S. consumer surplus, which dwarfs any welfare changes from net emissions.[37]

For welfare calculations, we adopt a social marginal cost of $CO_2$ equal to 40 USD per ton. However, if we assume a higher marginal cost, as recommended by EPA (2022) with base year figures ranging from 120 to 340 USD per ton as a function of higher to lower discount rates, the welfare estimate changes only in magnitude and not in direction. In fact, higher $CO_2$ marginal cost estimates would exacerbate the welfare losses resulting from increased net emissions in all scenarios accounting for inter-modal substitution. Specifically, for scenarios (1) and (4) in Table 4, the welfare-neutral value of $CO_2$ abatement, defined as the marginal social cost of carbon that exactly offsets consumer welfare loss from less trade at higher prices, would range between $\frac{6.8 \text{ bln USD}}{2.4 \text{ mln } CO_2 \text{ tons}} = 2,833 \frac{\text{USD}}{\text{ton}}$ and $\frac{7.0 \text{ bln USD}}{2.2 \text{ mln } CO_2 \text{ tons}} = 3,182 \frac{\text{USD}}{\text{ton}}$. These welfare-neutral values are roughly one order of magnitude larger than even the highest estimates of carbon's social cost.

Table 4: Short Run IMO2023 Results (OLS $\varepsilon = 7.3$)

| **Scenario** | (1) | (2) | (3) | (4) | (5) | (6) |
|---|---|---|---|---|---|---|
| Adjust $\nu$? | | No | | | Yes | |
| Air Pass Through ($\zeta$) | 0 | 1/6 | 0 | 0 | 1/6 | 0 |
| %Δ Container Capacity | -5.9 | -5.9 | -5.9 | -5.9 | -5.9 | -5.9 |
| %Δ Air Capacity | 0.009 | 24.5 | 29.5 | 0.0 | 26.0 | 31.0 |
| %Δ Container Freight Rates | 144.8 | 121.6 | 115.6 | 145.1 | 120.4 | 114.4 |
| %Δ Air Freight Rates | 0.0 | 20.3 | 0.0 | 0.0 | 20.1 | 0.0 |
| %Δ Container Emissions | -16.5 | -16.5 | -16.5 | -16.5 | -16.5 | -16.5 |
| %Δ Air Emissions | 0.0 | 24.9 | 29.4 | 0.0 | 26.4 | 30.9 |
| Net %Δ $CO_2$ | -4.6 | 13.3 | 16.5 | -4.6 | 14.4 | 17.6 |
| Net Δ $CO_2$ (mln ton) | -2.4 | 7.0 | 8.7 | -2.4 | 7.5 | 9.2 |
| Net Δ Welfare (mln USD) | -6717 | -5194 | -4946 | -7022 | -5408 | -5166 |
| Net Δ $CO_2$ Welfare (mln USD) | 97 | -278 | -346 | 97 | -301 | -369 |
| Net Δ Consumer Surplus (mln USD) | -6814 | -4915 | -4600 | -7119 | -5107 | -4797 |
| Welfare Neutral Carbon Price (USD/ton) | 2833 | NA | NA | 3182 | NA | NA |

Asia-US West Coast freight rates increased by approximately 230% from April to July 2021.

[37] Please see Online Appendix A.5 for the derivation of consumer surplus and welfare changes.

Scenarios (1) and (4) are the most restrictive scenarios considered, as they preclude any possibility of substitution into air transportation. Consequently, in these scenarios, IMO2023 has no effect on the net emissions of air transportation. These scenarios are the only ones in which the IMO2023 leads to a reduction in combined emissions from both air and ocean transportation (-4.6%). In all other scenarios where substitution is allowed, net combined emissions increase.

There are two primary reasons for the increase in emissions. Firstly, lower cargo capacity and higher air freight rates have led to a significant increase of 25 to 31 percent in the quantity of goods being transported by air. Since air shipping is two orders of magnitude more carbon-intensive than ocean transportation, the combined net emissions increase by between 13% and 16%, as demonstrated in columns (2) and (3) of Table 4. Secondly, the slower delivery of goods imported by vessels reduces their utility for consumers, leading to a greater shift towards air-shipped imports. This effect further increases emissions. When taken into account, the combined net emissions increase by between 14% and 18%, as demonstrated in columns (5) and (6) of Table 4. These findings highlight the need for a more comprehensive approach to reducing carbon emissions in the shipping industry, one that considers the inter-modal substitution effects and the broader economic impacts.

Our findings raise the question of why the IMO would propose a reform that could potentially increase combined carbon emissions from both ocean and air transportation while also lowering consumer surplus. The answer is multifaceted. Firstly, the IMO is mandated to address the specific objective of reducing emissions from ocean transportation, and IMO2023 achieves this by incentivizing ocean carriers to avoid receiving "D" and "E" ratings from their shippers. Secondly, the IMO can be seen as a self-regulating cartel, composed of representatives from carriers, shipbuilders, and shipping-related financiers. In this sense, IMO2023 serves to satisfy other IMO-specific objectives, such as (i) boosting carriers' short-term profits and (ii) enhancing the demand for new vessels in the medium and long term.

Indeed, as demonstrated in our comprehensive scenarios in columns (5) and (6), the implementation of IMO2023 is projected to lead to more than doubling of of carriers' revenue. This is computed as a 114 to 120% increase in container freight rate minus a 6% reduction in quantity from columns (5)

and (6). Furthermore, shipbuilders can anticipate an increase in orders to restore shipping capacity, while bankers can expect a higher demand for shipbuilding financing. In summary, in addition to reducing carbon emissions in ocean transportation, IMO2023 also creates additional profit opportunities for all participants in the industry. This situation is similar to a hypothetical scenario in which OPEC reduces oil supply, citing environmental concerns to justify their actions.

## 5.2 Forced speed up in the short run?

Our inter-modal analysis of trade and emissions is based on the tight, short-run relationship between vessel speed and capacity. A reduction in speed decreases the number of round trips a vessel can make, effectively decreasing short-run capacity. This suggests that a modest increase in speed can expand short-run capacity, given that ocean containerized carriers operate at close to full capacity. This expansion can lead to lower ocean freight rates and substitution from air to maritime transportation. Faster delivery of vessel-shipped goods will further increase this substitution.

Forcing vessels to speed up may have an ambiguous impact on net-$CO_2$ emissions. Substituting away from air to maritime transportation leads to lower emissions per unit of substituted imports. However, linear increases in speed translate into quadratic increases in fuel consumption per trip. Still, despite the decreased fuel efficiency in maritime transportation, a sufficient inter-modal substitution from air to ocean transportation can lead to lower net emissions.

As a self-contained thought experiment, we apply our **Identification Algorithm I** to a 1% increase in speed. With inter-modal substitution, net emissions fall by 1.8% to 2.3%, and welfare increases by $830 - 910$ million USD. We report all short-run counterfactual outcomes in a manner similar to Table 4 in our Online Appendix A.11.[38] It is worth noting that these results are not applicable to the long-run analysis. The relationship between speed and additional capacity in the long run is looser due to potential entry and exit of vessels. If anything, long-run speed increases for ocean routes without different technology could lead to net-emission increases. In Section 6, we provide a long-run analysis of IMO2023, and in Section 7, we discuss alternative policies and the potential for

[38] Please see Online Appendix Table A15 for our OLS $\varepsilon$ based results and Table A16 for our IV $\varepsilon$ based results.

technologically driven welfare-improving outcomes.

# 6 Long-Run Effects of IMO2023

In the long-run, carriers' ability to put new containerships into operation will eventually ease slow-steaming's negative impact on ocean capacity. Nonetheless, longer delivery times will still adversely affect demand for ocean transportation demand and contribute to carbon leakage into air shipping. In addition, slow-steaming will reduce bunker costs but increase non-fuel costs per ton-mile.[39] As a result, the net impact of IMO2023 on long-run marginal costs, freight rates, and quantities depends on the parameters of the model. To evaluate these effects, we proceed in a similar fashion to our short-run analysis. Specifically, we start by using equation (11), to derive long-run proportional changes in quantities compared to the pre-refrom level indexed by $t$:

$$\underline{\omega}_{ij}^{\text{LR}} \equiv \underline{q}_{ij}^{LR}/\underline{q}_{ijt} = (\omega_{K_i}^{LR})^{-\varepsilon}(\underline{\omega}_{P}^{LR})^{-\varepsilon}(\omega_{\nu}^{LR})^{\varepsilon} \qquad \overline{\omega}_{ij}^{\text{LR}} \equiv \overline{q}_{ij}^{LR}/\overline{q}_{ijt} = (\omega_{K_i}^{LR})^{-\varepsilon}(\overline{\omega}_{P}^{LR})^{-\varepsilon}, \tag{18}$$

where superscript $LR$ denotes long-run objects; $\omega_{K_i}^{LR} \equiv \frac{K_i^{LR}}{K_{it}}$; $\underline{\omega}_{P}^{LR} \equiv \frac{\underline{p}_{ijt}\underline{\tau}_{ijt}+\underline{f}_{ijt}^{LR}}{\underline{p}_{ijt}\underline{\tau}_{ijt}+\underline{f}_{ijt}}$ and $\overline{\omega}_{P}^{LR} \equiv \frac{\overline{p}_{ij}\overline{\tau}_{ijt}+\overline{f}_{ij}^{LR}}{\overline{p}_{ijt}\overline{\tau}_{ijt}+\overline{f}_{ijt}}$ are the changes in the delivered prices by ocean and air, respectively; and $\omega_{\nu}^{LR} \equiv \frac{(\nu_i\nu_j)^{LR}}{(\nu_i\nu_j)_t}$ is the change in the preferences parameter due to the slow-steaming. Note that $\omega_{\nu}^{LR}$ is determined by changes in vessel speed, which remain the same as in the short run, as well as changes in port traffic, which differ from the short-run. Thus, the value of $\omega_{\nu}^{LR}$ will be somewhat different from the short-run $\omega_{\nu}$.

The values of $\omega_{P}^{LR}$ depend on the cost structure in containerized shipping and the naval engineering relationship between speed and fuel consumption. For the sake of clarity, we provide a detailed derivation of $\omega_{P}^{LR}$ in Online Appendix A.7.

That leaves us with three components, $\underline{\omega}_{ij}^{\text{LR}}$, $\overline{\omega}_{ij}^{\text{LR}}$, and $\omega_{K_i}^{LR}(\underline{\omega}_{ij}^{\text{LR}}, \overline{\omega}_{ij}^{\text{LR}})$. To obtain these components, we solve a system of non-linear equations using numerical optimization techniques. The detailed derivations of these equations are presented in Online Appendix A.7. We also present a de-

[39] Non-fuel costs include labor costs, financing costs, etc., which accumulate on a daily basis and are thus proportional to the time it takes to deliver cargo.

composition of $\underline{\omega}_{ij}^{LR}$ in terms of changes in round-trip delivery ($\omega_n$) and changes in new ship capacity ($\omega_B$) since by definition $\underline{\omega}_{ij}^{LR} = \omega_n \omega_B$. Our long-run results are shown below in Table 5.[40]

Table 5: Long-Run IMO Scenarios (OLS $\varepsilon = 7.3$)
*Note*: Two long-run outcomes are presented below. "2023 Standards" consider long-run outcomes with IMO 2023 standards, which are 95% of the IMO's 2019 reference line. Likewise, "2026 Standards" consider long-run outcomes which are 89% of the IMO's 2019 reference line. We assume that fuel costs make up 30% of ship's marginal costs and that $\nu$ adjusts to changes in speed.

| **Scenario** | (1) | (2) | (3) | (4) |
|---|---|---|---|---|
| Standard | 2023 | | 2026 | |
| Air Pass Through ($\zeta$) | 0 | 1/6 | 0 | 1/6 |
| %Δ Container Capacity | 0.00 | 0.00 | -0.05 | -0.05 |
| %Δ Number of Vessels | 5.56 | 5.56 | 10.56 | 10.56 |
| %Δ Round-Trips per Vessel | -5.26 | -5.26 | -9.60 | -9.60 |
| %Δ Air Capacity | 0.28 | 0.25 | 0.49 | 0.43 |
| %Δ Container Freight Rates | 0.42 | 0.42 | 1.15 | 1.15 |
| %Δ Air Freight Rates | 0.00 | 0.06 | 0.00 | 0.19 |
| %Δ Container Emissions | -11.38 | -11.37 | -18.05 | -18.05 |
| %Δ Air Emissions | 0.24 | 0.22 | 0.45 | 0.39 |
| Net %Δ Emissions | -3.02 | -3.04 | -4.75 | -4.79 |
| Net Δ Emissions (mln tons) | -1.53 | -1.54 | -2.41 | -2.43 |
| Net Δ Welfare (mln USD) | -234 | -235 | -466 | -469 |
| Net Δ $CO_2$ Welfare (mln USD) | 61 | 62 | 96 | 97 |
| Net Δ Consumer Surplus (mln USD) | -295 | -297 | -563 | -566 |
| Welfare Neutral Carbon Price (USD/ton) | 153 | 153 | 194 | 193 |

As mentioned earlier, construction of ocean vessels typically takes around three years to complete (Kalouptsidi, 2014; Chokshi, 2020), and the International Maritime Organization (IMO) mandates annual increases in environmental standards beyond 2023. To account for this three-year lag, we model two different sets of standards: 2023 Standards and 2026 Standards.[41] This approach helps us better understand how stricter standards over time may impact the outcomes. Similar to the short-run analysis, Table 5 also presents the outcomes with and without adjustments to air freight rates in

[40] Please see Online Appendix Table A12 for our IMO long-run predictions using our IV estimates of $\varepsilon$ and all other parameters.

[41] Please refer to IMO Resolution MEPC.338(76) *Table 1: Reduction factor (Z%) for the CII relative to the 2019 reference line* for a complete standard schedule.

response to changes in ocean freight rates.

A summary of our findings. First, in equilibrium with free entry, capacity will practically revert to its pre-reform level. To achieve this goal, the industry will require 5.6% more vessels under the 2023 Standards and 10.6% more vessels under the 2026 Standards. Even if a 10.6% increase in vessels is possible within 3-5 years, the projected decrease in annual $CO_2$ is not significant: $(-3\%)$ for the 2023 Standards and $(-4.8\%)$ for the 2026 Standards. While efficiency gains in ocean transportation are significant, up to 18%, these gains will be largely offset by the continuing leakage to air shipping due to pronounced (up to 10% slower) slow-steaming in ocean transportation. These projections put a big question mark on the policy outcome, even in the long-run. Especially because carbon emissions are accumulative over time, and with relatively low reductions in $CO_2$ in the long-run, it will take a decade just to offset the initial short-run annual increases in $CO_2$ (assuming that short run will last for at least 3 years). Second, in the long-run, the IMO 2023's effect on consumer and total surpluses will continue to be negative and substantial. To justify the IMO 2023, the negative price externality from a ton of $CO_2$ should have been \$153 under the 2023 Standards and \$193 under the 2026 Standards.

As demonstrated by our findings, agencies with narrow specializations tend to prioritize agency-specific objectives when regulating activities. This is evident within the various United Nations entities responsible for developing environmental policies for different sectors such as ocean transportation, air travel, production, and more.[42] To address the issue of inter-sectoral and other types of environmental spillovers, the United Nations could consider restructuring its organizational framework or assigning broader mandates to specialized agencies. In the following section, we present examples of well-designed policies that can serve as models.

[42]Examples of specialized agencies within the United Nations include the International Maritime Organization, the International Civil Aviation Organization, and the United Nations Environment Programme, among others.

# 7 Welfare Improving Counterfactuals

## 7.1 Subsidies and Taxes

In this section, we evaluate an alternative policy of regulating air and ocean transportation emissions by means of taxes or subsidies. We explore taxes and subsidies rather than quantitative restrictions because these are widely used policy tools applied to environmental regulation in many contexts.[43] The proposed policies are designed to decrease the most carbon-intensive mode of transportation—air transportation. Specifically, we propose two policies: (i) subsidizing goods delivered by ocean shipping and (ii) taxing goods delivered by air shipping. For ease of comparison, we set the targeted carbon reduction for both policies to be at the level of the long-run IMO2023 reduction under 2023 Standards, which is 3.02% per year.

We set both subsidies and taxes to be ad-valorem, with the following resulting function form of the final prices: $(\underline{p}_{ij}\underline{\tau}_{ij}\underline{\psi} + \underline{f}_{ij})$ for ocean subsidy $\underline{\psi}$ and $(\overline{p}_{ij}\overline{\tau}_{ij}\psi + \overline{f}_{ij})$ for air tax $\overline{\psi}$, where $\underline{\psi} < 1$ and $\overline{\psi} > 1$. Given this setup, we applied the same procedure for deriving the long-run equilibrium as in the previous section. For brevity, we present only the scenarios in which there is variation in preferences for timely delivery $(\nu_j\nu_{it})$. This leaves us with two scenarios per policy: (i) without changes in air freight rates $(\zeta = 0)$ and (ii) with changes in air freight rates $(\zeta = 1/6)$. Based on these scenarios, we have derived that the required ocean subsidy amount is 0.787% for (i) and 0.791% for (ii), whereas the required air tax is 0.655% for (i) and 0.658% for (ii).[44] Using these values, we model policy impacts on air and ocean transportation in terms of both environmental effects and resulting welfare effects.

The results are presented in Table 6.[45] The results illustrate that the suggested alternative policies provide significantly better welfare results, given the same net reduction in carbon emissions. Specif-

[43] In the context of international transportation, one of the largest containerized ocean carriers, Maersk, voiced its discontent with IMO2023 and proposed an alternative in the form of a carbon tax of 150 dollars per ton of $CO_2$ (Wittels, 2021).

[44] The corresponding values of $\underline{\psi}$ are 0.99213 for (i) and 0.99209 for (ii); the corresponding values of $\overline{\psi}$ are 1.00655 for (i) and 1.00658 for (ii).

[45] Please see Online Appendix Table A13 for our IV parameter long-run results.

Table 6: Long-Run Alternative Policies (OLS $\varepsilon = 7.3$)

*Note*: All scenario results assume that $\nu$ changes with respect to changes in round-trip time. We calculate subsidy(tax) rates by solving for $\underline{\psi}$ ($\overline{\psi}$) that delivers the same long-run change in net emissions as the appropriate IMO2023 scenario; we use our long-run code to solve for equilibrium given $\underline{\psi} p_{ijt} \tau_{ijt}$ ($\overline{\psi} p_{ijt} \overline{\tau}_{ijt}$).

When $\zeta = 0$, container subsidy rate is 0.787% (air tax rate is 0.655%). When $\zeta = 1/6$, container subsidy rate is 0.791% (air tax rate is 0.658%).

| **Scenario** | IMO2023 | | Container Subsidy | | Air Tax | |
|---|---|---|---|---|---|---|
| Air Pass Through ($\zeta$) | 0 | 1/6 | 0 | 1/6 | 0 | 1/6 |
| %Δ Container Capacity | 0.00 | 0.00 | 0.97 | 0.98 | 0.18 | 0.18 |
| %Δ Container round-trips | -5.26 | -5.26 | -0.67 | -0.67 | -0.65 | -0.65 |
| %Δ Container additional boats | 5.56 | 5.56 | 1.66 | 1.66 | 0.84 | 0.84 |
| %Δ Air Capacity | 0.28 | 0.25 | -4.57 | -4.59 | -4.25 | -4.27 |
| %Δ Container Freight Rates | 0.42 | 0.42 | 0.02 | 0.02 | 0.01 | 0.01 |
| %Δ Air Freight Rates | 0.00 | 0.06 | 0.00 | 0.00 | 0.00 | 0.00 |
| %Δ Container Emissions | -11.38 | -11.37 | 0.97 | 0.98 | 0.18 | 0.18 |
| %Δ Air Emissions | 0.24 | 0.22 | -4.58 | -4.61 | -4.27 | -4.29 |
| Net %Δ Emissions | -3.02 | -3.04 | -3.02 | -3.04 | -3.02 | -3.04 |
| Net Δ Emissions (mln ton) | -1.53 | -1.54 | -1.53 | -1.54 | -1.53 | -1.54 |
| Net Δ Welfare (mln USD) | -234 | -235 | 179 | 180 | 3889 | 3907 |
| Net Δ $CO_2$ Welfare (mln USD) | 61 | 62 | 61 | 62 | 61 | 62 |
| Net Δ Consumer Surplus (mln USD) | -295 | -297 | 6770 | 6802 | -334 | -336 |
| Subsidy Amount/Tax Revenue (mln USD) | 0 | 0 | -6653 | -6684 | 4162 | 4181 |
| Welfare Neutral Carbon Price (USD/ton) | 153 | 153 | NA | NA | NA | NA |

ically, subsidies increase consumer welfare to the extent that even after accounting for the subsidy payments, the net welfare is positive, resulting in up to $180 million. In the case of air taxes, the consumer surplus decreases, but the amount of collected taxes greatly overcompensates for the lost consumer surplus, resulting in a $3.9 billion net welfare increase. To summarize, both policies would perform much better than IMO2023 as they will shift part of the air transportation to the ocean one.

## 7.2 Technological Improvements

The discourse on emission-reducing technologies often focuses on those that decrease fuel consumption per unit of transportation. However, given the substitutability between air and ocean transporta-

tion, we want to highlight technologies that enable faster ocean transportation without increasing fuel consumption.[46] Such technologies can have both positive economic and environmental implications. To illustrate this point, we will examine a technological improvement that keeps trip fuel consumption constant while increasing ocean transport speed by 10%.[47]

Table 7: New Technology Alternative Policy with increased speed (OLS $\varepsilon = 7.3$)

| **Scenario** | (1) | (2) | (3) | (4) |
|---|---|---|---|---|
| Adjust $\nu$? | No | | Yes | |
| Air Pass Through ($\zeta$) | 0 | 1/6 | 0 | 1/6 |
| %Δ Container Capacity | 0.21 | 0.21 | 0.23 | 0.23 |
| %Δ Number of Vessels | -7.80 | -7.81 | -7.78 | -7.79 |
| %Δ Round-Trips per Vessel | 8.69 | 8.69 | 8.69 | 8.69 |
| %Δ Air Capacity | -0.74 | -0.62 | -0.79 | -0.67 |
| %Δ Container Freight Rates | -3.24 | -3.24 | -3.25 | -3.25 |
| %Δ Air Freight Rates | 0.00 | -0.48 | 0.00 | -0.48 |
| %Δ Container Emissions | 0.21 | 0.21 | 0.23 | 0.23 |
| %Δ Air Emissions | -0.73 | -0.62 | -0.78 | -0.67 |
| Net %Δ Emissions | -0.46 | -0.39 | -0.49 | -0.42 |
| Net Δ Emissions (mln tons) | -0.24 | -0.20 | -0.26 | -0.22 |
| Net Δ Welfare (mln USD) | 980 | 987 | 1049 | 1053 |
| Net Δ $CO_2$ Welfare (mln USD) | 10 | 8 | 10 | 9 |
| Net Δ Consumer Surplus (mln USD) | 970 | 978 | 1038 | 1044 |

Using the same methodology as in the previous sections, we calculate the long-run annual effects of the technological improvement discussed. The results, presented in Table 7, indicate that this technology would increase consumer surplus (from imports) and decrease emissions. The increase in consumer surplus would occur through three channels: (i) more trade (an increase in ocean-delivered imports outweighs a decrease in air-delivered imports), (ii) lower prices of delivered goods due to lower transportation costs, and (iii) faster delivery of ocean-imported goods. The last channel, which is often overlooked in the trade literature, would contribute 7% to the increase in consumer surplus.

[46] Please see Section A.7.3 for calculation details.

[47] Please see Table A14 for our IV based results using the fuel-saving technology along with a 10% increase in speed.

Faster delivery times are also crucial in increasing ocean transportation and decreasing air transportation of US imports, resulting in a net decrease in net emissions by 0.5%. These insights underscore the importance of relative speed as a critical factor in economic analysis and targeted technological improvements.

# 8 Conclusion

In our paper, we argue that the mechanism proposed by IMO2023 will have unintended consequences, resulting in carbon leakage into air transportation. This leakage will cause a short-term increase in joint emissions from air and ocean transportation. In the long-run, the efficiency gains in ocean transportation will be greatly offset by the carbon leakage, resulting in a relatively small overall effect. Additionally, both in the short and long-runs, IMO203 will have substantial negative effects on consumer surplus, as it will decrease import volumes and slow down their delivery by ocean.

To address these issues, we propose alternative policies that could reduce emissions and increase consumer surplus. One option is to subsidize ocean-transported goods or tax air-transported goods. We also highlight the potential benefits of faster delivery by ocean with a ocean-speed improving technology in a counterfactual scenario.

# References


Matt Apuzzo and Sarah Hurtes. Tasked to Fight Climate Change, a Secretive U.N. Agency Does the Opposite. *The New York Times*, June 3:53–82, 2021.

Adina Ardelean and Volodymyr Lugovskyy. It Pays to Be Big: Price Discrimination in Maritime Shipping. Technical report, 2023.

Jose Asturias. Endogenous transportation costs. *European Economic Review*, 123:103366, 2020.

Randy Becker and Vernon Henderson. Effects of air quality regulations on polluting industries. *Journal of Political Economy*, 108(2):379–421, 2000. doi: 10.1086/262123. URL https://doi.org/10.1086/262123.

Marc F Bellemare, Takaaki Masaki, and Thomas B Pepinsky. Lagged explanatory variables and the estimation of causal effect. *The Journal of Politics*, 79(3):949–963, 2017.

Elyakim Ben-Hakoun, Mordechai Shechter, and Yehuda Hayuth. Economic evaluation of the environmental impact of shipping from the perspective of co2 emissions. *Journal of Shipping and Trade*, 1, 2016. ISSN 2364-4575. doi: https://doi.org/10.1186/s41072-016-0011-5.

Tibor Besedeš and Antu Panini Murshidb. Experimenting with ash: The trade-effects of airspace closures in the aftermath of eyjafjallajökull. *Mimeo*, 2022.

Timothy Besley, Thiemo Fetzer, and Hannes Mueller. The welfare cost of lawlessness: Evidence from somali piracy. *Journal of the European Economic Association*, 13(2):203–239, 2015.

Bruce A. Blonigen and Wesley W. Wilson. Port Efficiency and Trade Flows. *Review of International Economics*, 16(1):21–36, February 2008.

Lucy Budd and Stephen Ison. The role of dedicated freighter aircraft in the provision of global airfreight services. *Journal of Air Transport Management*, 61:34–40, 2017. ISSN 0969-6997. doi: https://doi.org/10.1016/j.jairtraman.2016.06.003. URL https://www.sciencedirect.com/science/article/pii/S0969699715301642. Special Issue on Air Cargo: A By-Product or Success Factor?

Ching-Cheng Chao. Assessment of carbon emission costs for air cargo transportation. *Transportation Research Part D: Transport and Environment*, 33:186–195, 2014. ISSN 1361-9209. doi: https://doi.org/10.1016/j.trd.2014.06.004. URL https://www.sciencedirect.com/science/article/pii/S1361920914000698.

Niraj Chokshi. How Giant Ships Are Built. *New York Times*, 2020. URL https://www.nytimes.com/interactive/2020/06/17/business/economy/how-container-ships-are-built.html.

Brian R Copeland. Pollution content tariffs, environmental rent shifting, and the control of cross-border pollution. *Journal of International Economics*, 40(3):459–476, 1996. ISSN 0022-1996. doi: https://doi.org/10.1016/0022-1996(95)01415-2. URL https://www.sciencedirect.com/science/article/pii/0022199695014152. Symposium on Growth and International Trade: Empirical Studies.

James J Corbett, Haifeng Wang, and James J Winebrake. The effectiveness and costs of speed reductions on emissions from international shipping. *Transportation Research Part D: Transport and Environment*, 14(8):593–598, 2009.

Anca Cristea, David Hummels, Laura Puzzello, and Misak Avetisyan. Trade and the greenhouse gas emissions from international freight transport. *Journal of Environmental Economics and Management*, 65(1):153–173, 2013. doi: 10.1016/j.jeem.2012.06.00. URL https://ideas.repec.org/a/eee/jeeman/v65y2013i1p153-173.html.

Edwin Van der Werf and Corrado Di Maria. Imperfect environmental policy and polluting emissions: The green paradox and beyond. *International Review of Environmental and Resource Economics*, 6(2):153–194, 2012. ISSN 1931-1465. doi: 10.1561/101.00000050. URL http://dx.doi.org/10.1561/101.00000050.

Naihua Duan. Smearing estimate: a nonparametric retransformation method. *Journal of the American Statistical Association*, 78(383):605–610, 1983.

Joshua Elliott, Ian Foster, Samuel Kortum, Todd Munson, Fernando Pérez Cervantes, and David Weisbach. Trade and carbon taxes. *American Economic Review*, 100(2):465–69, May 2010. doi: 10.1257/aer.100.2.465. URL https://www.aeaweb.org/articles?id=10.1257/aer.100.2.465.

EPA. *Report on the Social Cost of Greenhouse Gases: Estimates Incorporating Recent Scientific Advances*. September 2022. URL https://subscriber.politicopro.com/eenews/f/eenews/?id=00000184-77c6-d07e-a5fd-f7df41f80000. This document is *Supplementary Material for the Regulatory Impact Analysis for the Supplemental Proposed Rulemaking, "Standards of Performance for New, Reconstructed, and Modified Sources and Emissions Guidelines for Existing Sources: Oil and Natural Gas Sector Climate Review."*.

Jasper Faber, Maarten 't Hoen, Marnix Koopman, Dagmar Nelissen, and Saliha Ahdour. Estimated Index Values of New Ships. Analysis of EIVs of Ships That Have Entered The Fleet Since 2009. CE Delft 15.7E50.14, 2015.

Farid Farrokhi and Ahmad Lashkaripour. Can Trade Policy Mitigate Climate Change? Mimeo, indiana university, September 2021.

Sharat Ganapati, Woan Foong Wong, and Oren Ziv. Entrepôt: Hubs, Scale, and Trade Costs. Technical report, University of Oregon, 2020.

Michael Greenstone. The impacts of environmental regulations on industrial activity: Evidence from the 1970 and 1977 clean air act amendments and the census of manufactures. *Journal of Political Economy*, 110(6): 1175–1219, 2002. doi: 10.1086/342808. URL https://doi.org/10.1086/342808.

Howard K Gruenspecht. Differentiated regulation: The case of auto emissions standards. *American Economic Review*, 72(2):328–31, 1982. URL https://EconPapers.repec.org/RePEc:aea:aecrev:v:72:y:1982:i:2:p:328-31.

Antonio Guterres. UN Secretary-General: "Making Peace with Nature is the Defining Task of the 21st century", Dec 2020. URL https://tinyurl.com/a74bwarn.

Rema Hanna. Us environmental regulation and fdi: Evidence from a panel of us-based multinational firms. *American Economic Journal: Applied Economics*, 2(3):158–89, July 2010. doi: 10.1257/app.2.3.158. URL https://www.aeaweb.org/articles?id=10.1257/app.2.3.158.

Jamie Hansen-Lewis and Michelle M Marcus. Uncharted waters: Effects of maritime emission regulation. Technical report, National Bureau of Economic Research, 2022.

Hercules E Haralambides. Gigantism in container shipping, ports and global logistics: a time-lapse into the future, 2019.

James Harrigan. Airplanes and comparative advantage. *Journal of International Economics*, 82(2):181–194, November 2010.

David Hummels, Volodymyr Lugovskyy, and Alexandre Skiba. The trade reducing effects of market power in international shipping. *Journal of Development Economics*, 89(1):84–97, May 2009.

David L. Hummels and Georg Schaur. Hedging price volatility using fast transport. *Journal of International Economics*, 82(1):15–25, September 2010.

David L. Hummels and Georg Schaur. Time as a Trade Barrier. *American Economic Review*, 103(7):2935–59, 2013.

David L. Hummels and Alexandre Skiba. Shipping the good apples out? an empirical confirmation of the alchian-allen conjecture. *Journal of Political Economy*, 112(6):1384–1402, 12 2004.

IMO. Third IMO GHG Study. Technical report, International Maritime Organization, 2014. URL https://www.imo.org/en/ourwork/environment/pages/greenhouse-gas-studies-2014.aspx.

IMO. Fourth IMO GHG Study. Technical report, International Maritime Organization, 2020. URL https://wwwcdn.imo.org/localresources/en/OurWork/Environment/Documents/Fourth%20IMO%20GHG%20Study%202020%20-%20Full%20report%20and%20annexes.pdf.

IMO. IMO progress on revised GHG strategy, Mediterranean ECA adopted. *IMO Press Release*, 2022. URL https://www.imo.org/en/MediaCentre/PressBriefings/pages/MEPC-79.aspx.

IPCC. Climate change 2014: Synthesis report. *Contribution of Working Groups I, II and III to the Fifth Assessment Report of the Intergovernmental Panel on Climate Change*, 2014. URL https://www.ipcc.ch/report/ar5/syr/.

Jota Ishikawa and Nori Tarui. Backfiring with backhaul problems. *Journal of International Economics*, 111(C): 81–98, 2018.

Mark R. Jacobsen and Arthur A. van Benthem. Vehicle scrappage and gasoline policy. *American Economic Review*, 105(3):1312–38, March 2015. doi: 10.1257/aer.20130935. URL https://www.aeaweb.org/articles?id=10.1257/aer.20130935.

Myrto Kalouptsidi. Time to build and fluctuations in bulk shipping. *American Economic Review*, 104(2):564–608, February 2014. doi: 10.1257/aer.104.2.564. URL https://www.aeaweb.org/articles?id=10.1257/aer.104.2.564.

David Kershaw. Hapag-lloyd preparing for turbulent 2023, Nov 2022. URL https://www.heavyliftpfi.com/sectors/hapag-lloyd-preparing-for-turbulent-2023/21719.article.

Valentina Keys. Bimco cii clause finally released: Does it make any sense of cii?, Dec 2022a. URL https://www.wfw.com/articles/bimco-cii-clause-finally-released-does-it-make-any-sense-of-cii/.

Valentina Keys. The cii conundrum – will it sink or swim?, Dec 2022b. URL https://www.wfw.com/articles/the-cii-conundrum-will-it-sink-or-swim/.

Brian G. Kinyua. Shipping's decarbonization outlook for 2023. *Maritime Executive*, January 2023. URL https://maritime-executive.com/editorials/shipping-s-decarbonization-outlook-for-2023.

Samuel Kortum and David A. Weisbach. Optimal Unilateral Carbon Policy. Technical report, 2021.

Jasmina Ovcina Mandra. Maersk ceo: We will need 5-15% more capacity to meet imo 2023, Aug 2022. URL https://www.offshore-energy.biz/maersk-ceo-we-will-need-5-15-more-capacity-to-meet-imo-2023/.

James R. Markusen. International externalities and optimal tax structures. *Journal of International Economics*, 5 (1):15–29, 1975. ISSN 0022-1996. doi: https://doi.org/10.1016/0022-1996(75)90025-2. URL https://www.sciencedirect.com/science/article/pii/0022199675900252.

Gabriela Mundaca, Jon Strand, and Ian R. Young. Carbon pricing of international transport fuels: Impacts on carbon emissions and trade activity. *Journal of Environmental Economics and Management*, 110:102517, 2021. ISSN 0095-0696. doi: https://doi.org/10.1016/j.jeem.2021.102517. URL https://www.sciencedirect.com/science/article/pii/S009506962100084X.

William Nordhaus. Climate clubs: Overcoming free-riding in international climate policy. *American Economic Review*, 105(4):1339–70, April 2015. doi: 10.1257/aer.15000001. URL https://www.aeaweb.org/articles?id=10.1257/aer.15000001.

Ian Parry, Mr Dirk Heine, Kelley Kizzier, and Tristan Smith. *Carbon taxation for international maritime fuels: Assessing the options*. International Monetary Fund, 2018.

Arthur Pigou. *The Economics of Welfare*. Macmillan, London, 1920.

Joseph S Shapiro. Trade costs, co2, and the environment. *American Economic Journal: Economic Policy*, 8(4): 220–54, 2016.

Joseph S Shapiro. The Environmental Bias of Trade Policy*. *The Quarterly Journal of Economics*, 136(2):831–886, 12 2020. ISSN 0033-5533. doi: 10.1093/qje/qjaa042. URL https://doi.org/10.1093/qje/qjaa042.

Powell Slaughter. Next year's carbon emissions standards could further complicate ocean shipping, May 2022. URL https://www.furnituretoday.com/supply-chain/next-years-carbon-emissions-standards-could-further-complicate-ocean-shipping/.

S. Solomon, G.-K. Plattner, R. Knutti, and P. Friedlingstein. Irreversible climate change due to carbon dioxide emissions. *Proceedings of the National Academy of Sciences*, 106, 2009. URL https://www.pnas.org/doi/full/10.1073/pnas.0812721106.

Martin Stopford. page 669–673. Routledge, 2009.

Mark Szakonyi. Slow steaming, congestion to blunt container capacity injections: Zim, Aug 2021. URL https://www.joc.com/maritime-news/container-lines/zim-integrated-shipping-services/slow-steaming-congestion-blunt-2023-container-capacity-injections-zim_20210818.html.

Shinsuke Tanaka, Kensuke Teshima, and Eric Verhoogen. North-south displacement effects of environmental regulation: The case of battery recycling. *American Economic Review: Insights*, 4(3):271–88, September 2022. doi: 10.1257/aeri.20210201. URL https://www.aeaweb.org/articles?id=10.1257/aeri.20210201.

Jens Thomsen. Congestion keeps growing—427 vessels idle in major container ports. *Shippingwatch.com*, 2021. URL https://shippingwatch.com/carriers/Container/article13312358.ece.

UN. The State of Climate. Technical report, The United Nations, April 2021. URL https://www.unep.org/explore-topics/climate-action/what-we-do/climate-action-note/state-of-climate.html?gclid=CjwKCAjwsvujBhAXEiwA_UXnAMAUHPU-2sZw0bIx8uZ3wlD2ePdeHR5CRs2yiahTkUYRZyXSkvXV6xoCj1UQAvD_BwE.

UNCTAD. UNCTAD Assessment of the Impact of the IMO Short-Term GHG Reduction Measure on States. Tech. report, United Nations Conference on Trade and Development, 2021.

USCG. Office of commercial vessel compliance (cg-cvc): International convention for the prevention of pollution by ships - marpol 73/78, 2022. URL https://www.dco.uscg.mil/Our-Organization/Assistant-Commandant-for-Prevention-Policy-CG-5P/Inspections-Compliance-CG-5PC-/Commercial-Vessel-Compliance/Domestic-Compliance-Division/MARPOL/.

Tony R. Walker, Olubukola Adebambo, Monica C. Del Aguila Feijoo, Elias Elhaimer, Tahazzud Hossain, Stuart Johnston Edwards, Courtney E. Morrison, Jessica Romo, Nameeta Sharma, Stephanie Taylor, and Sanam Zomorodi. Chapter 27 - environmental effects of marine transportation. In Charles Sheppard, editor, *World Seas: An Environmental Evaluation (Second Edition)*, pages 505–530. Academic Press, second edition edition, 2019. ISBN 978-0-12-805052-1. doi: https://doi.org/10.1016/B978-0-12-805052-1.00030-9. URL https://www.sciencedirect.com/science/article/pii/B9780128050521000309.

Hulda Winnes, Linda Styhre, and Erik Fridell. Reducing ghg emissions from ships in port areas. *Research in Transportation Business & Management*, 17:73–82, 2015.

Jack Wittels. Maersk Seeks $150-a-Ton Carbon Tax on Shipping Fuel. *Bloomberg.com*, June 2:53–82, 2021.

Woan Foong Wong. The Round Trip Effect: Endogenous Transport Costs and International Trade. Technical report, University of Oregon, 2020.

Woan Foong Wong and Simon Fuchs. Multimodal transport networks. 2022.

Tianle Yuan, Hua Song, Robert Wood, Chenxi Wang, Lazaros Oreopoulos, Steven E Platnick, Sophia von Hippel, Kerry Meyer, Siobhan Light, and Eric Wilcox. Global reduction in ship-tracks from sulfur regulations for shipping fuel. *Science advances*, 8(29):eabn7988, 2022.

# A Online Appendix—For Online Publication

## A.1 Detailed Data Description

**Technical characteristics of each vessel** (vessel size, engine type, eco-equipment, design fuel consumption, etc.), which will allow us to predict speed changes to meet the required IMO 2023 CII. These data come from the *World Fleet Register* (WFR), maintained by Clarksons PLC—the world's leading shipbroker—and include all major commercial vessels.

**Actual (observed) fuel consumption, distance traveled, and carbon emissions** provided by THETIS-MRV (alternatively THETIS), an online, port state control/inspection database maintained by the European Maritime Safety Agency (EMSA). It was launched in August 2017 in an effort to support new owner reporting requirements pursuant to Regulation (EU) 2015/757 on Monitoring, Reporting, and Verification of $CO_2$ from marine transport. Regulation 2015/757 requires the owners to report carbon emissions per transport work for all vessels that (i) are larger than 5,000 gross tonnage (GT); and (ii) make at least one call to an EU territory port subsequent to January 1st, 2018. THETIS-MRV makes provisions for third party monitoring and verification of a ship owner's reported carbon emissions. THETIS-MRV's data on owner-reported technical efficiency is publicly available, and features annual emissions reports from 2018-2020.

There are roughly 15,000 unique IMO number-vessels in the THETIS-MRV database across 2018-2020. Our preferred efficiency rating is the Energy Efficiency Design Index (EEDI), which measures grams of $CO_2$ generated per ton-nautical mile. THETIS also records vessel Estimated Index Values (EIV). EIV ratings, relative to EEDI ratings, are: (i) better thought of as vessel design efficiency metric versus as a fuel efficiency rating; (ii) less data-intensive to calculate due to making simplifying assumptions about vessel operation; and (iii) tend to slightly overestimate EEDI ratings (Faber et al., 2015).

**Data on container carriers, their service rotations and capacities** on all routes worldwide between 2012 and 2020, provided by BlueWater Reporting. These data will allow us to determine the capacity and speed of ocean transportation on importing routes to the U.S.

**Matching different datasets.** We link each vessel found in the THETIS-MRV registry back to the Clarksons' World Fleet Registry through the vessel's unique IMO number. The Clarksons-THETIS merge of the global containerized ocean fleet results in a match of 39.7% by count and 54.1% by capacity. The match is less than 100% because under THETIS carbon emissions were measured only from the vessels entering European ports, while Clarksons contains information about the entire global fleet. For comparison, the corresponding numbers for the bulk fleet are 42.3% and 38.5%, respectively. BlueWater Reporting contains all containerized maritime routes, which allows us matching (using IMO number) each containership present in either Clarksons or THETIS with its route in a given month.

## A.2 Route Construction and Carrier Count

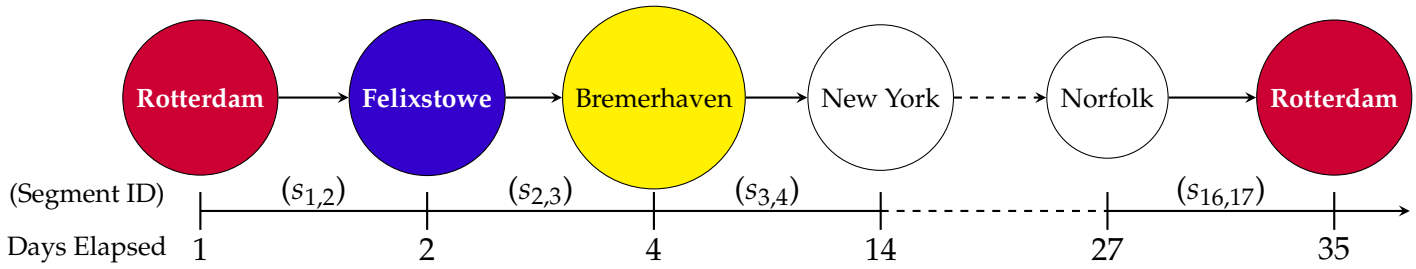


Figure A1: Container Rotation Example

*Note*: Port nodes are colored by country. Port to port pairs are identified by Segment ID $s_{i,j}$, where $i, j$ indexes port stops (from stop $i$ to stop $j$). Ports can be visited more than once whereas stop numbers are unique, e.g. Rotterdam is the 1st and 17th stop in the rotation. Finally, port stops between New York and Norfolk are excluded for illustrative simplicity. Carriers APL, CMA CGM, Hyundai, and Maersk Line service this rotation at various points throughout 2013.

A typical observation within BlueWater Reporting's historical rotation data lists the origin and destination port pair alongside the rotation that the pair belongs to. The rotation is a semi-colon separated string in the following form: "PortX 1 ; PortY 2" where a port name is followed by the number of days that have elapsed since the start of the rotation. In this way, a rotation can be thought of a sequence of port-to-port segments with a corresponding travel time given by the difference in the number of days elapsed. Additionally, each rotation lists the names of servicing carriers.

A BlueWater route is thus a sub-sequence of a larger rotation. The listed origin-destination pair, which serve as the endpoints of the route, *are not necessarily the endpoints* of a rotation. Moreover, BlueWater does not necessarily breakout all segments of a rotation. To put the problem in concrete terms, consider the example provided by Figure A1. BlueWater lists Rotterdam (origin port) to New York (destination port) as a route with the larger rotation. This rotation is serviced by four (4) carriers: APL, CMA CGM, Hyundai, and Maersk Line. Rotterdam (NL) to New York includes intermediate stops in Felixstowe (GB) and Bremerhaven (DE). Thus, there are at least four (4) carriers that serve New York from: the Netherlands; the United Kingdom; and Germany. However, BlueWater might *explicitly* report the four (4) carriers between the Netherlands and New York but not report the four (4) carriers between the United Kingdom and New York.

We clean our BlueWater rotation data to determine the number of carriers that service Country-U.S. Customs District *routes* according to the following steps:

1. **Identify all unique ports across all rotations**. Port names are not necessarily unique. After cleaning, our sample includes 462 ports.

2. **Geo-code ports**. For each of the 462 ports, we determine the longitude/latitude coordinates.

3. **Map ports into countries and/or U.S. Customs Districts**. Based on the port name and coordinates, we then map ports to countries. If the port is American, we further map the port into the relevant U.S. Customs district.

4. **Determine each rotation's total distance and time**. Since each rotation can be broken down into port-to-port pairs, we compute the sea distance traveled for each port pair.[48] Interestingly enough, at 3,769

[48] Besley et al. (2015) provides details about how to use GIS data and R to compute shortest paths over sea between port pairs.

unique pairs, the total number of unique port-to-port pairs is small relative to the theoretical maximum: $\frac{3,769}{462\times(461)/2} \approx 3.5\%$. Port pair travel time is based on the difference in total time elapsed. For example, Figure A1's segment $s_{3,4}$ implies a travel time of 10 days. Moreover, we calculate a sea distance of 4,230 miles (compared to the 4,000 mile estimate from SP PortWorld.

## A.3 From ship speed to route capacity changes

The following details how we process our shipping micro data to determine both changes in speed, capacity and $CO_2$ per ton mile post IMO2023 reforms on a per route basis (e.g. U.S. Customs District-country or $ij$) relative to our 2019 base year.

### A.3.1 Identify which ships service which routes for 2019

We look to our BlueWater Reporting and Panjiva datasets to determine which container ships serviced route $ij$ in 2019. Both our datasets report individual vessel IMO numbers (i.e. unique vessel identifiers) and report which port/country a vessel originated from and the U.S. port of arrival in 2019. Our first step is to identify unique ships across both datasets. All told, we have $n = 1,826$ unique vessels: 985 vessels are common to both datasets whereas 226 (615) ships are unique to BlueWater Reporting (Panjiva). Denote this list of unique (U.S. 2019 bound) vessels as `imo_vessel_list19`.

### A.3.2 Determine vessel speed for 2019

Once we have `imo_vessel_list19`, our next step is to determine the average speed for each vessel: we use BlueWater Reporting and THETIS-MRV to determine average vessel speed.

1. BlueWater Reporting data provides a rotation schedule for a given ship where we can see each port visited and transit duration between ports measured in days. BlueWater specifies the origin-destination ports within a rotation (e.g. London (UK) to Boston (US)): we use these end points to define a ship's trip. Using Dijkstra's algorithm as adapted by Besley et al. (2015), we compute the sea-distance between each port-to-port segment. Next, we sum up distance and transit time across all segments so that we know total (sea) travel distance and time. Average transit speed is thus total (sea) distance divided by total travel time. We use a vessels assigned weekly capacity as weights when computing average speed. In this way, we are able to compute 1,138 average vessel speeds.

2. THETIS data indirectly allows us to compute average vessel speed. THETIS reports a ship's annual $CO_2$ emissions; THETIS also reports a ship's $CO_2$ output while at berthing at port. We subtract a ship's berthing emissions from its annual emissions to determine its annual emissions while at moving at sea. THETIS lists a ship's average $CO_2$ emissions per nautical mile; combining average emissions per nautical mile with total emissions from movement at sea allows us to recover a ship's total mileage at sea. Converting this sea-mileage figure, we then use THETIS's reported annual hours at sea to come up with an average mile-per-hour estimate for each ship. In this way, we compute an additional 338 average speed estimates for ships in `imo_vessel_list19`.

BlueWater and THETIS thus allow us to estimate average traveling speed for 1,470 out of 1,826 ships (or 81 % of our sample). Figure A2 charts the relationship between vessel size and average speed. BlueWater and THETIS derived speeds share comparable distributions and both datasets convey a positive relationship between vessel size[49] and average speed. However, the relationship between vessel size and average speed

[49] Vessel size in Figure A2 comes from Clarksons WFR.

holds relatively modest explanatory power, with a simple regression line's $R^2 = 0.18$. For this reason, we impute a median speed of 16.245 mph to all remaining 356 ships. Our imputed speed is close to Clarksons' SIN 2019 average containership speed (for all containerships) of 14.36 knots or 16.53 mph.

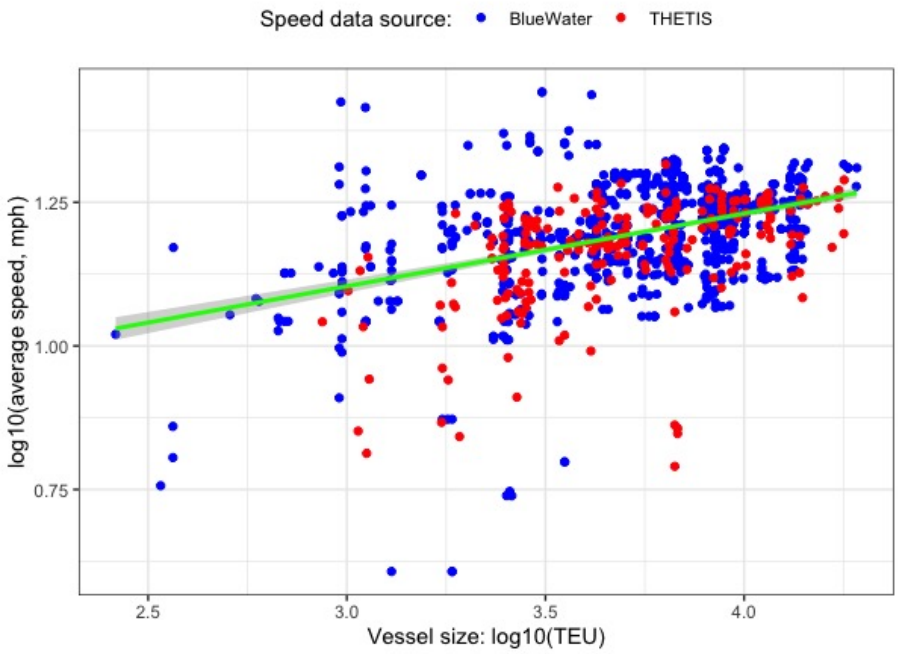


Figure A2: Ship size vs operational speed

*Note*: Green line is the regression line that comes from regressing (log) average vessel speed on (log) vessel size. The slope coefficient is positive and statistically different from zero, namely $\beta = 0.127$ 95% CI[ 0.112, 0.141], and the model's $R^2 = 0.18$.

### A.3.3 Approximating vessel technical characteristics related to fuel consumption

We use data from Clarksons WFR, which allows us to match vessel $v$'s size expressed in deadweight tonnage, $Dwt_v$, with engines' main and auxiliary fuel consumption and design speed ($s_v^{\text{Des}}$). We use the following specification:

$$\log(x_v) = \alpha_1 + \alpha_2 \log(Dwt_v) + \epsilon_v,$$

where $x_v$ sequentially represents $F_v^{\text{Main}}$, $F_v^{\text{Aux}}$, and $s_v^{\text{Des}}$. We apply a Seemingly Unrelated Regression (SUR) estimator to simultaneously estimate all coefficients. Table A1 presents the results.

Table A1: Vessel Size as a predictor of Fuel Consumption and Speed

| *Dependent variable*: | $\log(F_v^{\text{Main}})$ | $\log(F_v^{\text{Aux}})$ | $\log(s_v^{\text{Des}})$ |
|---|---|---|---|
| (Intercept) | $-4.861^{***}$ | $-5.087^{***}$ | $6.068^{***}$ |
| | (0.057) | (0.194) | (0.512) |
| $\log(Dwt_v)$ | $0.884^{***}$ | $0.632^{***}$ | $0.308^{***}$ |
| | (0.005) | (0.018) | (0.047) |
| $R^2$ | 0.867 | 0.484 | 0.430 |
| Num. obs. | 4046 | 329 | 370 |
| Duan Smear | 1.041 | 1.080 | 1.034 |

$^{***}p < 0.01$; $^{**}p < 0.05$; $^{*}p < 0.1$

**Filling in missing vessel size**. There are 297 vessels that are in `imo_vessel_list19` that do not appear in Clarksons' WFR. We use Vessel Tracking to look up each of these 297 vessels and retrieve vessel information as available: this website lists vessel TEU capacity rather than Dwt capacity. Our use of Vessel Tracking returns 220 vessels that $TEU_v > 0$. We use data from Clarksons' WFR to translate TEUs into Dwt via a simple linear model. Table A2 presents this simple "conversion" model:

Table A2: Mapping TEU to Dwt

| *Dependent variable*: | $Dwt_v$ |
|---|---|
| (Intercept) | $5703.848^{***}$ |
| | (146.036) |
| TEU | $10.637^{***}$ |
| | (0.026) |
| $R^2$ | 0.982 |
| Adj. $R^2$ | 0.982 |
| Num. obs. | 3189 |
| RMSE | 6101.592 |

$^{***}p < 0.01$; $^{**}p < 0.05$; $^{*}p < 0.1$

For the remaining 297-220=77 vessels, we impute our data's median Dwt of 66,940 tons. Once we have Dwt information for all vessels, we impute any missing information on engines' main and auxiliary fuel consumption and design speed; we default to Clarksons' WFR if those characteristics are present there.

### A.3.4 Imputing vessel CII

We use pooled THETIS data across the 2018-2021 reporting periods and vessel size (e.g. Dwt) from Clarksons' WFR to compute vessel CII scores, $CII_{v,t}^{obs}$. We estimate two regression models—one model that simply uses vessel size measured in Dwt to predict $CII_{v,t}^{obs}$ and another model that controls for year effects—and report our results in Table A3:[50]

[50]We trim one vessel-year from the merged THETIS (Year)-Clarksons dataset because it is an outlier: $CII_{v,t}^{obs} > 1000$.

Table A3: Imputing CII

| *Dependent variable*: $\log(CII^{obs}_{v,t})$ | | |
|---|---|---|
| | (1) | (2) |
| (Intercept) | $7.650^{***}$ | $7.671^{***}$ |
| | (0.023) | (0.023) |
| log(Dwt) | $-0.490^{***}$ | $-0.490^{***}$ |
| | (0.002) | (0.002) |
| 2019 | | $-0.027^{***}$ |
| | | (0.006) |
| 2020 | | $-0.043^{***}$ |
| | | (0.006) |
| 2021 | | $-0.015^{**}$ |
| | | (0.006) |
| $R^2$ | 0.879 | 0.880 |
| Adj. $R^2$ | 0.879 | 0.880 |
| BIC | -4584.829 | -4617.023 |
| Num. obs. | 7190 | 7190 |
| Duan Smear | 1.015 | 1.015 |

$^{***}p < 0.01$; $^{**}p < 0.05$; $^{*}p < 0.1$

We use the regression model specification of column (2) within Table A3 to impute CII scores for vessels in `imo_vessel_list19` that don't appear in THETIS.

### A.3.5 Vessel data source summary

Table A4 summarizes where/what combination of sources/methods our vessel data from when we construct `imo_vessel_list19`: Figure A3 depicts the empirical cumulative distribution function (ECDF) for vessel capacity per data series/source. Broadly speaking, all data series have similar capacity distributions.

Table A4: Vessel data sources for `imo_vessel_list19`

| Speed | Dwt | Main Engine ($F^{\text{Main}}$) | Auxiliary Engine ($F^{\text{Aux}}$) | Design Speed ($s_v^{\text{Des}}$) | $CII_{v,t}^{obs}$ | Count |
|---|---|---|---|---|---|---|
| BW | Clarksons | Clarksons | (II) | (II) | (III) | 379 |
| BW | Clarksons | Clarksons | (II) | (II) | THETIS | 374 |
| THETIS | Clarksons | Clarksons | (II) | (II) | THETIS | 176 |
| (I) | Clarksons | Clarksons | (II) | (II) | (III) | 149 |
| (I) | Vessel Track | (II) | (II) | (II) | (III) | 130 |
| BW | Clarksons | (II) | (II) | (II) | (III) | 109 |
| THETIS | Vessel Track | (II) | (II) | (II) | (III) | 68 |
| BW | Clarksons | (II) | (II) | (II) | THETIS | 62 |
| BW | Clarksons | Clarksons | (II) | Clarksons | (III) | 59 |
| BW | Clarksons | Clarksons | Clarksons | (II) | (III) | 58 |
| THETIS | (I) | (II) | (II) | (II) | (III) | 43 |
| (I) | (I) | (II) | (II) | (II) | (III) | 33 |
| BW | Clarksons | Clarksons | (II) | Clarksons | THETIS | 24 |
| THETIS | Clarksons | (II) | (II) | (II) | THETIS | 23 |
| BW | Vessel Track | (II) | (II) | (II) | (III) | 22 |
| BW | Clarksons | Clarksons | Clarksons | (II) | THETIS | 19 |
| (I) | Clarksons | Clarksons | Clarksons | (II) | (III) | 17 |
| (I) | Clarksons | Clarksons | (II) | Clarksons | (III) | 17 |
| BW | Clarksons | (II) | (II) | Clarksons | (III) | 16 |
| BW | Clarksons | (II) | (II) | Clarksons | THETIS | 15 |
| THETIS | Clarksons | Clarksons | (II) | Clarksons | THETIS | 11 |
| THETIS | Clarksons | Clarksons | Clarksons | (II) | THETIS | 8 |
| (I) | Clarksons | (II) | (II) | (II) | (III) | 7 |
| (I) | Clarksons | (II) | (II) | Clarksons | (III) | 3 |
| THETIS | Clarksons | (II) | (II) | Clarksons | THETIS | 3 |
| BW | (I) | (II) | (II) | (II) | (III) | 1 |

Imputation Method (I): We use the median speed and Dwt across our pooled BlueWater (BW) and THETIS data to impute missing values.
Imputation Method (II): We use a seemingly unrelated regression (SUR) estimator, built on Clarksons WFR data, to impute vessel characteristics as function of vessel Dwt.
Imputation Method (III): We estimate a simple regression model where observed carbon intensity is a function of vessel Dwt and use this model to impute carbon intensity.

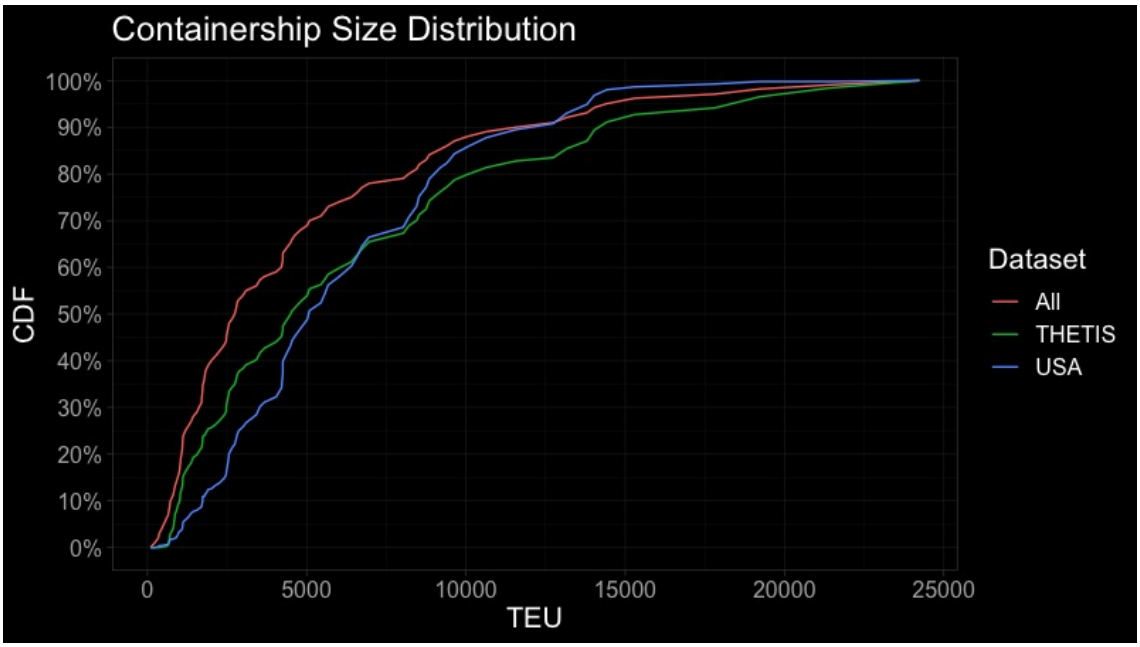


Figure A3: Size Comparison

### A.3.6 Modeling IMO Speed Adjustments

Now that `imo_vessel_list19` is complete with respect to technical characteristics, speed, and carbon intensity, we use Corbett et al. (2009)'s formula, equation (A19), to model the relationship between a vessel's speed and fuel consumption (subject to vessel characteristics):

$$F_{ijv}(s_v) = \left[F_v^{\text{Main}}\left(\frac{s_v}{s_v^{\text{Des}}}\right)^3 + F_v^{\text{Aux}}\right]\frac{d_{ij}}{24 s_v},, \tag{A19}$$

where $d_{ij}$ is the route distance. Suppose that $s_v^{\text{IMO}} = \rho_v s_v$ is the speed that will ensure that $v$ is compliant with IMO2023 carbon intensity standards, namely that ships are no more than 107% over the required emissions line (as to score a letter "C" or better):

$$CII_{v,t}^{req}(Z_t) = \left[1984 \times (Dwt_v)^{-0.489}\right](1 - Z_t) \implies \frac{CII_{v,t}^{obs}}{CII_{v,t}^{req}} \times \leq 107\%$$

where $(1 - Z_t) = 0.95$ for $t = 2023$.[51]
For each ship in `imo_vessel_list19`, we use Brent's method to find the speed adjustment factor $\rho_v^*$ that solves:

$$\rho_v^*(Z_t) \in \arg\min H(\rho_v) \equiv \left(1 - \left(\frac{\overline{CII}_v^{obs}}{\overline{CII}_v^{req}(Z_t)} - 1.07\right) - \frac{F_v\left(s_{1v}^{\text{IMO}}(\rho_v(Z_t))\right)}{F_v(s_{1v})}\right)^2 \tag{A20}$$

We set $\rho_v^* = 1$ for IMO2023 compliant ships (e.g. "C" grade or better). Figure 2 in the text visualizes our results

[51] See MEPC.338(76) for the $Z_t$ schedule over the next several years: starting in 2023, $Z_t = 5\%$ with an additional 2 percentage points added each year after 2023.

for $\rho_v^*$ across all `imo_vessel_list19` containerships. In the event that we calculate $\rho_v > 1$ for ships that are currently rated as "D" or "E", this means that these ships will be unable to reduce their speed enough to comply with IMO standards. In this case of IMO2023 standards, the number of these ships is less than five (5). When we take our speed estimates over to our capacity adjustment calculations, we drop these ships from our capacity-analysis.

### A.3.7 Estimating time in port

The number of trips that a ship can make in a year partially depends on how much time is spent in port. We follow a similar strategy to Wong and Fuchs (2022) in using Automatic Identification System (AIS) provided by MarineCadastre.gov. These AIS data are the result of collaborative efforts between the U.S. Bureau of Ocean Energy Management (OECM), the National Oceanic and Atmospheric Administration (NOAA), and the U.S. Coast Guard Navigation Center. In total, these AIS data cover nearly all vessel movements off the U.S. coastline reported in one minute intervals for every day since January 1st, 2015 (with more limited coverage stretching back to 2009). Downloading all of these data would require several terabytes (TB) of computer storage.

Awash in a sea of data, we make a number of judgement calls to make these vessel tracking data more amenable to our purposes.

- **First**, we limit our attention to January 2019 vessel tracking.
- **Second**, using Clarksons's WFR data on all containership MMSI (Maritime Mobile Service Identity) numbers—a unique number that identifies individual ships—we are able to filter out all non-containerships from the MarineCadastre data. This filtering step leaves us with 3,105,5772 AIS readings for 610 containerships.
- **Third**, our AIS data include COLREGS (International Regulations for Preventing Collisions at Sea) vessel navigational codes. These codes describe what the vessel is doing when it transmits the AIS signal. We limit our attention to AIS readings with navigation status codes "0" (Under way using its engine),"1" (anchored), and "5" (Moored or tied to another object to limit free movement): these codes describe the two statuses we are interesting, namely whether the vessel is moving or docked. Filtering on these navigation status codes brings our sample down to 3,090,059 AIS signals and keeps at 610 vessels. As a sanity check, we use the AIS's SOG (speed over ground, knots per hour) data to confirm that ship is relatively stationary while a "1" of "5" code is active.
- **Fourth**, we re-code our three reminaing COLREGS status to capture whether or not a containership is moving. For each containership in our MarineCadastre, we identify runs in our data between moving/non-moving (e.g. if we code moving status as "M" and non-moving status as "N", then we look for the first time an uninterrupted sequence of "M"'s is broken by an "N"). Once we the terminal points of non-moving code sequence, we find the corresponding (terminal) time stamps and so compute the duration of the vessel's stationary episode.
- **Fifth**, we use Panjiva U.S. 2019 bill of lading data to identify all U.S container ports and geo-reference all container port. For every vessel's stationary period, we take the average longitude/latitude position of the vessel and use that point to find the closest Panijvia U.S. container port. If the vessel's non-stationary location is more than 50 miles away from the port, we exclude this stationary episode from our analysis.
- Figure A4 gives an example of what our clean AIS data look like for a given ship, the COSCO Excellence (IMO: 9472189), and its various stops in the early part of January 2019. In particular, we see that

COSCO Excellence first stopped outside of Savannah, GA (denoted by "A" across panels) before entering and unloading that port (denoted by "B") before repeating the waiting and unloading stages in Charleston, SC ("C" and "D" respectively) before heading west out to sea. In context, we consider the sum of the times in periods "A" and "B" ("C" and "D") as COSCO Excellence's port time period for Savannah, GA (Charleston, SC). The port time for COSCO Excellence is roughly 164 (43) hours for Savannah,GA (Charleston, SC).

- **Sixth**, we compute a rough measure of port-day traffic in a manner similar to Wong and Fuchs (2022). For each ship in our sample, we calculate the share of a given day that a ship spends in a port and multiply this share by the deadweight (Dwt) tonnage capacity of the ship. For example, if a 78,300 Dwt container ship were docked outside of Oakland, CA from January 2nd 2:00AM to January 4th 6:00PM, we would add $22/24 \times 78,300 = 71,790$ tons on January 2nd to Oakland's traffic measure and $24/24 \times 78,300 = 78,300$tons on January 3rd and $6/24 \times 78,300 = 19,575$ tons on January 4th. We then sum over each port-day to compute our traffic measure, port traffic$_{pd}$.

- **Seventh**, we aggregate port locations together such that if our data have two or more ports within a 20 miles radius of each other, we group them together. In this way, we jointly consider the ports of Los Angeles/Long Beach, Seattle/Tacoma, New York/Newark, etc.

- **Eighth**, armed with 50 ports, 524 container ships, and 1,236 port visits, we estimate a set of simple fixed effect regression models that predict a vessel's port time as function of its deadweight capacity. Our unit of analysis here is a ship $v$ on day $d$ visiting port $p$: the dependent variable is (log) days in port for ship $v$ on day $d$ visiting port $p$. Each column of Table A5 indicates that increases in vessel size are associated with higher expected port times: even in the most stringent specification in column (3), a 10% increase in vessel time raises expected dwell time by 2.8%. Column (3)'s $p \times d$ fixed effects encompass port and day specific influences on a vessel's expected dwell time, such as *port congestion*. We use the port fixed effects from column (2) to create the dwell time map presented by Figure A5. With the exception of Wilmington DE, containerships entering any major U.S. container port experience between 20 to 80% less dwell time conditional on vessel size relative to Los Angeles/Long Beach.

Table A5: Port time as a function of vessel size?

| | *Dependent variable*: log (port time$_{vpd}$) | | |
|---|---|---|---|
| | (1) | (2) | (3) |
| (Intercept) | 1.418*** | | |
| | (0.506) | | |
| log(Dwt$_{vd}$) | 0.181*** | 0.111* | 0.284*** |
| | (0.046) | (0.064) | (0.079) |
| Num. obs. | 1236 | 1236 | 1236 |
| $R^2$ (full model) | 0.013 | 0.350 | 0.700 |
| $R^2$ (proj model) | | 0.004 | 0.032 |
| Adj. $R^2$ (full model) | 0.012 | 0.305 | 0.421 |
| Adj. $R^2$ (proj model) | | 0.003 | 0.030 |
| FE: port ($p$) | | ✓ | |
| FE: day ($d$) | | ✓ | |
| FE: port $\times$ day ($p \times d$) | | | ✓ |

$^{***}p < 0.01$; $^{**}p < 0.05$; $^{*}p < 0.1$

We also (partially) replicate Wong and Fuchs (2022) regression analysis connecting port traffic to port service times. As a quick outline of differencesWong and Fuchs (2022): (i) use data on a wider selection of ships from June 2015 to December 2021; (ii) focus on a ship's *dwell time*, or the time a vessel "spends being moored at a pier and has zero speed" (e.g. periods in "B" and "D" in our Figure A4); and (iii) calculate port traffic over moving multi-day/week averages. These differences notwithstanding, we find similar a qualitatively similar port time elasticity with respect to traffic: a 10% increase in traffic today is associated with a 1.97% increase in a ship's vessel time in port (e.g. column 4) compared to Wong and Fuchs (2022) preferred elasticity of 1.3%.

Table A6: Port time as function of port traffic?

| | *Dependent variable*: log (port time$_{vpd}$) | | | |
|---|---|---|---|---|
| | (1) | (2) | (3) | (4) |
| (Intercept) | 0.437* | | | |
| | (0.256) | | | |
| log(port traffic$_{pd}$) | 0.205*** | 0.234*** | 0.210*** | 0.197*** |
| | (0.017) | (0.068) | (0.051) | (0.058) |
| Num. obs. | 1236 | 1236 | 1236 | 1236 |
| $R^2$ (full model) | 0.101 | 0.317 | 0.382 | 0.764 |
| $R^2$ (proj model) | | 0.070 | 0.053 | 0.057 |
| Adj. $R^2$ (full model) | 0.100 | 0.288 | 0.339 | 0.542 |
| Adj. $R^2$ (proj model) | | 0.069 | 0.052 | 0.055 |
| FE: port ($p$) | | ✓ | ✓ | ✓ |
| FE: day ($d$) | | | ✓ | ✓ |
| FE: vessel ($v$) | | | | ✓ |

$^{***}p < 0.01$; $^{**}p < 0.05$; $^{*}p < 0.1$

- **Ninth**, our Table A5 regression specifications' relatively low *adjusted* $R^2$'s suggest that considerable explanatory power is left unaccounted for. For this reason, we choose to adopt a uniform measure of port time via a two step weighted average: (i) we average January 2019 port time per container port in our sample using our definition of port traffic$_{pdv}$ as weights; and, (ii) we use Panjiva bill of lading data to compute 2019 annual traffic per port which we use to identify the top 20 ports by TEU volume. We then use average these twenty container port times (from the previous step) while using their annual TEU volumes as weights. In this way, we compute an aggregated port time measure of **2.53 days (60.8 hours)**.

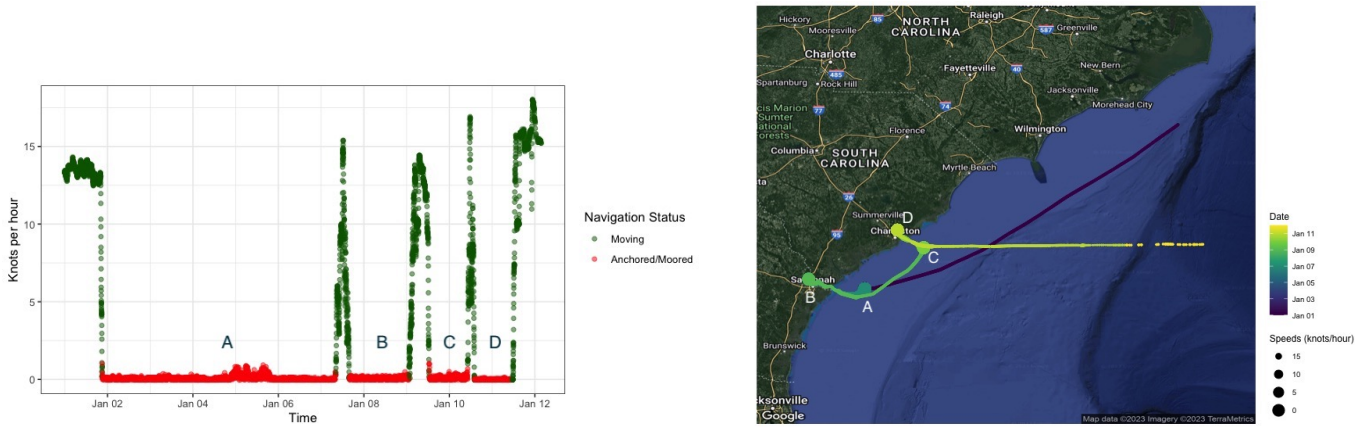


(a) Vessel speed vs movement status (b) Vessel path

Figure A4: COSCO Excellence (IMO: 9472189) trip to Savannah, GA and Charleston, SC




Figure A5: 2019 estimated port time for top 20 U.S. container ports

*Note*: Ports are scaled in size to proportion of their annual TEU volume. Port time's are weighted by the container's port traffic$_{pd}$ flows across January 2019.

### A.3.8 Filling in missing values on route distance, time, and carbon intensity

In order to analyze changes in vessel speed and their impact on route time, carbon intensity, and carbon output, it is first necessary to establish a route's distance, time, and carbon intensity. Directly observed data mapping ships to routes and route times can be used to assign vessel-capacity weighted averages of ship speed and carbon intensity per route. However, the available Census trade data on containerized imports includes U.S. Customs District-country pairs that are not covered by our vessel microdata. To address this issue, we have developed a route characteristics imputation approach, which we describe in detail below.

(a) **Direct measurements**

(a) Our analysis of trade routes involves the use of **direct measurements of distance and time, obtained from the BlueWater platform.** Priority is given to distance and travel time data for a specific route $ij$ that is either directly reported by BlueWater (e.g., the total days in transit between ports), or that can be inferred from BlueWater data (e.g., port-to-port distance calculations converted into route distances). In total, we have access to 615 U.S. Customs District-country pairs from the BlueWater platform, along with associated IMO vessel numbers.

(b) **Direct route measures of carbon intensity:** We use our BlueWater vessel/route data to compute a vessel-capacity weighted average of carbon intensity $CII^{obs}_{v,t}$ per route.

(b) **Indirect measurements**

(a) **Indirect distance measurements**. For all remaining routes, we utilize indirect distance measurements to calculate the sea distance between BlueWater U.S. Customs District-country pairs. Specifically, we use the coordinates of a country's largest city, obtained from CEPII's GeoDist database, and average coordinates of a U.S. Customs District as our distance endpoints.[52] By incorporating these distance estimates, we are able to analyze an additional 2,684 routes in our analysis.

(b) **Indirect travel speed and distance estimates**. Once we have obtained sea distance measurements for each $ij$ route, we utilize our non-BlueWater Panjiva vessels and their voyages' U.S. Customs District-country endpoints to calculate travel time, assuming a constant moving speed that we have previously computed. It is important to note a subtle but significant distinction between the Panjiva bill of lading data and the BlueWater data. Specifically, the bill of lading information pertains to the city/port (and therefore, the country) of origin, the port of lading (and therefore, the country), and the U.S. port of unlading (and therefore, the U.S. Customs District). We treat the country of origin as $j$, but we compute the distance for route $ij$ as a shipment-weighted average distance and shipping speed between U.S. Customs District $i$ and the port of lading in country $j'$. Formally, our indirect measure of $x \in$ distance, speed for ships $v$ serving route $ij$ and using country $j'$ as a stop is:

$$\overline{x}^{\text{indirect}}_{ij} = \frac{\sum_{v \in ij} x_{v,ij'j} \times ship_{v,ij'j}}{\sum_{v \in ij} ship_{v,ij'j}} \tag{A21}$$

where $ship_{v,ij'j}$ is $v$'s total shipment volume to $ij$ using $j'$ measured in TEUs. Using (A21), we compute average travel distance and speed for 364 additional routes.

[52] To the extent that a country's largest city is not on the country's coastline (or even if the country is landlocked), our shortest sea-path code still takes the shortest path to the nearest point of coastline and then draws a straight line (as the crow flies) over land.

(c) **Indirect estimates travel time, vessel size, and carbon efficiency**. At this stage, we have route characteristics for only 979 out of 3,295 routes. To impute the remaining route characteristics, we have devised the following strategy. If route $ij$ is missing vessel data, we first utilize ship-capacity size weighted average speed/Dwt/$\overline{CII}_v^{obs}$ values based on country $j$. In the event that we are unable to compute a country average, we then attempt to compute a U.S. Customs District $i$ average. Finally, if we cannot calculate an average using either $i$ or $j$, we compute an average over all geographies.

(c) **Other measurements**. As a measure of air route distance, we compute the great circle distance between the average coordinates of the U.S. Customs Districts and the country coordinates from CEPII's GeoDist database.

Table A7 presents a summary of our maritime route-level characteristics and their respective sources. Notably, the median summary statistics pertaining to route travel speed and carbon intensity are relatively consistent across our different data sources and imputation methods, providing reassurance of the validity and reliability of our findings.

Table A7: Route characteristics data sources

| Route Sources | | Count | (I) values | | | | |
|---|---|---|---|---|---|---|---|
| Travel time | Other characteristics | | Dwt | Distance (miles) | Travel time (days) | Speed (mph) | $CII^{obs}$ |
| BW | Route Average | 611 | 62000 | 7958 | 22.4 | 15.8 | 10.2 |
| Country Average | Country Average | 2243 | 77411 | 7826 | 22.2 | 15.0 | 9.1 |
| Country Average | Route Average | 205 | 77859 | 6702 | 19.8 | 14.6 | 8.9 |
| District Average | District Average | 31 | 90804 | 7855 | 21.3 | 16.1 | 7.7 |
| Panjiva | Country Average | 11 | 92766 | 7202 | 23.9 | 17.0 | 8.2 |
| Panjiva | Route Average | 194 | 78962 | 6903 | 20.3 | 15.5 | 9.0 |

### A.3.9 Modeling capacity adjustments caused by speed adjustments

The number of annual round trips that a ship $v$ can make during the year on route $ij$ is equal to:

$$\text{Round Trips} : n_{ij,v} = \frac{A}{2(d_{ij}/(24s_{ij,v}) + \text{port time})}$$

$A$ is the number of sailing days in the year and $d_{ij}/(24s_{ij,v})$ is the average route time of vessel $v$ moving distance $d_{ij}$ at average speed $s_{ij,v}$ (mph).[53] A vessel's reduced capacity on route

[53] We assume that vessels are active for $A$ =340 days out of the year to reflect off-hire periods or when statutory maintenance, dry docking, etc. This is the number used by Haralambides (2019). The choice of $A$ arguably is inconsequential since when we calculate the ratio of round trips, we are assuming that the number of sailing days per year is unaffected.

## A.4 Additional Results from the Demand-Side Estimation

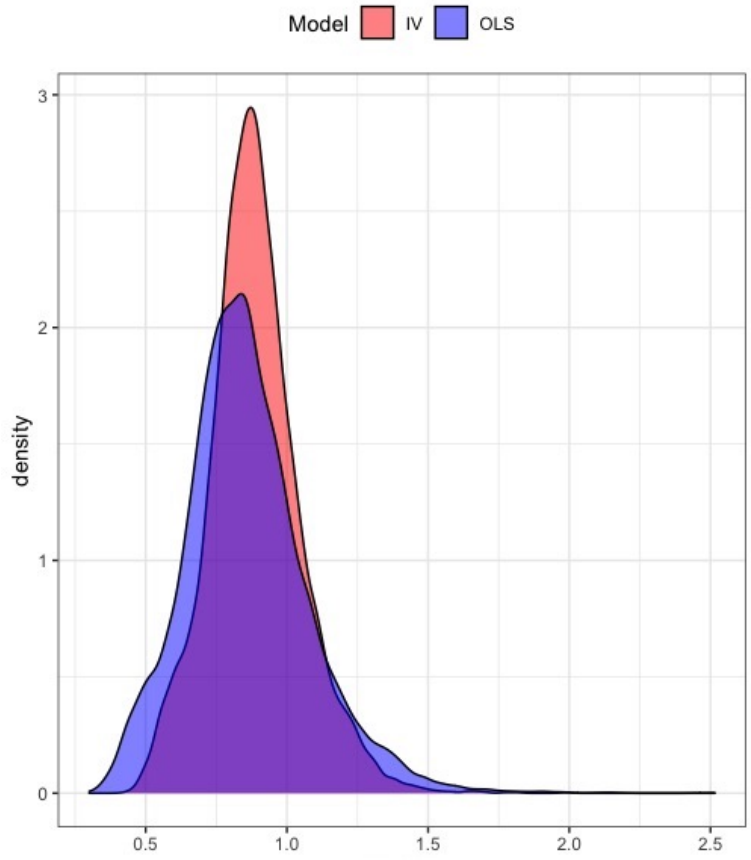


Figure A6: Distribution of $\theta_j \theta_{it}$ (i.e., $\widehat{\nu}_j \widehat{\nu}_{it}$) from equation (14).

## A.5 Additional Theoretical Derivations

### A.5.1 Deriving ocean equilibrium freight rates

Let us focus on the containerized ocean transportation on a given route $ij$. Recall that carriers compete à la Cournot, with all carriers having the same symmetric marginal cost and no differentiation or loyalty incentives in ocean transportation. As a result, in equilibrium, all carriers will charge the same freight rate, $f_{ij}$. This freight rate will be a function of the aggregate equilibrium quantity on that route, $\underline{q}_{ij}$. Specifically, from the demand function (11), we can express the freight rate as:

$$\underline{f}_{ij} = \underline{q}_{ij}^{-\frac{1}{\epsilon}} \frac{q_{0,it} \nu_{ij}(s_{ij})}{K_{it}} - \underline{p}_{ij} \underline{\tau}_{ij} = \left(\sum \underline{Q}_{ij}^{l}\right)^{-\frac{1}{\epsilon}} \frac{q_{0,it} \nu_{ij}(s_{ij})}{K_{it}} - \underline{p}_{ij} \underline{\tau}_{ij},$$

where $\underline{Q}_{ij}^{l}$ is the quantity supplied on $ij$ by carrier $l$. Using the above equation we can calculate the freight rate elasticity with respect to $\underline{Q}_{ij}^{l}$ :

$$\frac{\partial \underline{f}_{ij}}{\partial \underline{Q}_{ij}^{l}} \frac{\underline{Q}_{ij}^{l}}{\underline{f}_{ij}} = -\frac{1}{\varepsilon} \frac{(\underline{f}_{ij} + \underline{p}_{ij}\underline{\tau}_{ij})}{\underline{f}_{ij}} \frac{\underline{Q}_{ij}^{l}}{\underline{q}_{ij}} \left(1 + \frac{1}{K_{it}} \frac{1-\mu}{\mu} \nu_{ij} (\varepsilon - 1) \underline{q}_{ij}^{\frac{\varepsilon-1}{\varepsilon}}\right) \tag{A22}$$

The profit functions of carrier $l$ delivering from country $j$ to district $i$ is:

$$\pi_{ij}^{l} = Q_{ij}^{l}(f_{ij} - c_{ij}) - C \qquad \forall l = 1, 2, ..., n_{ij}$$

The nx1 vector of the first order conditions is:

$$\frac{\partial \underline{\pi}_{ij}^{l}}{\partial \underline{Q}_{ij}^{l}} = \underline{f}_{ij} \left(1 + \frac{\partial \underline{f}_{ij}}{\partial \underline{Q}_{ij}^{l}} \frac{\underline{Q}_{ij}^{l}}{\underline{f}_{ij}}\right) - c_{ij} = 0$$

Next, we substitute for $\frac{\partial \underline{f}_{ij}}{\partial \underline{Q}_{ij}^{l}} \frac{\underline{Q}_{ij}^{l}}{\underline{f}_{ij}}$ with the result in equation (A22) noting also that, in the symmetric equilibrium $n_{ij}\underline{Q}_{ij}^{l} = \underline{q}_{ij}$ :

$$\underline{f}_{ij} \left(1 - \frac{1}{\varepsilon} \frac{(\underline{f}_{ij} + \underline{p}_{ij}\underline{\tau}_{ij})}{\underline{f}_{ij}} \frac{1}{n_{ij}} \left(1 + \frac{1}{K_{it}} \frac{1-\mu}{\mu} \nu_{ij} (\varepsilon - 1) \underline{q}_{ij}^{\frac{\varepsilon-1}{\varepsilon}}\right)\right) - c_{ij} = 0,$$

from which:

$$\underline{f}_{ij} = c_{ij} + \frac{c_{ij} + \underline{p}_{ij}\underline{\tau}_{ij}}{n_{ij}\sigma_{ij} - 1},$$

where

$$\sigma_{ij} \equiv \varepsilon \left(1 + \frac{1}{K_{it}} \frac{1-\mu}{\mu} \nu_{ij} (\varepsilon - 1) \underline{q}_{ij}^{\frac{\varepsilon-1}{\varepsilon}}\right)^{-1} = \varepsilon \left(1 + \frac{(\varepsilon - 1)\nu_{ij} \underline{q}_{ij}^{\frac{\varepsilon-1}{\varepsilon}}}{\sum_{j} \left(\nu_{ij} \underline{q}_{ij}^{\frac{\varepsilon-1}{\varepsilon}} + \overline{q}_{ij}^{\frac{\varepsilon-1}{\varepsilon}}\right)}\right)^{-1}.$$

### A.5.2 Calculating changes in consumer surplus

IMO2023 is likely to impose economic cost on consumers. We will use the following procedure to evaluate the corresponding changes in consumer surplus. First, using demand functions (11), we will calculate pre-reform surplus on each route using the following formula:

$$CS_{it}^{pre} = \sum_j \int_0^{\underline{q}_{ijt}^{pre}} \left[\underline{\Lambda}_{ijt}\underline{q}_{ijt}^{-\frac{1}{\varepsilon}} - (\underline{p}_{ijt}^{pre}\underline{\tau}_{ijt}^{pre} + \underline{f}_{ijt}^{pre})\right] d\underline{q}_{ijt} + \sum_j \int_0^{\overline{q}_{ijt}^{pre}} \left[\overline{\Lambda}_{ijt}\overline{q}_{ijt}^{-\frac{1}{\varepsilon}} - (\overline{p}_{ijt}^{pre}\overline{\tau}_{ijt}^{pre} + \overline{f}_{ijt}^{pre})\right] d\overline{q}_{ijt}$$

where $\underline{\Lambda}_{ijt} = \frac{\nu_{it}\nu_j q_{0,it}}{K_{it}}$ and $\overline{\Lambda}_{ijt} = \frac{q_{0,it}}{K_{it}}$. Denoting our vector of post-reform changes as $\mathbf{\Omega}$, we express the ratio of post to pre utilities for $i$ as:

$$U_{i,t+1}^{post}(\mathbf{\Omega}) \Big/ U_{it}^{pre} = \left[\sum_j \left(\nu(\mathbf{\Omega})[\underline{q}_{ijt}(\mathbf{\Omega})]^{\frac{\varepsilon-1}{\varepsilon}} + [\overline{q}_{ijt}(\mathbf{\Omega})]^{\frac{\varepsilon-1}{\varepsilon}}\right)\right]^{\frac{\mu\varepsilon}{\varepsilon-1}} \Big/ \left[\sum_j \left(\nu \underline{q}_{ijt}^{\frac{\varepsilon-1}{\varepsilon}} + \overline{q}_{ijt}^{\frac{\varepsilon-1}{\varepsilon}}\right)\right]^{\frac{\mu\varepsilon}{\varepsilon-1}},$$

and calculate changes in consumer surplus post reform as: $\Delta CS = \sum_{it} CS_{it}^{pre}\left(\frac{U_{it}^{post}(\mathbf{\Omega})}{U_{it}^{pre}} - 1\right)$.

### A.5.3 Other welfare calculations

Welfare changes in transportation related to changes $CO_2$ emissions are more straightforward to quantify. Change in $CO_2$ emissions comes from evaluating:

$$\Delta CO_2 = \sum_{ij} \underline{q}_{ij}\underline{d}_{ij}(\underline{\omega}_{ij} - 1)(\underline{\xi}_{ij}^{post} - \underline{\xi}_{ij}^{pre}) + \sum_{ij} \overline{q}_{ij}\overline{d}_{ij}(\overline{\omega}_{ij} - 1)\overline{\xi}_{ij}$$

where $\underline{\xi}_{ij}^{post}$ ($\underline{\xi}_{ij}^{pre}$) is the amount of carbon generated per ton-mile after (pre) reform for conatinerships; likewise, $\overline{\xi}_{ij}$ is the amount of carbon generated per ton-mile for airplanes. Changes in net welfare are then $\Delta CS - \Delta CO_2 \times$ social cost of carbon.

## A.6 Estimating the Containerized Shipping Price elasticity of Air-Shipping Price

Given the substantial excess capacity previously identified in the air-shipping industry, it's unclear if an expected rise in ocean freight rates would correspondingly boost air freight rates. To further investigate, we analyze US imports data from 2013 to 2019 A.6. The data, organized on a monthly-(HS6 product)-(customs district)-(exporting country) basis, is used to estimate the relationship between these two freight rates. Our simple pass-through model has ad-valorem iceberg associated with the air-transported imports $\overline{\phi}_{ijkt}$ (defined as the ratio of the factory price and air freight rate over factory price) regressed on the corresponding iceberg cost of vessel imports ($\underline{\phi}_{ijkt}$):

$$\ln(\overline{\phi}_{ijkt}) = \beta_1 \ln(\underline{\phi}_{ijkt}) + \beta_2 \ln(bunker_t) + \theta_{ijk} + \mu_{ijkt}$$

where, as controls, we also include the average monthly high sulfur bunker fuel cost (USD/tonne) across 400 ports from Clarksons SIN, $bunker_t$ and (HS6 product)-(customs district)-(exporting country) fixed effects.

The results are presented in Table A8. The "pass through" estimate of $\beta_1$ is the primary object of interest. We find it to be 0.021, an economically insignificant figure. For instance, a 5% increase in the average ad-valorem vessel rate in 2019 (from 1.048 to 1.10) would result in a mere 0.011% rise in the average ad-valorem air rate

(from 1.123 to 1.1242). In other words, doubling the vessel freight rate would only lead to a 1% increase in air freight rates. In our analysis, we also include as controls the average monthly high sulfur bunker fuel cost (USD/tonne) across 400 ports from Clarksons SIN, denoted as $bunker_t$, along with (HS6 product)-(customs district)-(exporting country) fixed effects. Our primary focus is the "pass-through" estimate of $\beta_1$. We find it to be 0.021, an economically insignificant figure. To illustrate, a 5% rise in the average ad-valorem vessel rate in 2019 (from 1.048 to 1.10) would trigger just a 0.011% increase in the average ad-valorem air rate (from 1.123 to 1.1242). Simply put, if the vessel freight rate were to double, it would lead to merely a 1% increase in air freight rates.

Table A8: Simple Pass Through Model

| | (1) |
|---|---|
| $\ln(\underline{\phi}_{ijkt})$ | $0.021^{***}$ |
| | $(0.001)$ |
| $\ln(bunker_t)$ | $0.007^{***}$ |
| | $(0.000)$ |
| Num. obs. | $18,849,010$ |
| FE: District $i$ × Country $j$ × HS6 $k$ | $620,230$ |
| $R^2$ | 0.437 |
| Adj. $R^2$ | 0.418 |

$^{***}p < 0.01$; $^{**}p < 0.05$; $^{*}p < 0.1$

## A.7 Deriving Long-run Changes in Ocean and Air Transportation

This section presents a derivation of the long-run changes in air- and ocean-transported imports to the US, denoted as $\underline{\omega}_{ij}^{\text{LR}}$ and $\overline{\omega}_{ij}^{\text{LR}}$, respectively, resulting from the implementation of IMO2023. Our approach utilizes a theoretical model, shipping cost structure, and naval engineering formulas. In accordance with the derivation presented in equation (18) of the main body of the paper, these changes can be expressed as a function of four other changes, namely $\omega_{K_i}^{\text{LR}}$, $\underline{\omega}_{P}^{\text{LR}}$, $\overline{\omega}_{P}^{\text{LR}}$, and $\omega_{v}^{\text{LR}}$. As in the short-run analysis, we will assume the air-freight rate change to be proportional to the ocean-freight change as defined by equation (17).

### A.7.1 Setup

Assume a representative vessel type for route $ij$. Fuel cost per trip for such a vessel moving at speed $s_{ij}$ is:

$$\text{Fuel cost per trip per vessel}(s_{ij}) = \underbrace{\left[F^{\text{Main}}\left(\frac{s_{ij}}{s_v^{\text{Des}}}\right)^3 + F^{\text{Aux}}\right]\frac{d_{ij}}{s_{ij}}}_{=\text{Fuel consumption (ton)}} \times \underbrace{b}_{=\text{Bunker price (per ton)}}$$

Adopting hat notation such that $\widehat{x} = x'/x$, denote relative fuel cost per trip as:

$$\widehat{\text{Fuel}}_{ij}(\widehat{s}_{ij}) = \widehat{b}\left[\frac{F^{\text{Main}}\left(\frac{\widehat{s}_{ij}s_{ij}}{s_v^{\text{Des}}}\right)^3 + F^{\text{Aux}}}{F^{\text{Main}}\left(\frac{s_{ij}}{s_v^{\text{Des}}}\right)^3 + F^{\text{Aux}}}\right]\frac{1}{\widehat{s}_{ij}}$$

We assume that non-fuel expenses are proportional to total route time. Changes in trip time are inversely proportional to the change in round trips. If the number of round trips per year (e.g. the number voyages) at speed $s_{ij}$ is $n_{ij} = \frac{A}{2(d_{ij}/(24s_{ij})+port)} = \frac{A}{2(\text{Route time}_{ij})}$ and if we also allow for port congestion, then:

$$\widehat{n}_{ij}(\widehat{s}_{ij};\underline{\omega}_{ij}^{LR}) = \widehat{s}_{ij}\left(\frac{d_{ij}+24s_{ij}\overline{\text{port}}}{d_{ij}+24\widehat{s}_{ij}s_{ijt}\overline{\text{port}}(\underline{\omega}_{ij}^{LR})^{\kappa}}\right) = \frac{1}{\widehat{\text{Route time}}(\widehat{s}_{ij};\underline{\omega}_{ij}^{LR})} \tag{A23}$$

Since changes in the number of round trips are inversely proportional to round-trip time, changes in our preference parameter $\nu$ can be written compactly by:

$$\omega_{\nu}^{LR} = \frac{\nu_{ij}^{LR}}{\nu_{ij}} = \left(\frac{1}{\widehat{n}_{ij}(\widehat{s}_{ij};\underline{\omega}_{ij}^{LR})}\right)^{-\beta_k} \tag{A24}$$

Assuming that $k_0 = \frac{1-\mu_{\text{Fuel}}}{\mu_{\text{Fuel}}}$ and that bunker fuel doesn't change, we can write the relative change to marginal cost as:

$$\begin{aligned}
\widehat{c}_{ij}(\widehat{s}_{ij};\underline{\omega}_{ij}^{LR}) =& \frac{\widehat{\text{Fuel}}_{ij}\times\text{Fuel}_{ij}+\widehat{\text{Other}}_{ij}\times\text{Other}_{ij}}{\text{Fuel}_{ij}+\text{Other}_{ij}} \\
=& \frac{\widehat{\text{Fuel}}_{ij}\times\text{Fuel}_{ij}+\widehat{\text{Other}}_{ij}\times k_0\text{Fuel}_{ij}}{\text{Fuel}_{ij}(1+k_0)} \\
=& \frac{1}{k_0+1}\left(\widehat{\text{Fuel}}_{ij}\times\widehat{\text{Other}}_{ij}k_0\right) \\
=& \frac{1}{k_0+1}\left(\left[\frac{F^{\text{Main}}\left(\frac{\widehat{s}_{ij}s_{ij}}{s_v^{\text{Des}}}\right)^3+F^{\text{Aux}}}{F^{\text{Main}}\left(\frac{s_{ij}}{s_v^{\text{Des}}}\right)^3+F^{\text{Aux}}}\right]\frac{1}{\widehat{s}_{ij}}+\frac{k_0}{\widehat{n}_{ij}(\widehat{s}_{ij};\underline{\omega}_{ij}^{LR})}\right) \\
=& \mu_{\text{Fuel}}\left(\left[\frac{F^{\text{Main}}\left(\frac{\widehat{s}_{ij}s_{ij}}{s_v^{\text{Des}}}\right)^3+F^{\text{Aux}}}{F^{\text{Main}}\left(\frac{s_{ij}}{s_v^{\text{Des}}}\right)^3+F^{\text{Aux}}}\right]\frac{1}{\widehat{s}_{ij}}\right)+\frac{(1-\mu_{\text{Fuel}})}{\widehat{n}_{ij}(\widehat{s}_{ij};\underline{\omega}_{ij}^{LR})}
\end{aligned} \tag{A25}$$

We know from earlier that:

$$\underline{f}_{ij} = c_{ij}+\frac{c_{ij}+\underline{p}_{ij}\underline{\tau}_{ij}}{n_{ij}\sigma-1} \implies \underline{f}_{ij}+\underline{p}_{ij}\underline{\tau}_{ij} = \frac{N_{ij}\sigma(c_{ij}+\underline{p}_{ij}\underline{\tau}_{ij})}{N_{ij}\sigma-1}$$

Therefore we can write:

$$\underline{\omega}_{P}^{LR} = \frac{\underline{f}_{ij}^{LR}+\underline{p}_{ijt}\underline{\tau}_{ijt}}{\underline{f}_{ijt}+\underline{p}_{ijt}\underline{\tau}_{ijt}} = \frac{\sigma^{LR}(N_{ij}\sigma-1)}{\sigma(N_{ij}\sigma^{LR}-1)}\times\frac{\widehat{c}_{ij}(\widehat{s}_{ij};\underline{\omega}_{ij}^{LR})c_{ij}+\underline{p}_{ij}\underline{\tau}_{ij}}{c_{ij}+\underline{p}_{ij}\underline{\tau}_{ij}} \tag{A26}$$

given:

$$\sigma^{LR} = \varepsilon \left( 1 + \frac{(\varepsilon - 1)\omega_{\nu}^{LR} \nu_{ij} [\underline{\omega}_{ij}^{LR} \underline{q}_{ij}]^{\frac{\varepsilon-1}{\varepsilon}}}{\sum_j \left( \omega_{\nu}^{LR} \nu_{ij} [\underline{\omega}_{ij}^{LR} \underline{q}_{ij}]^{\frac{\varepsilon-1}{\varepsilon}} + [\overline{\omega}_{ij}^{LR} \overline{q}_{ij}]^{\frac{\varepsilon-1}{\varepsilon}} \right)} \right)^{-1} \tag{A27}$$

Changes in air freight rates come from:

$$\underline{\omega}_f^{LR} = \frac{\underline{f}_{ij}^{LR}}{\underline{f}_{ij}} = \frac{N_{ij}\sigma^{LR}\widehat{c}_{ij}(\widehat{s}_{ij}; \underline{\omega}_{ij}^{LR})c_{ij} + \underline{p}_{ij}\underline{\tau}_{ij}}{N_{ij}\sigma c_{ij} + \underline{p}_{ij}\underline{\tau}_{ij}} \times \frac{N_{ij}\sigma - 1}{N_{ij}\sigma^{LR} - 1} \implies \overline{\omega}_f^{LR} = \zeta(\underline{\omega}_f^{LR} - 1) + 1$$

So changes in air delivered prices is given by:

$$\overline{\omega}_P^{LR} = \frac{\overline{\omega}_f^{LR}\overline{f}_{ij} + \overline{p}_{ij}\overline{\tau}_{ij}}{\overline{f}_{ij} + \overline{p}_{ij}\overline{\tau}_{ij}} \tag{A28}$$

Finally, we can write changes in container capacity via:

$$\underline{\omega}_{ij}^{LR} = \frac{\underline{q}_{ijt}^{LR}}{\underline{q}_{ijt}} = \left(\frac{\nu_{ij}^{LR}}{\nu_{ijt}}\right)^{\varepsilon} \left(\frac{K_i}{K_i^{LR}}\right)^{\varepsilon} \left(\frac{\underline{f}_{ij}^{LR} + \underline{p}_{ijt}\underline{\tau}_{ijt}}{\underline{f}_{ijt} + \underline{p}_{ijt}\underline{\tau}_{ijt}}\right)^{-\varepsilon} = (\omega_{\nu}^{LR})^{\varepsilon} \times (\omega_{K_i}^{LR})^{-\varepsilon} \times (\underline{\omega}_p^{LR})^{-\varepsilon} \tag{A29}$$

And correspondingly, changes for air capacity are

$$\overline{\omega}_{ij}^{LR} = \frac{\overline{q}_{ij}^{LR}}{\overline{q}_{ijt}} = \left(\frac{K_i}{K_i^{LR}}\right)^{\varepsilon} \left(\frac{\overline{f}_{ij}^{LR} + \overline{p}_{ijt}\overline{\tau}_{ijt}}{\overline{f}_{ijt} + \overline{p}_{ijt}\overline{\tau}_{ijt}}\right)^{-\varepsilon} = (\omega_{K_i}^{LR}\overline{\omega}_P^{LR})^{-\varepsilon} \tag{A30}$$

### A.7.2 Solving for long-run or Alternative Policy Equilibrium

We use the following algorithm to solve for long-run changes brought on my IMO2023 as well as alternative policies. We initially choose change in route speed $\widehat{s}_{ij}$ in accordance to an IMO carbon efficiency standard. Alternatively, we can set container/air subsidy/tax multipliers $\boldsymbol{\psi} = (\underline{\psi}, \overline{\psi})$.

1. Place a guess on $\underline{\omega}_{ij}^{LR,N}$. This allows us to calculate $\widehat{n}_{ij}(\widehat{s}_{ij}; \underline{\omega}_{ij}^{LR,N})$ , which in turn drives our calculation of $\omega_{\nu}(\widehat{s}_{ij}; \underline{\omega}_{ij}^{LR,N})$ via (A24) and our calculation of $\widehat{c}_{ij}(\widehat{s}_{ij}; \underline{\omega}_{ij}^{LR,N})$ via equation (A25).

2. Knowing changes in marginal cost allows to calculate changes in container delivered price $\underline{\omega}_p$ via equation (A26) and changes in air delivered price $\overline{\omega}_p$ via equation (A28). If the alternative scenario involves container subsidies and/or air taxes, we still use equations (A26) and (A28) to calculate changes in container and air delivered prices, respectively. New $K_{it}$ is equal to:

$$\begin{aligned} K_i^{LR} =& \frac{1-\mu}{\mu} \sum_j \nu_{ij}^{LR} [\underline{q}_{ij}^{LR}]^{\frac{\varepsilon-1}{\varepsilon}} + [\overline{q}_{ij}^{LR}]^{\frac{\varepsilon-1}{\varepsilon}} \\ =& \frac{1-\mu}{\mu} \sum_j \omega_{\nu}^{LR}(\widehat{s}_{ij}; \underline{\omega}_{ij}^{LR,N}) \nu_{ij} [\omega_{\nu}^{LR}(\widehat{s}_{ij}; \underline{\omega}_{ij}^{LR,N})^{\varepsilon} \widehat{K}_i^{-\varepsilon} (\underline{\omega}_P^{LR})^{-\varepsilon} \underline{q}_{ijt}]^{\frac{\varepsilon-1}{\varepsilon}} + [\widehat{K}_i^{-\varepsilon} (\overline{\omega}_P^{LR})^{-\varepsilon} \overline{q}_{ijt}]^{\frac{\varepsilon-1}{\varepsilon}} \end{aligned}$$

which implies that:

$$\omega_{K_i}^{LR} = (\omega_{K_i}^{LR})^{1-\varepsilon} \frac{\sum_j \omega_v^{LR}(\widehat{s}_{ij}; \underline{\omega}_{ij}^{LR,N})^{\varepsilon} \nu_{ijt} \underline{\omega}_P^{LR}(\widehat{s}_{ij}, \underline{\psi}; \underline{\omega}_{ij}^{LR,N})^{1-\varepsilon} [\underline{q}_{ijt}]^{\frac{\varepsilon-1}{\varepsilon}} + \overline{\omega}_P^{LR}(\widehat{s}_{ij}, \overline{\psi}; \underline{\omega}_{ij}^{LR,N})^{1-\varepsilon} [\overline{q}_{ijt}]^{\frac{\varepsilon-1}{\varepsilon}}}{\sum_j \nu_{ijt} [\underline{q}_{ijt}]^{\frac{\varepsilon-1}{\varepsilon}} + [\overline{q}_{ijt}]^{\frac{\varepsilon-1}{\varepsilon}}}$$

and further that:

$$(\omega_{K_i}^{LR})^{-\varepsilon} = \frac{\sum_j \nu_{ijt} [\underline{q}_{ijt}]^{\frac{\varepsilon-1}{\varepsilon}} + [\overline{q}_{ijt}]^{\frac{\varepsilon-1}{\varepsilon}}}{\sum_j \omega_v^{LR}(\widehat{s}_{ij}; \underline{\omega}_{ij}^{LR,N})^{\varepsilon} \nu_{ijt} \underline{\omega}_P^{LR}(\widehat{s}_{ij}, \underline{\psi}; \underline{\omega}_{ij}^{LR,N})^{1-\varepsilon} [\underline{q}_{ijt}]^{\frac{\varepsilon-1}{\varepsilon}} + \overline{\omega}_P^{LR}(\widehat{s}_{ij}, \overline{\psi}; \underline{\omega}_{ij}^{LR,N})^{1-\varepsilon} [\overline{q}_{ijt}]^{\frac{\varepsilon-1}{\varepsilon}}} \tag{A31}$$

$\widehat{K}_{it}^{-\varepsilon}$ depends on current guess of $\underline{\omega}_{ij}^{LR,N}$ through changes in delivered prices.

3. Use equation (A29) to compute changes in container volume:

$$\underline{\omega}_{ij}^{LR,N'} = \widehat{v}_{ij}(\widehat{s}_{ij})^{\varepsilon} \omega_{K_i}^{LR}(\widehat{s}_{ij}, \psi; \underline{\omega}_{ij}^{LR,N})^{-\varepsilon} \underline{\omega}_p(\widehat{s}_{ij}, \underline{\psi}; \underline{\omega}_{ij}^{LR,N})^{-\varepsilon}$$

Check that for some sufficiently small $\delta_1$ that:

$$\frac{\sum_{ij} \underline{q}_{ijt} |\underline{\omega}_{ij}^{LR,N'} - \underline{\omega}_{ij}^{LR,N}|}{\sum_j \underline{q}_{ijt} \underline{\omega}_{ij}^{LR,N}} < \delta_1$$

If no, move outer iteration counter forward to $N = N + 1$, set $\underline{\omega}_{ij}^{LR,N+1} = \underline{\omega}_{ij}^{LR,N'}$, and repeat until convergence. If yes, then we've found our solution and use equation (A30) to compute changes in air traffic.

### A.7.3 Alternative Policy: New Technology

Suppose for a given route that there is an increase in speed but that fuel consumption per trip remains constant. Let $\lambda_{ij}$ be a technology that improves the fuel efficiency of a ship such that $\lambda_{ij}$ satisfies:

$$\left[F^{\text{Main}}\left(\frac{s_{ij}}{s_v^{\text{Des}}}\right)^3 + F^{\text{Aux}}\right] \frac{d_{ij}}{s_{ij}} = \left[F^{\text{Main}}\left(\frac{s'_{ij}}{s_v^{\text{Des}}}\right)^3 + F^{\text{Aux}}\right]^{\lambda_{ij}} \frac{d_{ij}}{s'_{ij}}$$

where $s'_{ij}$ is a new given speed. Assuming that $s'_{ij} = \rho s_{ij}$, we can formulate this technology as:

$$\lambda_{ij}(\rho) = \frac{\log(\rho) + \log\left(F^{\text{Main}}\left(s_{ij}/s_v^{\text{Des}}\right)^3 + F^{\text{Aux}}\right)}{\log\left(F^{\text{Main}}\left((\rho s_{ij})/s_v^{\text{Des}}\right)^3 + F^{\text{Aux}}\right)}$$

## A.8 Calibrating Marginal Costs

We take our freight rate formula and invert it to express marginal costs as function of observables and import demand elasticity:

$$c_{ij} = \frac{\underline{f}_{ij}(N_{ij}\sigma - 1) - \underline{p}_{ij}\underline{\tau}_{ij}}{N_{ij}\sigma} \tag{A32}$$

We turn to BlueWater data to come up with estimates for the number of carriers $N_{ij}$. There are two problems we have to overcome when using (A32) to measure marginal costs.

1. **Missing carrier data**. We use BlueWater Reporting data to calculate the number of carriers per route. The table below shows that there is modest overlap between BlueWater and U.S. Census data routes when it comes to carrier data: a mere 22%. However, looking at the total share of traffic, this overlap increases to over 75%.

| Carrier-Route Status | Traffic Share (%) | Frequency Share (%) |
|---|---|---|
| Observed | 75.6 | 22.4 |
| Country | 13.5 | 25.8 |
| All Routes | 6.3 | 22.0 |
| District | 4.6 | 29.7 |

   We adopt the following imputation strategy: (i) if a U.S. Census route is found in BlueWater, we use observed carrier counts; (ii) if a U.S. Census route is NOT found in BlueWater AND we can calculate the median number of carriers per U.S. Customs district $i$ AND country $j$ OR we can only calculate the median number of carriers per country $j$, we impute the median carrier count per country $j$; (iii) if a U.S. Census route is NOT found in BlueWater AND we can only calculate the median carrier per U.S. Customs District $i$, we impute the median carrier count per U.S. Customs District $i$; and, (iv) otherwise, we impute the median number of carriers.

2. **Negative marginal costs**. Equation (A32) implies that the number of carriers on a route must satisfy $N_{ij} > (\underline{p}_{ij}\underline{\tau}_{ij} + \underline{f}_{ij})/(\sigma \underline{f}_{ij})$ to ensure positive marginal costs. From a frequency standpoint, we calculate positive marginal costs for more than half our routes. As with before, if we instead adjust by route traffic volume, we calculate positive marginal costs for more than 80% of routes. Table A9 reports the traffic/frequency share of positive/negative marginal costs by carrier-route.

Table A9: Marginal Cost Sign Table

| Positive marginal cost? | Carrier-Route Status | Traffic Share (%) | Frequency Share (%) |
|---|---|---|---|
| Yes | | **82.6** | **62.6** |
| | Observed | 67.6 | 14.2 |
| | Country | 9.3 | 15.6 |
| | District | 3.2 | 17.0 |
| | All Routes | 2.5 | 15.8 |
| No | | **17.4** | **37.4** |
| | Observed | 8.0 | 8.2 |
| | Country | 4.2 | 10.2 |
| | All Routes | 3.9 | 6.3 |
| | District | 1.3 | 12.7 |

We eliminate negative marginal costs by looking at the route-traffic weighted average markup for positive marginal cost routes, namely $\alpha_0$. We then use this markup to scale freight rates to back out marginal costs.

$$\alpha_0 = \frac{\sum_{ij}\left(\frac{\underline{f}_{ij}-c_{ij}}{\underline{f}_{ij}}\right)\mathbb{1}\{c_{ij}>0\}\underline{q}_{ij}}{\sum_{ij}\mathbb{1}\{c_{ij}>0\}q_{ij}} \implies c_{ij} = \begin{cases} \frac{\underline{f}_{ij}(N_{ij}\varepsilon-1)-\underline{p}_{ij}\underline{\tau}_{ij}}{N_{ij}\varepsilon} & \text{if } N_{ij} > \frac{\underline{p}_{ij}\underline{\tau}_{ij}+\underline{f}_{ij}}{\varepsilon \underline{f}_{ij}} \\ (1-\alpha_0)\underline{f}_{ij} & \text{otherwise} \end{cases}$$

In practice, we calculate $\alpha_0 = 0.402$. Our distribution of marginal costs (per kilogram) are plotted below in Figure A7:[54]

[54]Our calibration of $c_{ij}$ depends on our estimate of $\varepsilon$. Figure A7 presents the distribution of marginal costs assuming our OLS estimate of $\widehat{\varepsilon} = 7.3$. Our marginal cost distribution using our IV $\widehat{\varepsilon} = 10.3$ is qualitatively similar.

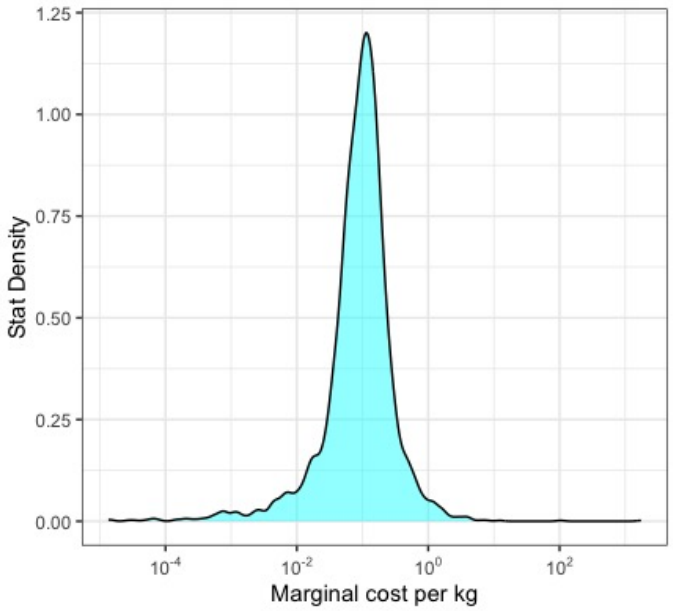


Figure A7: Marginal cost ($c_{ij}$) Distribution

## A.9 Data Analysis of Shipping Speed and Route Stability

When analyzing IMO2023, we assume that routes are stable and will not be affected by the reform. In this section, we provide support for this assumption through the distribution of two types of route stability measures. The first measure is the **route-specific coefficient of variation of ports** which is calculated as the ratio of the standard deviation of number of ports to the average number of ports. The higher the measure, the more (relatively) disperse the number of ports are on a given route.

The second route stability measure, **"Port share,"** is defined as the average number of ports used by a given route in a given month, normalized by the total number of ports that the route ever uses. The formula to calculate it is:

$$\frac{1}{|T_i||n_i|}\sum_{t_i \in T_i} n_i(t)$$

Here, $T_i$ is the number of time periods that route $i$ appears, $n_i$ is the list of all ports ever used by route $i$, and $n_i(t)$ is the number of ports used by rotation $i$ for month $t$. A score of zero (one) means no (perfect) port overlap for a given route.

Table A10 lists our stability results. The average port share of roughly 60% suggests that on average, each route uses 60% of its total ports in a given month. This indicates that, at least on a short-term basis, the routes are relatively stable and not subject to significant changes. The coefficient of variation, which measures the dispersion of the number of ports used by a route, is close to 20%, indicating that there is some variability in the number of ports used by different routes, but overall the routes remain relatively stable.

Table A10: Route Stability Measures

| Stat | Port Coefficient of Variation | Port Share |
|---|---|---|
| Min. | 0.0% | 15.4% |
| 1st Qu. | 6.9 | 43.5 |
| (I) | 16.5 | 54.3 |
| Mean | 19.4 | 59.5 |
| 3rd Qu. | 28.7 | 73.6 |
| Max. | 105.3 | 100.0 |

## A.10 Algorithm I's Proofs of Existence and Uniqueness

In this section, we will initially establish a series of preliminary Lemmas before proceeding to the proofs of existence and uniqueness. We aim to demonstrate that our method of calculating $\omega_{K_i}$ yields a unique result. If we assume away substitution from ocean to air transportation and fix the quantity transported by air, determining $\omega_{K_i}$ is straightforward. Instead, when we allow for such substitution, the proof of uniqueness is required.

### A.10.1 Rearranging and redefing key model objects

We begin with reminding and rearranging the definitions of $\omega_{K_i}$, $\overline{\omega}_{ij}(\omega_{K_i})$, and $\underline{\omega}_p(\omega_{K_i})$.

$$\omega_{K_i} = \frac{\sum_{j=1}^{n} \omega_v \nu_{ij} [\underline{\omega}_{ij} \underline{q}_{ij}]^{\frac{\varepsilon-1}{\varepsilon}} + [\overline{\omega}_{ij}(\omega_{K_i}) \overline{q}_{ij}]^{\frac{\varepsilon-1}{\varepsilon}}}{\sum_{j=1}^{n} \nu_{ij} \underline{q}_{ij}^{\frac{\varepsilon-1}{\varepsilon}} + \overline{q}_{ij}^{\frac{\varepsilon-1}{\varepsilon}}} = \frac{\sum_{j=1}^{n} \omega_v \nu_{ij} [\underline{\omega}_{ij} \underline{q}_{ij}]^{\frac{\varepsilon-1}{\varepsilon}}}{\sum_{j=1}^{n} \nu_{ij} \underline{q}_{ij}^{\frac{\varepsilon-1}{\varepsilon}} + \overline{q}_{ij}^{\frac{\varepsilon-1}{\varepsilon}}} + \frac{\sum_{j=1}^{n} [\overline{\omega}_{ij}(\omega_{K_i}) \overline{q}_{ij}]^{\frac{\varepsilon-1}{\varepsilon}}}{\sum_{j=1}^{n} \nu_{ij} \underline{q}_{ij}^{\frac{\varepsilon-1}{\varepsilon}} + \overline{q}_{ij}^{\frac{\varepsilon-1}{\varepsilon}}} \tag{A33}$$

from which, only the second term is a function of $\omega_{K_i}$.

$$\begin{aligned}
\overline{\omega}_{ij}(\omega_{K_i}) =& \overline{\omega}_{K_i}{}^{-\varepsilon} \overline{\omega}_p^{-\varepsilon} \\
=& \overline{\omega}_{K_i}{}^{-\varepsilon} \frac{\overline{\omega}_f \overline{f}_{ijt} + \overline{p}_{ijt} \overline{\tau}_{ijt}}{\overline{f}_{ijt} + \overline{p}_{ijt} \overline{\tau}_{ijt}} \\
=& \overline{\omega}_{K_i}{}^{-\varepsilon} \left( \frac{\overline{f}_{ijt}}{\overline{f}_{ijt} + \overline{p}_{ijt} \overline{\tau}_{ijt}} \left( \zeta(\underline{\omega}_f - 1) + 1 \right) + \frac{\overline{p}_{ijt} \overline{\tau}_{ijt}}{\overline{f}_{ijt} + \overline{p}_{ijt} \overline{\tau}_{ijt}} \right) \\
=& \overline{\omega}_{K_i}{}^{-\varepsilon} \left( \frac{\overline{f}_{ijt}}{\overline{f}_{ijt} + \overline{p}_{ijt} \overline{\tau}_{ijt}} \left( \zeta \left( \frac{\underline{\omega}_p(\omega_{K_i})(\underline{f}_{ijt} + \underline{p}_{ijt} \underline{\tau}_{ijt}) - \underline{p}_{ijt} \underline{\tau}_{ijt}}{\underline{f}_{ijt}} - 1 \right) + 1 \right) + \frac{\overline{p}_{ijt} \overline{\tau}_{ijt}}{\overline{f}_{ijt} + \overline{p}_{ijt} \overline{\tau}_{ijt}} \right)
\end{aligned}$$

$$\underline{\omega}_p(\omega_{K_i}) = \underline{\omega}_{ij}{}^{-\frac{1}{\varepsilon}} \times \overline{\omega}_{K_i}{}^{-1} \times \omega_v(\underline{\omega}_{ij}) \tag{A34}$$

Next, we define function $\Phi$ as:

$$\Phi(\omega_{K_i}) \equiv \frac{\sum_{j=1}^{n} \omega_v \nu_{ij} [\underline{\omega}_{ij} \underline{q}_{ij}]^{\frac{\varepsilon-1}{\varepsilon}}}{\sum_{j=1}^{n} \nu_{ij} \underline{q}_{ij}^{\frac{\varepsilon-1}{\varepsilon}} + \overline{q}_{ij}^{\frac{\varepsilon-1}{\varepsilon}}} + \frac{\sum_{j=1}^{n} [\overline{\omega}_{ij}(\omega_{K_i}) \overline{q}_{ij}]^{\frac{\varepsilon-1}{\varepsilon}}}{\sum_{j=1}^{n} \nu_{ij} \underline{q}_{ij}^{\frac{\varepsilon-1}{\varepsilon}} + \overline{q}_{ij}^{\frac{\varepsilon-1}{\varepsilon}}} - \omega_{K_i} \tag{A35}$$

The intuition behind $\Phi$ in (A35) is translating our statement of relative or hat equilibrium objects into a root-finding problem. We take our initial guess of $\omega_{K_i}$ and use our demand functions to recompute the ratio of $K_{it}$ terms (e.g new to old $K_{it}$) as function of this initial guess. If our guess of $\omega_{K_i}$ is correct, then the difference between our guess and our computed ratio of $K_{it}$ terms should be zero; that is $\Phi(\omega_{K_i}) \equiv K'_{it}(\omega_{K_i})/K_{it} - \omega_{K_i} = 0$. If our guess were incorrect, then $\Phi(\omega_{K_i}) > 0$ or $\Phi(\omega_{K_i}) < 0$. Put differently, $g(\omega_{K_i}) = \Phi(\omega_{K_i})^2$ from our initial statement of **Identification Algorithm I**, where in practice we minimize the squared difference of our guess and (demand)functional evaluation of our guess.

Next, we define notational short-hands:

$$\chi_1 = \frac{\overline{f}_{ijt}}{\overline{f}_{ijt} + \overline{p}_{ijt}},$$

$$\chi_2 = \frac{\overline{p}_{ijt}\overline{\tau}_{ijt}}{\overline{f}_{ijt} + \overline{p}_{ijt}\overline{\tau}_{ijt}}$$

$$\gamma_1 = (\underline{f}_{ijt} + \underline{p}_{ijt}\underline{\tau}_{ijt})/\underline{f}_{ijt},$$

and

$$\gamma_2 = \underline{p}_{ijt}\underline{\tau}_{ijt}/\underline{f}_{ijt}.$$

This allows us to write:

$$\begin{aligned}
\overline{\omega}_{ij}(\omega_{K_i}) =& {\omega_{K_i}}^{-(\varepsilon+1)} \left( {\underline{\omega}_{ij}}^{-\frac{1}{\varepsilon}} \omega_v(\underline{\omega}_{ij}) \chi_1 \gamma_1 \zeta \right) + {\omega_{K_i}}^{-\varepsilon} \left( \chi_1 \left( 1 - \zeta(\gamma_2 + 1) \right) + \gamma_2 \right) \\
=& {\omega_{K_i}}^{-\varepsilon} \left( \left( {\underline{\omega}_{ij}}^{-\frac{1}{\varepsilon}} \omega_v(\underline{\omega}_{ij}) \chi_1 \gamma_1 \zeta \right) / \omega_{K_i} + \left( \chi_1 \left( 1 - \zeta(\gamma_2 + 1) \right) + \gamma_2 \right) \right)
\end{aligned}$$

Introduce further shorthand: $\alpha_1 = \sum_{j=1}^{n} \omega_v \nu_{ij} [\underline{\omega}_{ij} \underline{q}_{ij}]^{\frac{\varepsilon-1}{\varepsilon}}$ and $\alpha_2 = \sum_{j=1}^{n} \nu_{ij} \underline{q}_{ij}^{\frac{\varepsilon-1}{\varepsilon}} + \overline{q}_{ij}^{\frac{\varepsilon-1}{\varepsilon}}$. Thus,

$$\Phi(\omega_{K_i}) = \frac{\alpha_1}{\alpha_2} + \frac{\sum_{j=1}^{n} [\overline{\omega}_{ij}(\omega_{K_i}) \overline{q}_{ij}]^{\frac{\varepsilon-1}{\varepsilon}}}{\alpha_2} - \omega_{K_i}$$

And so further:

$$\begin{aligned}
\Phi(\omega_{K_i}) =& \frac{\alpha_1}{\alpha_2} + \frac{1}{\alpha_2} \left( \sum_j \left( {\omega_{K_i}}^{-\varepsilon} \left( \left( {\underline{\omega}_{ij}}^{-\frac{1}{\varepsilon}} \omega_v(\underline{\omega}_{ij}) \chi_1 \gamma_1 \zeta \right) / \omega_{K_i} + \left( \chi_1 \left( 1 - \zeta(\gamma_2 + 1) \right) + \gamma_2 \right) \right) \overline{q}_{ij} \right)^{\frac{\varepsilon-1}{\varepsilon}} \right) - \omega_{K_i} \\
=& \frac{\alpha_1}{\alpha_2} + \frac{1}{\alpha_2 {\omega_{K_i}}^{\varepsilon-1}} \sum_j \left( \left( \frac{{\underline{\omega}_{ij}}^{-\frac{1}{\varepsilon}} \omega_v(\underline{\omega}_{ij}) \chi_1 \gamma_1 \zeta}{\omega_{K_i}} + \left( \chi_1 \left( 1 - \zeta(\gamma_2 + 1) \right) + \gamma_2 \right) \right) \overline{q}_{ij} \right)^{\frac{\varepsilon-1}{\varepsilon}} - \omega_{K_i}
\end{aligned}$$

Let $\Gamma_1 = (\underline{\omega}_{ij}{}^{-\frac{1}{\varepsilon}}\omega_v(\underline{\omega}_{ij})\chi_1\gamma_1\zeta)$ and $\Gamma_2 = (\chi_1(1-\zeta(\gamma_2+1))+\gamma_2)$. Reformulate $\Phi(\omega_{K_i})$ as:

$$\begin{aligned}\Phi(\omega_{K_i}) =& \frac{\alpha_1}{\alpha_2} + \frac{1}{\alpha_2}\sum_j \left(\left(\omega_{K_i}{}^{-(\varepsilon+1)}\Gamma_1 + \omega_{K_i}{}^{-\varepsilon}\Gamma_2\right)\overline{q}_{ij}\right)^{\frac{\varepsilon-1}{\varepsilon}} - \omega_{K_i} \\ =& \frac{\alpha_1}{\alpha_2} + \frac{\omega_{K_i}{}^{1-\varepsilon}}{\alpha_2}\sum_j \left(\left(\frac{\Gamma_1}{\omega_{K_i}} + \Gamma_2\right)\overline{q}_{ij}\right)^{\frac{\varepsilon-1}{\varepsilon}} - \omega_{K_i} \end{aligned} \tag{A36}$$

We define the domain of $\omega_{K_i} \in (0,\infty)$.

### A.10.2 Essential Lemmas and Theorems

Proving that **Identification Algorithm I** admits a solution and that this solution requires us to show that: (i) $\Phi(\omega_{K_i})$ is continuous; (ii) the limiting behavior of $\Phi(\omega_{K_i})$ is such that arbitrarily small (large) values of $\omega_{K_i}$ mean that $\Phi(\omega_{K_i})$ tends towards infinity (negative infinity); and, that (iii) $\Phi(\omega_{K_i})$ is strictly monotone. With these three (3) elements, we can invoke the Intermediate Value Theorem and prove existence and uniqueness. In this section, we focus on proving each of the three (3) core propositions. Section A.10.3 proves a number of background lemmas that support our continuity proposition.

**Theorem 1.** $\Phi(\omega_{K_i}) = \frac{\alpha_1}{\alpha_2} + \frac{\omega_{K_i}{}^{1-\varepsilon}}{\alpha_2}\sum_j \left(\left(\frac{\Gamma_1}{\omega_{K_i}} + \Gamma_2\right)\overline{q}_{ij}\right)^{\frac{\varepsilon-1}{\varepsilon}} - \omega_{K_i}$ *is continuous.*

*Proof.* We will take advantage of each of our Lemmas to prove this result.

1. $1/\omega_{K_i}$ is continuous by Lemma 7.
2. $\Gamma_1/\omega_{K_i}$ is a continuous function since constant function $\Gamma_1$ is continuous by Lemma 6 and the product of continuous functions is a continuous function by Lemma 3.
3. $\Gamma_1/\omega_{K_i} + \Gamma_2$ is a continuous function since constant function $\Gamma_2$ is continuous by Lemma 6 and the sum of continuous functions is a continuous function by Lemma 2.
4. $\left(\frac{\Gamma_1}{\omega_{K_i}} + \Gamma_2\right)\overline{q}_{ij}$ is a continuous function since constant function $\overline{q}_{ij}$ is continuous by Lemma 6 and the sum of continuous functions is a continuous function by Lemma 2.
5. $\left(\left(\frac{\Gamma_1}{\omega_{K_i}} + \Gamma_2\right)\overline{q}_{ij}\right)^{\frac{\varepsilon-1}{\varepsilon}}$ is continuous since a continuous function raised to a real exponent is also a continuous function by Lemma 4.
6. Function
$$\left(\left(\frac{\Gamma_1}{\omega_{K_i}} + \Gamma_2\right)\overline{q}_{i1}\right)^{\frac{\varepsilon-1}{\varepsilon}} + \cdots + \left(\left(\frac{\Gamma_1}{\omega_{K_i}} + \Gamma_2\right)\overline{q}_{in}\right)^{\frac{\varepsilon-1}{\varepsilon}} = \sum_j \left(\left(\frac{\Gamma_1}{\omega_{K_i}} + \Gamma_2\right)\overline{q}_{ij}\right)^{\frac{\varepsilon-1}{\varepsilon}}$$
is continuous since the sum of continuous functions is continuous by Lemma 2.
7. $\frac{\omega_{K_i}{}^{1-\varepsilon}}{\alpha_2}$ is continuous since: $\omega_{K_i}$ is continuous by Lemma 5; $\omega_{K_i}{}^{1-\varepsilon}$ is continuous by Lemma 4; $1/\alpha_2$ is continuous by Lemma 6; and, so $\frac{\omega_{K_i}{}^{1-\varepsilon}}{\alpha_2}$ is continuous by Lemma 3.

8. Function

$$\frac{{\omega_{K_i}}^{1-\varepsilon}}{\alpha_2}\sum_j\left(\left(\frac{\Gamma_1}{\omega_{K_i}}+\Gamma_2\right)\bar{q}_{ij}\right)^{\frac{\varepsilon-1}{\varepsilon}} \tag{A37}$$

is continuous by Lemma 3.

9. Condensing the last steps, we arrive at our desired result by noting that function $\frac{\alpha_1}{\alpha_2}-\omega_{K_i}$ is continuous by Lemmas 6, 5, 3 and 2. Summing together $\frac{\alpha_1}{\alpha_2}-\omega_{K_i}$ with the function represented by equation (A37) yields our desired continuous function, namely $\Phi(\omega_{K_i})$, by Lemma 2.

□

**Lemma 1.** $\lim_{\omega_{K_i}\to 0}\Phi(\omega_{K_i})=\infty$ *and* $\lim_{\omega_{K_i}\to\infty}\Phi(\omega_{K_i})=-\infty$

*Proof.* Consider the limit case where $\omega_{K_i}$ converges to zero. Then,

$$\begin{aligned}\lim_{\omega_{K_i}\to 0}\Phi(\omega_{K_i}) &= \underbrace{\lim_{\omega_{K_i}\to 0}\left(\frac{\alpha_1}{\alpha_2}\right)}_{=\alpha_1/\alpha_2}+\underbrace{\lim_{\omega_{K_i}\to 0}\left(\frac{1}{\alpha_2{\omega_{K_i}}^{\varepsilon-1}}\sum_j\left(\left(\frac{\Gamma_1}{\omega_{K_i}}+\Gamma_2\right)\bar{q}_{ij}\right)^{\frac{\varepsilon-1}{\varepsilon}}\right)}_{=\infty}-\underbrace{\lim_{\omega_{K_i}\to 0}(\omega_{K_i})}_{=0}\\ &=\frac{\alpha_1}{\alpha_2}+\infty\\ &=\infty\end{aligned}$$

Likewise, consider the limit case where $\omega_{K_i}$ tends toward infinity. Then,

$$\begin{aligned}\lim_{\omega_{K_i}\to \infty}\Phi(\omega_{K_i}) &= \underbrace{\lim_{\omega_{K_i}\to \infty}\left(\frac{\alpha_1}{\alpha_2}\right)}_{=\alpha_1/\alpha_2}+\underbrace{\lim_{\omega_{K_i}\to \infty}\left(\frac{1}{\alpha_2{\omega_{K_i}}^{\varepsilon-1}}\sum_j\left(\left(\frac{\Gamma_1}{\omega_{K_i}}+\Gamma_2\right)\bar{q}_{ij}\right)^{\frac{\varepsilon-1}{\varepsilon}}\right)}_{=0}-\underbrace{\lim_{\omega_{K_i}\to \infty}(\omega_{K_i})}_{=-\infty}\\ &=\frac{\alpha_1}{\alpha_2}-\infty\\ &=-\infty\end{aligned}$$

□

Now that we have proved continuity and the limiting behavior for $\Phi(\omega_{K_i})$, we can fully demonstrate solution existence and uniqueness for $\Phi(\omega_{K_i})$.

**Theorem 2.** $\Phi(\omega_{K_i})=0$ *has at least one solution in the interval* $\omega_{K_i}\in(0,\infty)$. *Moreover, this solution is unique.*
***Existence:***

*Proof.* Consider an interval $[a,b]$, where without loss of generality, $0<a<b<\infty$. $\Phi(\omega_{K_i})$ is defined on this interval. By choosing $\omega_{K_i}$ arbitrarily small, Lemma 1 shows that $\Phi(\omega_{K_i})$ tends towards $\infty$. Likewise, by choosing $\omega_{K_i}$ arbitrarily large, Lemma 1 shows that $\Phi(\omega_{K_i})$ tends towards $-\infty$. Moreover, Theorem 1 demonstrates that $\Phi(\omega_{K_i})$ is continuous.
The Intermediate Value Theorem (IVT) states that if $f(x)$ is continuous on $[a,b]$ and that $f(a)<k<f(b)$, then there exists some $c\in(a,b)$ such that $f(c)=k$.
Apply the IVT $\Phi(\omega_{K_i})$ and set $k=0$. Picking $a$ to be arbitrarily small means that $\Phi(a)$ is positive and picking $b$ arbitrarily large means $\Phi(b)$. IVT (or its Bolzano Theorem corollary) guarantees that $\exists c\in(a,b)$ such that $\Phi(b)<\Phi(c)=0<\Phi(a)$. □

***Uniqueness**:*

*Proof.* Demonstrating that $\Phi$ is strictly monotonic (decreasing) is sufficient to show that there at most one $c$ that satisfies $\Phi(c) = 0$ a la Lemma 8. Rewrite $\Phi(\omega_{K_i})$ as:

$$\begin{aligned}\Phi(\omega_{K_i}) =& \frac{\alpha_1}{\alpha_2} + \frac{{\omega_{K_i}}^{1-\varepsilon}}{\alpha_2} \sum_j \left( \left( \frac{\Gamma_1}{\omega_{K_i}} + \Gamma_2 \right) \overline{q}_{ij} \right)^{\frac{\varepsilon-1}{\varepsilon}} - \omega_{K_i} \\ =& \frac{\alpha_1}{\alpha_2} + \frac{{\omega_{K_i}}^{1-\varepsilon}}{\alpha_2} \left( \frac{\Gamma_1}{\omega_{K_i}} + \Gamma_2 \right)^{\frac{\varepsilon-1}{\varepsilon}} \sum_j (\overline{q}_{ij})^{\frac{\varepsilon-1}{\varepsilon}} - \omega_{K_i}\end{aligned}$$

Taking first order conditions with respect to $\omega_{K_i}$ yields:

$$\frac{d\Phi}{d\omega_{K_i}} = \underbrace{-\frac{1}{\alpha_2} \left( (\varepsilon - 1) {\omega_{K_i}}^{-\varepsilon} \left( \frac{\Gamma_1}{\omega_{K_i}} + \Gamma_2 \right)^{\frac{\varepsilon-1}{\varepsilon}} + {\omega_{K_i}}^{1-\varepsilon} \left( \frac{\varepsilon - 1}{\varepsilon} \right) \left( \frac{\Gamma_1}{\omega_{K_i}} + \Gamma_2 \right)^{-\frac{1}{\varepsilon}} \frac{\Gamma_1}{{\omega_{K_i}}^2} \right)}_{<0} - 1 < 0$$

Therefore for all $\omega_{K_i} \in (0, \infty)$, $\frac{d\Phi}{d\omega_{K_i}} < 0$, which means that $\Phi$ is strictly monotone (decreasing). □

### A.10.3 Background Lemmas and Theorems

**Lemma 2.** *The sum of continuous functions is a continuous function.*

*Proof.* Suppose we have two continuous functions $f$ and $g$. Then we know that: $\forall \varepsilon > 0, \exists \delta_f$ such that $0 < |x - a| < \delta_f$ implies $|f(x) - f(a)| < \varepsilon$; and, $\forall \varepsilon > 0, \exists \delta_g$ such that $0 < |x - a| < \delta_g$ implies $|g(x) - g(a)| < \varepsilon$. Note that $a$ is an arbitrary point in the codomain of $f$ and/or $g$. Define $h(x) = f(x) + g(x)$ and $\delta_h = \min\{\delta_f, \delta_g\}$. Then by the continuity of $f$ and $g$, we know that

$$|f(x) - f(a)| < \varepsilon \text{ and } |g(x) - g(a)| < \varepsilon \implies |f(x) - f(a)| + |g(x) - g(a)| < 2\varepsilon$$

By the Triangle Inequality, $|f(x) + g(x) - f(a) - -g(a)| < |f(x) - f(a)| + |g(x) - g(a)|$. Thus,

$$|h(x) - h(a)| = |f(x) + g(x) - f(a) - g(a)| < |f(x) - f(a)| + |g(x) - g(a)| < 2\varepsilon$$

Therefore, $|x - a| < \delta_h \implies |h(x) - h(a)| < \varepsilon$ for $\forall \epsilon > 0$. □

**Lemma 3.** *The product of continuous functions is a continuous function.*

*Proof.* Let $f(x)$ and $g(x)$ be continuous functions. By definition, we know that: $\exists \delta_f > 0$ such that $|x - a| < \delta_f \implies |f(x) - f(a)| < \epsilon_f, \forall \epsilon_f > 0$; and, $\exists \delta_g > 0$ such that $|x - a| < \delta_g \implies |g(x) - g(a)| < \epsilon_g, \forall \epsilon_g > 0$. Define $h(x) = f(x)g(x)$. Trivially, $|h(x) - h(a)| = |f(x)g(x) - f(a)g(a)|$. Expanding this result and applying the triangular inequality yields:

$$\begin{aligned}|f(x)g(x) - f(a)g(a)| =& |f(x)g(x) - f(x)g(a) + f(x)g(a) - f(a)g(a)| \\ =& |f(x)\left(g(x) - g(a)\right) + g(a)\left(f(x) - f(a)\right)| \\ \leq& |f(x)||g(x) - g(a)| + |g(a)||f(x) - f(a)| \\ <& \epsilon_g |f(x)| + \epsilon_f |g(a)|\end{aligned}$$

Without loss of generality, assume $\epsilon_f = \frac{\epsilon}{2|g(a)|+1} < \frac{\epsilon}{2}$ for any $\epsilon > 0$. With this $\epsilon_f$, we can show that $\epsilon_f|g(a)| = \frac{\epsilon|g(a)|}{2|g(a)|+1} < \frac{\epsilon}{2}$ Now pick some $\delta_b$ such that $|x-a| < \delta_b \implies |f(x)-f(a)| < \epsilon$. By the (reverse) triangular inequality, we know that:

$$|f(x)| - |f(a)| \leq |f(x) - f(a)| < \epsilon \implies |f(x)| < |f(a)| + \epsilon$$

So we know then that $|f(x)| < |f(a)| + \epsilon \implies \epsilon_g|f(x)| < \epsilon_g(|f(a)| + \epsilon)$. Define $\epsilon_g = \frac{\epsilon}{2(\epsilon+|f(a)|)}$. This implies that $\epsilon_g(|f(a)| + \epsilon) = \frac{\epsilon(|f(a)|+\epsilon)}{2(\epsilon+|f(a)|)} = \frac{\epsilon}{2}$. To recap, we have shown that:

$$|h(x) - h(a)| = |f(x)g(x) - f(a)g(a)| < \epsilon_g|f(x)| + \epsilon_f|g(a)| < \frac{\epsilon}{2} + \frac{\epsilon}{2} = \epsilon$$

Finally, if we choose some $\delta$ that satisfies $0 < \delta < \min\{\delta_f, \delta_g, \delta_b\}$, then $|x-a| < \delta \implies |h(x) - h(a)| < \epsilon$ for $\forall \epsilon > 0$. □

**Lemma 4.** *If $f(x)$ is a continuous function, then for any $b \in \mathbb{R}$, $g(x) = f(x)^b$ is also continuous for any real exponent $b$.*

*Proof.* Define a sequence $x_n$ that converges to $c \in \mathbb{R}$, that is $\lim_{n\to\infty} x_n = c$. Since $f(x)$ is continuous, we know that:

$$\lim_{n\to\infty} \{f(x_i)\}_{i=1}^n = f(c)$$

Now define function $g(x) = f(x)^b$. Consider a sequence $\{g(x_i)\}_{i=1}^n$, and for notational simplicity let $f(x_n) = \{f(x_i)\}_{i=1}^n$ and $g(x_n) = \{g(x_i)\}_{i=1}^n$ Using limit properties,

$$\lim_{n\to\infty} g(x_n) = \lim_{n\to\infty} \left[f(x_n)^b\right] = \left[\lim_{n\to\infty} f(x_n)\right]^b = f(c)^b = g(c)$$

Since our choice of $c$ was arbitrary, we have proved that $g(x) = f(x)^b$ is continuous. □

**Lemma 5.** *$f(x) = x$ is continuous.*

*Proof.* Consider $|x-a| < \epsilon$ for arbitrary $\epsilon > 0$ and $\forall a \in \mathbb{R}$. Set $\delta = \epsilon > 0$. Then

$$|x-a| < \delta \iff 0 < |f(x) - f(a)| = |x-a| < \delta = \epsilon$$

Thus we have found a $\delta > 0$ such that $|x-a| < \delta \implies |f(x) - f(a)| < \epsilon, \forall \epsilon > 0$. □

**Lemma 6.** *Constant functions are continuous*

*Proof.* Let $f(x) = k$ and choose any $\epsilon > 0$. For any $a$, we have $|f(x) - f(a)| = |k-k| = 0 < \epsilon$. Thus, $\forall \delta > 0$, $|x-a| < \delta \implies |f(x) - f(a)| < \epsilon, \forall \epsilon > 0$.

□

**Lemma 7.** *$f(x) = \frac{1}{x}$ is continuous $\forall x \in (0, \infty)$.*

*Proof.* Pick any $c \in (0, \infty)$. Suppose that $x > c/2$ : this implies that $\frac{1}{xc} < \frac{2}{c^2}$. Further, we may write that:

$$\left|\frac{1}{x} - \frac{1}{c}\right| = \frac{|x-c|}{xc} < \frac{2}{c^2}$$

Choose $\delta < \min\{\frac{c^2\epsilon}{2}, \frac{c}{2}\}$. Then $|x-c| < \delta$ implies:

$$\frac{|x-c|}{xc} < \frac{\delta}{xc} < \frac{2}{c^2}\delta$$

Suppose that $\frac{c^2\epsilon}{2} > \frac{c}{2}$. This implies that $\epsilon > 1/c$. Thus:

$$|f(x) - f(c)| = |\frac{1}{x} - \frac{1}{c}| = \frac{|x-c|}{xc} < \frac{\delta}{xc} < \frac{2}{c^2}\delta < \frac{2}{c^2}\frac{c}{2} = \frac{1}{c} < \epsilon$$

Now suppose that $\frac{c^2\epsilon}{2} < \frac{c}{2}$. Then:

$$|f(x) - f(c)| = |\frac{1}{x} - \frac{1}{c}| = \frac{|x-c|}{xc} < \frac{\delta}{xc} < \frac{2}{c^2}\delta < \frac{2}{c^2}\frac{c^2}{2}\epsilon < \epsilon$$

Thus $\exists\delta > 0$ such that $|x-c| < \delta$ implies $|f(x) - f(c)| < \epsilon$ for any $\epsilon > 0$.
Alternatively, if we reformulate our function as $f(x) = x^a$, we can appeal Lemma 4 and set $a = -1$. □

**Lemma 8.** *A continuous, strictly monotone decreasing function $f(x)$ has at most one solution to $f(c) = k$.*

*Proof.* By definition of strictly monotone decreasing function, $a < b \implies f(a) > f(b)$. Since $f$ is continuous, the Intermediate Value Theorem (IVT) applies, so we know that there is a least one $c \in (a, b)$ such that $f(b) < f(c) < f(a)$ and that $f(c) = k$
Suppose that $c$ is not unique and that we have, $a < c_1, c_2 < b \implies (b) < f(c_1) = f(c_2) = k < f(a)$ and that $c_1 \neq c_2$. Without loss of generality, suppose that $c_1 < c_2$. Then by definition of strictly monotone decreasing function, $c_1 < c_2 \implies f(c_1) > f(c_2)$. However, we have already stated that $f(c_1) = k$ and that $f(c_2) = k$, so $f(c_1) > f(c_2) \iff k > k$ is a contradiction. Therefore $c$ is unique. □

## A.11 Additional Model Results

Table A11: Short Run IMO2023 Results (IV $\varepsilon = 10.3$)

| **Scenario** | (1) | (2) | (3) | (4) | (5) | (6) |
|---|---|---|---|---|---|---|
| Adjust $\nu$? | | No | | | Yes | |
| Air Pass Through ($\zeta$) | 0 | 1/6 | 0 | 0 | 1/6 | 0 |
| %Δ Container Capacity | -5.87 | -5.87 | -5.87 | -5.87 | -5.87 | -5.87 |
| %Δ Air Capacity | 0.00 | 34.50 | 40.78 | 0.00 | 35.99 | 42.23 |
| %Δ Container Freight Rates | 142.75 | 113.77 | 107.18 | 142.95 | 112.61 | 106.05 |
| %Δ Air Freight Rates | 0.00 | 18.07 | 0.00 | 0.00 | 17.54 | 0.00 |
| %Δ Container Emissions | -16.47 | -16.47 | -16.47 | -16.47 | -16.47 | -16.47 |
| %Δ Air Emissions | 0.00 | 35.23 | 40.97 | 0.00 | 36.71 | 42.44 |
| Net %Δ $CO_2$ | -4.63 | 20.71 | 24.84 | -4.63 | 21.77 | 25.89 |
| Net Δ $CO_2$ (mln ton) | -2.42 | 10.85 | 13.02 | -2.42 | 11.41 | 13.57 |
| Net Δ Welfare (mln USD) | -4500 | -3475 | -3343 | -4643 | -3576 | -3447 |
| Net Δ $CO_2$ Welfare (mln USD) | 97 | -434 | -521 | 97 | -456 | -543 |
| Net Δ Consumer Surplus (mln USD) | -4597 | -3041 | -2822 | -4740 | -3119 | -2905 |
| Welfare Neutral Carbon Price (USD/ton) | 1857 | NA | NA | 1915 | NA | NA |

Table A12: Long-Run IMO Scenarios (IV $\varepsilon = 10.3$)

*Note*: Two long-run outcomes are presented below. "2023 Standards" consider long-run outcomes with IMO 2023 standards, which are 95% of the IMO's 2019 reference line. Likewise, "2026 Standards" consider long-run outcomes which are 89% of the IMO's 2019 reference line. We assume that fuel costs make up 30% of ship's marginal costs and that $\nu$ adjusts to changes in speed.

| **Scenario** | (1) | (2) | (3) | (4) |
|---|---|---|---|---|
| Standards | 2023 | | 2026 | |
| Air Pass Through ($\zeta$) | 0 | 1/6 | 0 | 1/6 |
| %Δ Container Capacity | 0.00 | 0.01 | -0.05 | -0.05 |
| %Δ Round-Trips per Vessel | 5.56 | 5.56 | 10.56 | 10.56 |
| %Δ Round-Trips per Vessel | -5.26 | -5.26 | -9.60 | -9.60 |
| %Δ Air Capacity | 0.43 | 0.39 | 0.79 | 0.69 |
| %Δ Container Freight Rates | 0.46 | 0.46 | 1.24 | 1.24 |
| %Δ Air Freight Rates | 0.00 | 0.07 | 0.00 | 0.21 |
| %Δ Container Emissions | -11.37 | -11.37 | -18.06 | -18.05 |
| %Δ Air Emissions | 0.39 | 0.35 | 0.74 | 0.65 |
| Net %Δ Emissions | -2.92 | -2.94 | -4.54 | -4.61 |
| Net Δ Emissions (mln tons) | -1.48 | -1.49 | -2.30 | -2.34 |
| Net Δ Welfare (mln USD) | -255 | -256 | -520 | -522 |
| Net Δ $CO_2$ Welfare (mln USD) | 59 | 60 | 92 | 93 |
| Net Δ Consumer Surplus (mln USD) | -314 | -316 | -612 | -615 |
| Welfare Neutral Carbon Price (USD/ton) | 173 | 172 | 226 | 223 |

Table A13: Long-Run Alternative Policies (IV $\varepsilon = 10.3$)

*Note*: All scenario results assume that $\nu$ changes with respect to changes in round-trip time. We calculate subsidy(tax) rates by solving for $\underline{\psi}$ ($\overline{\psi}$) that delivers the same long-run change in net emissions as the appropriate IMO2023 scenario; we use our long-run code to solve for equilibrium given $\underline{\psi}\underline{p}_{ijt}\underline{\tau}_{ijt}$ ($\overline{\psi}\overline{p}_{ijt}\overline{\tau}_{ijt}$).

When $\zeta = 0$, container subsidy rate is 0.507% (air tax rate is 0.446%). When $\zeta = 1/6$, container subsidy rate is 0.511% (air tax rate is 0.450%).

| **Scenario** | IMO2023 | | Container Subsidy | | Air Tax | |
|---|---|---|---|---|---|---|
| Air Pass Through ($\zeta$) | 0 | 1/6 | 0 | 1/6 | 0 | 1/6 |
| %Δ Container Capacity | 0.00 | 0.01 | 0.66 | 0.67 | 0.15 | 0.15 |
| %Δ Number of Vessels | 5.56 | 5.56 | 1.33 | 1.34 | 0.81 | 0.81 |
| %Δ Round-Trips per Vessel | -5.26 | -5.26 | -0.66 | -0.66 | -0.65 | -0.65 |
| %Δ Air Capacity | 0.43 | 0.39 | -4.30 | -4.34 | -4.09 | -4.13 |
| %Δ Container Freight Rates | 0.46 | 0.46 | 0.02 | 0.02 | 0.01 | 0.01 |
| %Δ Air Freight Rates | 0.00 | 0.07 | 0.00 | 0.01 | 0.00 | 0.01 |
| %Δ Container Emissions | -11.37 | -11.37 | 0.66 | 0.67 | 0.15 | 0.15 |
| %Δ Air Emissions | 0.39 | 0.35 | -4.31 | -4.35 | -4.11 | -4.15 |
| %Δ Net Emissions | -2.92 | -2.94 | -2.92 | -2.94 | -2.92 | -2.94 |
| Net Δ $CO_2$ (mln ton) | -1.48 | -1.49 | -1.48 | -1.49 | -1.48 | -1.49 |
| Net Δ Welfare (mln USD) | -255 | -256 | -66 | -65 | 2693 | 2713 |
| Net Δ $CO_2$ Welfare (mln USD) | 59 | 60 | 59 | 60 | 59 | 60 |
| Net Δ Consumer Surplus (mln USD) | -314 | -316 | 4147 | 4183 | -205 | -207 |
| Subsidy Amount/Tax Revenue (mln USD) | 0 | 0 | -4272 | -4308 | 2839 | 2860 |
| Welfare Neutral Carbon Price (USD/ton) | 173 | 172 | 44 | 44 | NA | NA |

Table A14: New Technology Alternative Policy with increased speed (IV $\varepsilon = 10.3$)

| **Scenario** | (1) | (2) | (3) | (4) |
|---|---|---|---|---|
| Adjust $\nu$? | No | | Yes | |
| Air Pass Through ($\zeta$) | 0 | 1/6 | 0 | 1/6 |
| %Δ Container Capacity | 0.23 | 0.23 | 0.25 | 0.24 |
| %Δ Number of Vessels | -7.78 | -7.79 | -7.77 | -7.78 |
| %Δ Round-Trips per Vessel | 8.69 | 8.69 | 8.69 | 8.69 |
| %Δ Air Capacity | -1.25 | -1.06 | -1.32 | -1.13 |
| %Δ Container Freight Rates | -3.29 | -3.29 | -3.29 | -3.29 |
| %Δ Air Freight Rates | 0.00 | -0.52 | 0.00 | -0.52 |
| %Δ Container Emissions | 0.23 | 0.23 | 0.25 | 0.24 |
| %Δ Air Emissions | -1.24 | -1.06 | -1.30 | -1.12 |
| Net %Δ $CO_2$ | -0.82 | -0.70 | -0.87 | -0.74 |
| Net Δ $CO_2$ (mln ton) | -0.43 | -0.37 | -0.45 | -0.39 |
| Net Δ Welfare (mln USD) | 1103 | 1108 | 1162 | 1165 |
| Net Δ $CO_2$ Welfare (mln USD) | 17 | 15 | 18 | 16 |
| Net Δ Consumer Surplus (mln USD) | 1085 | 1094 | 1143 | 1149 |

Table A15: Short Run Uniform 1% Speedup (OLS $\varepsilon = 7.3$)

*Note*: Welfare neutral carbon price estimates in columns (1) and (4) refer to the social value of carbon abatement that *eliminates* consumer surplus gains from increasing speed; by contrast, IMO2023 induced slowdown welfare neutral carbon prices give a sense of social value of carbon abatement necessary to *reverse* consumer surplus *losses*. When inter-modal substitution is allowed, both net $CO_2$ emissions fall and consumer surplus rises, so there is no need to calculate a welfare neutral carbon price.

| **Scenario** | (1) | (2) | (3) | (4) | (5) | (6) |
|---|---|---|---|---|---|---|
| Adjust $\nu$? | | No | | | Yes | |
| Air Pass Through ($\zeta$) | 0 | 1/6 | 0 | 0 | 1/6 | 0 |
| %Δ Container Capacity | 1.00 | 1.00 | 1.00 | 1.00 | 1.00 | 1.00 |
| %Δ Air Capacity | 0.00 | -3.37 | -4.00 | 0.00 | -3.57 | -4.18 |
| %Δ Container Freight Rates | -22.32 | -19.16 | -18.70 | -22.27 | -19.06 | -18.48 |
| %Δ Air Freight Rates | 0.00 | -3.17 | 0.00 | 0.00 | -3.10 | 0.00 |
| %Δ Container Emissions | 2.61 | 2.61 | 2.61 | 2.61 | 2.61 | 2.61 |
| %Δ Air Emissions | 0.00 | -3.48 | -4.06 | 0.00 | -3.68 | -4.25 |
| Net %Δ $CO_2$ | 0.73 | -1.77 | -2.18 | 0.73 | -1.91 | -2.32 |
| Net Δ $CO_2$ (mln ton) | 0.38 | -0.93 | -1.14 | 0.38 | -1.00 | -1.22 |
| Net Δ Welfare (mln USD) | 1111 | 867 | 831 | 1164 | 906 | 871 |
| Net Δ $CO_2$ Welfare (mln USD) | -15 | 37 | 46 | -15 | 40 | 49 |
| Net Δ Consumer Surplus (mln USD) | 1126 | 830 | 785 | 1179 | 866 | 823 |
| Welfare Neutral Carbon Price (USD/ton) | 2887 | NA | NA | 3026 | NA | NA |

Table A16: Short Run Uniform 1% Speedup (IV $\varepsilon = 10.3$)

*Note*: Welfare neutral carbon price estimates in columns (1) and (4) refer to the social value of carbon abatement that *eliminates* consumer surplus gains from increasing speed; by contrast, IMO2023 induced slowdown welfare neutral carbon prices give a sense of social value of carbon abatement necessary to *reverse* consumer surplus *losses*. When inter-modal substitution is allowed, both net $CO_2$ emissions fall and consumer surplus rises, so there is no need to calculate a welfare neutral carbon price.

| **Scenario** | (1) | (2) | (3) | (4) | (5) | (6) |
|---|---|---|---|---|---|---|
| Adjust $\nu$? | | No | | | Yes | |
| Air Pass Through ($\zeta$) | 0 | 1/6 | 0 | 0 | 1/6 | 0 |
| %Δ Container Capacity | 1.00 | 1.00 | 1.00 | 1.00 | 1.00 | 1.00 |
| %Δ Air Capacity | 0.00 | -4.72 | -5.50 | 0.00 | -4.91 | -5.67 |
| %Δ Container Freight Rates | -22.46 | -18.88 | -18.07 | -22.43 | -18.79 | -17.96 |
| %Δ Air Freight Rates | 0.00 | -2.94 | 0.00 | 0.00 | -2.91 | 0.00 |
| %Δ Container Emissions | 2.61 | 2.61 | 2.61 | 2.61 | 2.61 | 2.61 |
| %Δ Air Emissions | 0.00 | -4.88 | -5.59 | 0.00 | -5.07 | -5.77 |
| Net %Δ $CO_2$ | 0.73 | -2.77 | -3.29 | 0.73 | -2.91 | -3.42 |
| Net Δ $CO_2$ (mln ton) | 0.38 | -1.45 | -1.72 | 0.38 | -1.52 | -1.79 |
| Net Δ Welfare (mln USD) | 761 | 592 | 572 | 786 | 611 | 592 |
| Net Δ $CO_2$ Welfare (mln USD) | -15 | 58 | 69 | -15 | 61 | 72 |
| Net Δ Consumer Surplus (mln USD) | 776 | 534 | 503 | 802 | 550 | 520 |
| Welfare Neutral Carbon Price (USD/ton) | 1978 | NA | NA | 2044 | NA | NA |